Structure and Function of the Viscous Capture Spiral and its Relationship to the Architecture of Spider Orb-Webs

Sarah Day Stellwagen

Dissertation submitted to the faculty of the Virginia Polytechnic Institute and State University in partial fulfillment of the requirements for the degree of Doctor of Philosophy In Biological Sciences

Brent D. Opell, Committee Chair

E. Fred Benfield

Todd A. Blackledge

Carlyle C. Brewster

July 27, 2015

Blacksburg, VA

Keywords: Orb-web, glycoprotein, temperature, ultraviolet, asymmetry

Structure and Function of the Viscous Capture Spiral and its Relationship to the Architecture of Spider Orb-Webs

Sarah Day Stellwagen

ABSTRACT

Spider orb-webs have evolved to intercept prey, absorb and dissipate the kinetic energy from prey impact, and retain prey until a spider can subdue their catch. Orb-web structure and function engages scientists from many disciplines, including engineering, behavior, materials science, ecology, and evolution. This dissertation examines the sticky capture spiral component of an orb-web. This composite material is made of supporting fibers covered in sticky glue droplets. These threads are both adhesive and extensible, and their performance is influenced by ambient conditions. The questions I addressed are framed in an ecological context, although they also add to our understanding of materials science. The results of the first study showed that temperature increased the viscosity of glycoproteins within *Argiope aurantia* droplets, mediating the effect of daily humidity changes, an important environmental effect on the glue's performance. The second study demonstrates that capture spiral droplets of spiders that build webs in habitats ranging from full sun to shade and nocturnal species (*Argiope aurantia, Leucauge venusta, Neoscona crucifera, Verrucosa areenata, Micrathena gracilis*) is resistant to degradation after a day's worth of UVB exposure. Conversely, after the equivalent of two days of UVB exposure the glue degrades in webs built by *M. gracilis* that build webs in the shade and *N. crucifera*, a nocturnal species. The less harsh UVA has little affect on capture spiral glue function, both for species that build webs in full sun and those that build webs at night. The third study documented web asymmetry in *Argiope trifasciata* orb-webs and identified differences in droplet characteristics across the webs. These spiders differently allocated resources, with the bottom region of the web having twice the droplet volume as the top, and half the ratio of aqueous to glycoprotein material as the inner droplets. Additionally, during foraging times, the bottom of the web experiences higher humidity than the top, which has the potential to increase droplet toughness in this region. This study expands the understanding of web asymmetry by examining the differences in glue characteristics as an additional level of flexibility for web fine-tuning.

ATTRIBUTIONS

I thank my advisor, Brent D. Opell, for his enduring support and dedication to helping me achieve my academic goals. He has been an inspiring mentor, has been patient and thorough, and I give endless thanks to him for seeing me through this graduate experience. I couldn't have asked for better guidance, and I know my career will be exciting and fruitful because of the scientific foundations I received in his lab.

I thank my committee, not only for investing their time and effort into improving my graduate projects, but for helping me grow as a scientist. I also thank the undergraduate and assistant laboratory researchers that contributed their time and effort to my projects. Their help was invaluable and they did excellent work.

I thank the faculty, staff, and fellow students of the Biological Sciences Department for making my time at Virginia Tech fulfilling and enjoyable. I appreciate the community this department offered, and I will always look back at my time as a graduate student at Virginia Tech with fondness.

I thank the American Arachnological Society for providing a supportive and exciting arena for the exchange and development of ideas for all things arachnids. This group has been incredibly inspirational, and I am grateful to have an outlet for my arachnological enthusiasm with like-minded individuals.

I thank my mom, Laurel Roland, for her love, encouragement, and support, and for allowing me to explore my interests as a child, as this no doubt led me to pursue a career in arachnology. It has been an enjoyable and fulfilling path, and I'm grateful to be able to study what I truly find fascinating. I also thank my loved ones and friends that have supported me during this adventure.

TABLE OF CONTENTS

LIST OF FIGURES

CHAPTER 1:

CHAPTER 2:

CHAPTER 3:

CHAPTER 4:

CHAPTER 5:

LIST OF TABLES

CHAPTER 2:

CHAPTER 3:

CHAPTER 4:

CHAPTER 5:

1. Introduction : Orb-web function and the importance of viscous capture theads

Sarah Stellwagen

The ability to spin silk has evolved multiple times in several orders of Arthropoda (Craig, 1997). Insects, myriapods, and arachnids all produce silk proteins for a variety of purposes including lining burrows and retreats, protecting eggs and pupae, constructing nets for capturing prey (e.g. spider orb-webs and caddisfly snares), and dispersal (e.g. silk ballooning in spiders and moths. Silk proteins consist of repetitive amino acid sequences that begin as a liquid dope within an organism and become fibrous as the material is 'spun' or polymerized. The arrangement of these amino acids produces varying levels of strength and extensibility (Swanson et al., 2007). Spiders, however, also produce silk proteins that remain liquid after extrusion: the sticky glycoprotein glue of the capture spiral silk component of orb-webs.

Scientists from many disciplines have been drawn to spider orb-webs (Fig. 1). Ethologists are inspired by the behavioral complexities involved in making such an intricate and functional structure in a relatively short period of time (Vollrath, 1988). Engineers are motivated to understand the integration of the web's components to yield powerful energy sinks (Sensenig et al., 2012). Material scientists examine the unique properties of the array of silks used in web construction (Swanson et al., 2006). Systematists are driven to discover the origin and subsequent modification of the physical and structural diversity of orb web architecture (Hormiga and Griswold, 2014), a field still under hot debate (Bond et al., 2014), while ecologists seek to understand the selective pressures that shape web elements (Blackledge, 2012). Each of these disciplines contributes important knowledge to a broader understanding of spider orb-web function.

Spider orb-webs must complete three tasks: intercept prey, absorb and dissipate preys' kinetic energy, and retain prey (Chacón and Eberhard, 1980; Blackledge et al., 2011). The outer frame of silk provides the primary foundational support for the web's inner components. Radial silk threads that extend from the center of the web like the spokes of a wheel absorb and dissipate kinetic energy from prey impact (Sensenig et al., 2012) and

provide support for the spiral of sticky capture silk responsible for prey retention (Fig. 2; Sahni et al., 2011). The retention time of an insect is critical to successful prey capture, as even a few seconds can mean the loss of a potential meal for a spider (Blackledge and Zevenbergen, 2006).

Most orb-weaving spiders follow a behavioral pattern that results in a general web design (Fig. 2; Eberhard, 1990). Spiders begin web construction by anchoring the top frame line between two structural supports. This is accomplished by releasing a strand of dragline silk, which, after becoming caught in an air current, is carried from the spider's resting place until it contacts another structure, such as a neighboring branch or twig (Eberhard, 1987). The spider then tests the line to determine if the opposing anchor of support is secure and the distance appropriate. Several more strands of silk are then laid down to strengthen the top frame line, after which the spider will drop from the center of this multi-thread frame line until reaching a third anchoring structure, usually adjacent vegetation, creating a Y-shaped silk framework. The remainder of the radial silk threads that will eventually support the sticky capture spiral are subsequently added. Before the sticky spirals are spun however, the spider creates a temporary spiral, starting from the web's center and moving to the web's periphery. Beginning at the web's perimeter the spider lays the capture spirals covered in viscoelastic glue, using the temporary spiral as a guide while simultaneously removing it, and progressing towards the center. The capture spiral is completed a short distance from the web's center leaving a 'free zone' between the final spirals and the web hub, where most orb-weaving spiders rest while waiting for prey interception (Levi, 1978).

Orb-web silks originate within glands that terminate at valved spigots supported by flexible appendages called spinnerets, located posteriorly on a spider's abdomen. There are up to seven types of silk produced by orb-weavers, each with unique properties. Major ampullate or dragline silk forms the outer frame and radial threads and serves as a lifeline as the spider moves around its habitat. This silk has been the focus of material science for decades, as it is as strong, but, owing to its great extensibility, tougher than steel. Minor ampullate silk is used to create a temporary scaffold spiral that serves as a guide for the web's sticky capture spiral silk, which is composed of a pair of supporting flagelliform lines covered in aggregate gland glue. Other forms of silk include tubiliform silk, which covers a spider's eggs creating a protective sac, aciniform silk, which is spun in sheets of hundreds of

individual strands and used to wrap subdued prey, and piriform silk, which forms attachment disks that fasten major ampullate silk threads to surfaces (Foelix, 2011).

Orb-webs are constructed by members of two spider clades, which can be distinguished by the type of silk used to form the sticky spiral: cribellate silk, produced by the more primitive Deinopoidea, and viscous silk, produced by the more derived and taxonomically diverse Araneiodea (Coddington and Levi, 1991). Cribellate silk consists of a pair of supporting pseudoflagelliform axial silk fibers covered by thousands of coiled and looped nanofibers to form a dry, adhesive surface (Opell, 1999, 2013). To adhere to prey, this silk relies on van der Waals and capillary forces, as well as entanglement with insect setae (Hawthorn and Opell, 2003), and absorbs energy from the breaking of individual nanofibers upon impact by an insect and as an insect struggles to escape (Blackledge and Hayashi, 2006). Most spiders have lost the cribellum spinning plate responsible for producing the adhesive nanofibers and, therefore, the ability to spin cribellar thread. However, cribellar thread appears to have been present as the sticky spiral element of the first orb-webs. Recent studies suggest that the orb-web has a more ancient and common web form than previously thought (Bond et al., 2014; Hormiga and Griswold, 2014) and that many spider families previously considered among the ancestors of the cribellate orb-weavers have, in fact, descended from orb-weaving spiders.

Viscous silk is formed of two elements. Like cribellar thread, it contains a pair of supporting axial flagelliform fibers (now considered homologous with the psuedoflagelliform fibers of cribellate silk; Blackledge et al., 2009)**,** but the nanofiber coating has been replaced by droplets of liquid viscoelastic glue. Each axial flagelliform fiber spigot is found on a pair of posterior lateral spinnerets and flanked by a pair of aggregate spigots that coat the silk with adhesive as it is spun. The glue initially forms a cylinder around the support fibers, but rapid absorption of atmospheric moisture builds surface tension and causes the material to break into evenly spaced droplets (Plateau, 1873; Rayleigh, 1892; Edmonds and Vollrath, 1992). Each droplet is composed of a glycoprotein core (Fig. 3; Vollrath and Tillinghast, 1991), which confers stickiness (Sahni et al., 2010) and contains a small granule that probably anchors the droplet to the axial fibers (Opell and Hendricks, 2010). This core is surrounded by a solution composed of inorganic salts and water-soluble low molecular mass organic compounds (LMMC) such as GABamide, choline, and isethionic acid (Fischer and

Brander, 1960; Andersen, 1970; Vollrath et al., 1990; Townley and Tillinghast, 2013). This liquid coating extends into the inter-droplet regions and conditions the axial fibers, causing them to supercontract, becoming taut but remaining extensible (Vollrath and Edmonds, 1989; Bonthrone et al., 1992). Flagelliform silk used in viscous webs is more elastic and more efficient at energy absorption than is cribellate silk (Blackledge and Hayashi, 2006). Moreover, viscous thread is less metabolically expensive, and takes the spider less time to spin: 30 minutes to spin a viscous orb-web versus 3 hours to spin a cribellate orb-web (Zschokke and Vollrath, 1995; Opell, 1997).

Viscous capture spiral glue has engaged scientists because it is a 'smart material', adapting to ambient environmental conditions by changing its properties. The low molecular weight compounds and salts within the outer aqueous material affect droplet performance in two ways: they solvate glycoproteins, enhancing their interaction with a surface (Sahni et al., 2014), and they cause droplet volume to fluctuate with ambient humidity, allowing them to remain hydrated (Opell et al., 2011, 2013). Some of the absorbed atmospheric water is also incorporated into the glycoprotein at the center of the droplet, altering performance properties such as extensibility and adhesion (Sahni et al., 2011; Opell et al., 2013).

Humidity affects droplet performance and adhesion, and appears to adapt a species to the conditions of its habitat (Sahni et al., 2011; Opell et al., 2013). Droplets from species adapted to dry conditions become over-lubricated when ambient humidity increases beyond their adaptive range, exhibiting a reduction in adhesion and energy absorption capabilities, while droplets from species that are adapted to high humidity habitats function optimally in the upper ranges of ambient humidity. Strain rates also influence droplet adhesive energy; faster strain rates increase adhesive energy and humidity mediates the optimum (Sahni et al. 2010, 2011). A complete understanding of the viscous capture system relies on investigating the selective pressures that shape glue performance. These pressures come from a variety of sources including abiotic conditions (humidity, temperature, wind, solar radiation, and precipitation) and biotic factors (metabolic energy requirements for glue production, prey characteristics, e.g. struggling behaviors, size, and cuticle structures), as well as synergism with the other structural components of the web (radial thread frequency, web size, and silk performance).

When I began considering project ideas examining the viscous capture system of orb-webs, we knew that humidity impacts the volume and performance of the thread's droplets, however the effects of other potentially important environmental factors were unknown. Therefore, I chose to examine the effect of several abiotic factors that have not previously been studied, and an aspect of web architecture that has not been considered. Specifically, I examined the effects of two other obvious environmental factors, temperature and ultraviolet radiation on the function of the capture spiral glue droplets. Additionally, large orb-webs are asymmetrical, with the bottom being larger than the top. Although this phenomenon has received a lot of attention in the past, the contribution of viscous droplet size, performance, and distribution to web asymmetry had not been considered. Therefore, I quantified intra-web differences in droplet distribution and performance in relation to ambient microhabitat gradients.

Chapter 2 demonstrates the influence of temperature on the viscous nature of the glycoprotein droplets and the mediation of humidity effects. Chapter 3 examines the resistance of this material to ultraviolet radiation by comparing the effects of different levels of UVB radiation on the performance of viscous droplets from the webs of five species that encounter different levels of UV exposure: species from sunny, partial and fully shaded habitats, and a nocturnal species. A short Chapter 4 examines the effect of UVA radiation on droplet performance in a diurnal and nocturnal species. The fifth chapter characterizes the composition and performance of droplets from threads taken from the top, top middle, inner, bottom middle, and bottom sections of the capture spiral of *Argiope trifasciata*. This chapter also characterizes the temperature and humidity gradient in which webs are found and examines these gradients in the context of observed differences in droplet distribution and performance. A short final chapter suggests a framework for questions that will continue to refine our understanding of the viscous thread adhesive delivery system and set the stage for applications that might be derived from this system.

The ability to ask questions about a viscous thread's response to environmental variables and to quantify performance differences within and between species depends on the instrumentation available for analysis. Our lab is equipped with a microscope system that has the capabilities of examining, manipulating, photographing, and video recording threads within a chamber whose temperature and humidity can be controlled (Fig. 4). Droplet

extensibility is measured by first inserting a probe through the side of the chamber and making contact with an individual suspended droplet. Next, a stepping motor is used to advance the microscope stage and chamber away from the anchored probe tip at a constant speed. This stretches the droplet until it releases from the probe's tip. Video of the stretching droplet is recorded and used to evaluate differences in droplet performance. To visualize glycoprotein size and its relationship to droplet volume and performance, droplets must be flattened (Fig. 3). This is accomplished by placing a cover slip onto the suspended droplets, which causes them to spread over the glass, allowing visualization of the layered components. Photographs of the flattened droplets are then recorded and used to determine the volume of the droplet's glycoprotein core. In Chapters 3-5, we are also able to use these data to approximate the force on an extending droplet and, from this, calculate the relative toughness of glycoprotein. The information derived from integrating these methods provides a unique ability to examine the influence of specific selection pressures on overall droplet performance.

FIGURES

Figure 1. Orb-web of *Argiope trifasciata* Forsskål 1775.

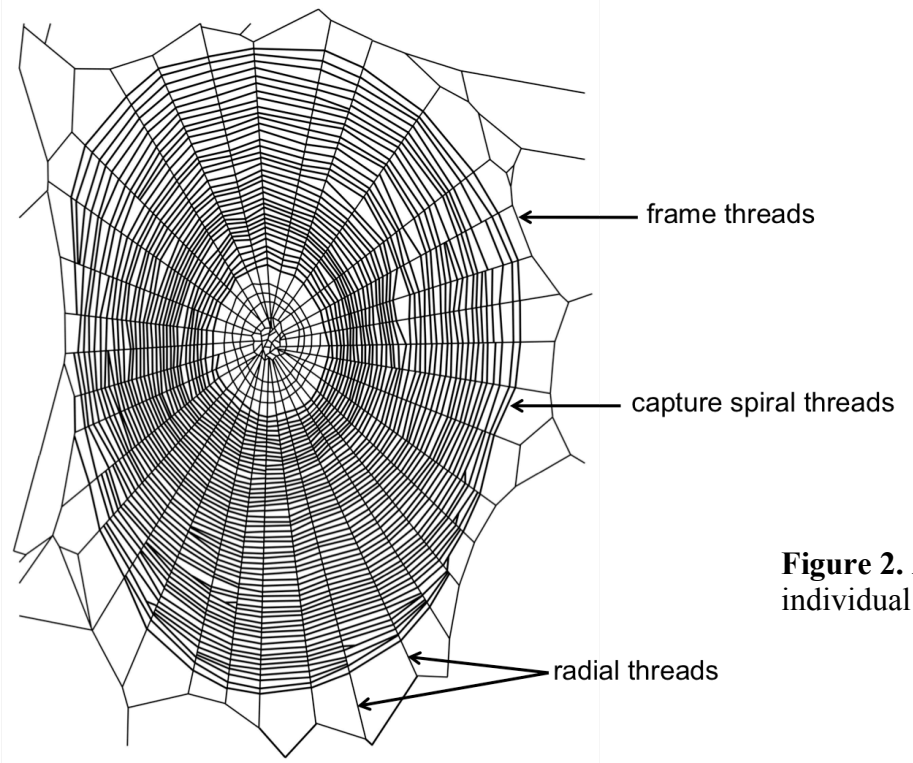

Figure 2. An orb-web and its individual components.

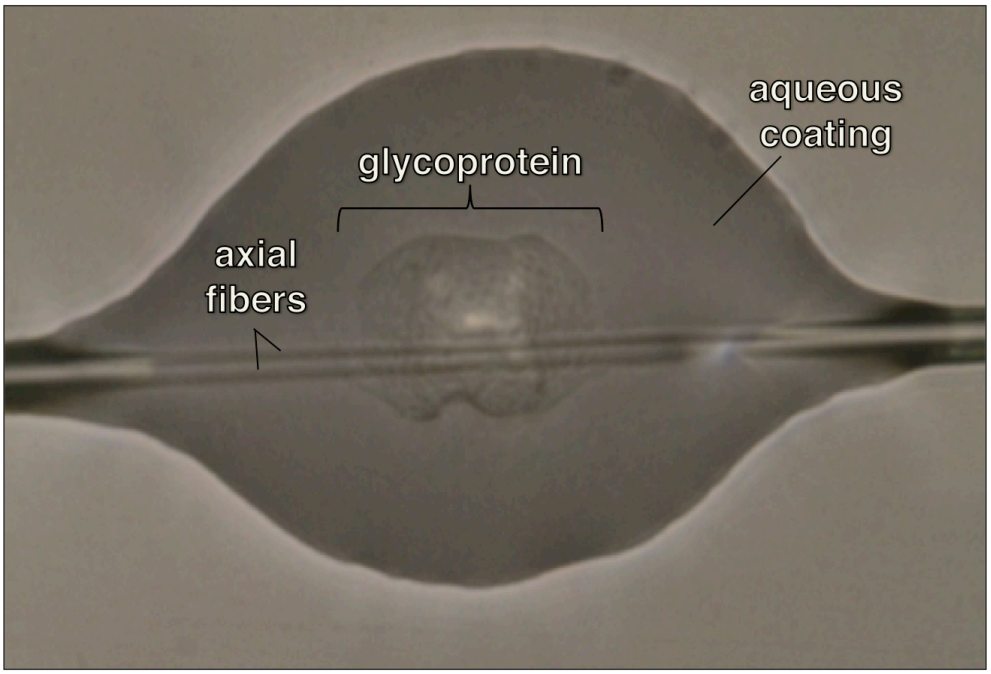

Figure 3. An aqueous glue droplet after flattening on a slide shows the pair of supporting axial fibers, outer aqueous coating, and the inner glycoprotein core.

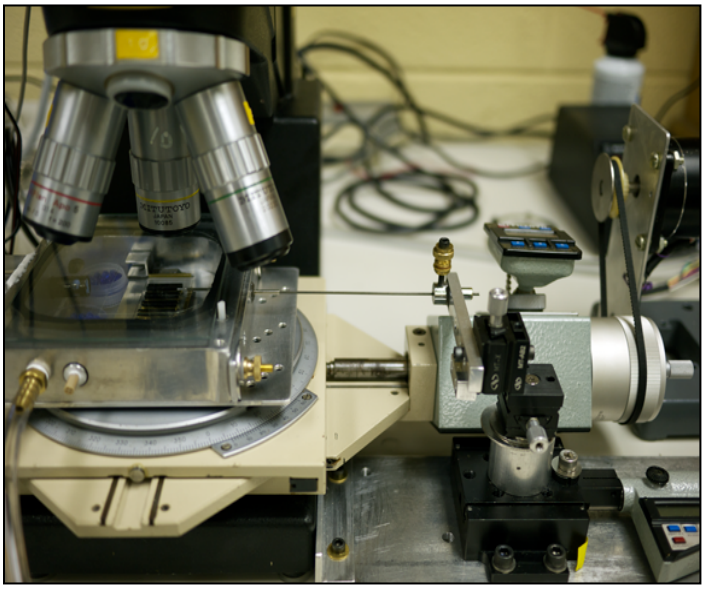

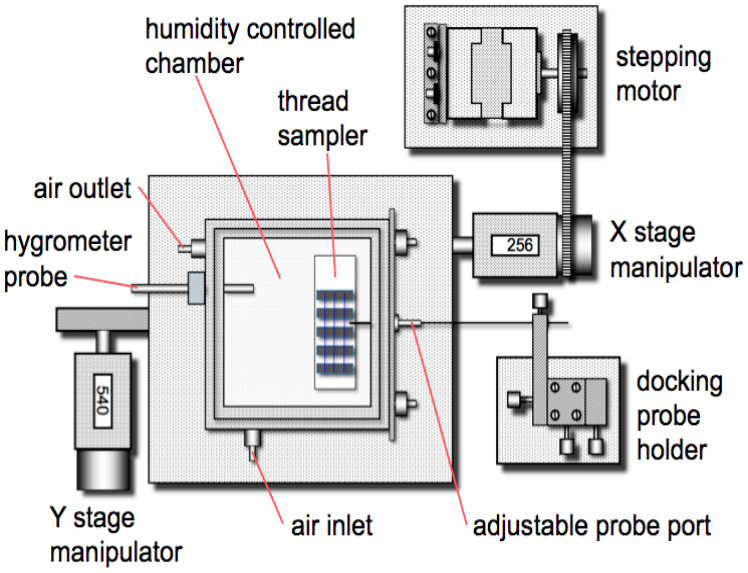

Figure 4. Microscope apparatus used to record and measure extending droplets. Silk strands are suspended across supports glued to thread samplers and placed in a humidity and temperature controlled chamber. A probe inserted into the side of the chamber is brought into contact with a single droplet, and then withdrawn at a constant speed while the extension is recorded. Figure and photograph courtesy: Brent D. Opell.

REFERENCES

Andersen, S. O. (1970). Amino acid composition of spider silks. *Comparative biochemistry and physiology* **35**, 705.

Blackledge, T. A. (2012). Spider silk: a brief review and prospectus on research linking biomechanics and ecology in draglines and orb webs. *Journal of Arachnology* **40**, 1-12.

Blackledge, T. A. and Hayashi, C. Y. (2006). Unraveling the mechanical properties of composite silk threads spun by cribellate orb-weaving spiders. *J Exp Biol* **209**, 3131-3140.

Blackledge, T. A. and Zevenbergen, J. M. (2006). Mesh Width Influences Prey Retention in Spider Orb Webs. *Ethology* **112**, 1194-1201.

Blackledge, T. A., Kuntner, M. and Agnarsson, I. (2011). The Form and Function of Spider Orb Webs: Evolution from Silk to Ecosystems. In *Advances in Insect Physiology*, vol. Volume 41 (ed. C. Jérôme), pp. 175-262: Academic Press.

Blackledge, T. A., Scharff, N., Coddington, J. A., Szuts, T., Wenzel, J. W., Hayashi, C. Y. and Agnarsson, I. (2009). Reconstructing web evolution and spider diversification in the molecular era. *Proceedings of the National Academy of Sciences of the United States of America* **106**, 5229-5234.

Bond, Jason E., Garrison, Nicole L., Hamilton, Chris A., Godwin, Rebecca L., Hedin, M. and Agnarsson, I. (2014). Phylogenomics Resolves a Spider Backbone Phylogeny and Rejects a Prevailing Paradigm for Orb Web Evolution. *Current Biology* **24**, 1765-1771.

Bonthrone, K. M., Vollrath, F., Hunter, B. K. and Sanders, J. K. M. (1992). The Elasticity of Spiders' Webs is Due to Water-Induced Mobility at a Molecular Level. *Proceedings of the Royal Society B: Biological Sciences* **248**, 141-144.

Chacón, P. and Eberhard, W. G. (1980). Factors affecting numbers and kinds of prey caught in artificial spider webs with considerations of how orb-webs trap prey. *Bulletin of the British Arachnological Society* **5**, 29-38.

Coddington, J. A. and Levi, H. W. (1991). Systematics and evolution of spiders (Araneae). *Annual Review of Ecology and Systematics* **22**, 565-592.

Craig, C. L. (1997). Evolution Of Arthropod Silks. *Annual Review of Entomology* **42**, 231-267.

Eberhard, W. G. (1987). How Spiders Initiate Airborne Lines. *Journal of Arachnology* **15**, 1-9.

Eberhard, W. G. (1990). Early Stages of Orb Construction by Philoponella Vicina, Leucauge Mariana, and Nephila Clavipes (Araneae, Uloboridae and Tetragnathidae), and Their Phylogenetic Implications. *Journal of Arachnology* **18**, 205-234.

Edmonds, D. and Vollrath, F. (1992). The contribution of atmospheric water vapour to the formation and efficiency of a spider's web. *Proceedings of the Royal Society of London* **248**, 145-148.

Fischer, F. G. and Brander, J. (1960). Eine Analyse der Gespinste der Kreuzspinne. *Hoppe-Seylers's Zeitschrift fur Physiologische Chemie* **320**, 92-102.

Foelix, R. F. (2011). Biology of spiders. Oxford: Oxford University Press.

Hormiga, G. and Griswold, C. E. (2014). Systematics, Phylogeny, and Evolution of Orb-Weaving Spiders. *Annual Review of Entomology* **59**, 487-512.

Levi, H. W. (1978). Orb-Weaving Spiders and Their Webs: Although we can learn much from studying spider webs, more taxonomic data is needed to unravel the mystery of orb-web origins and evolution. *American Scientist* **66**, 734-742.

Opell, B. (2013). Cribellar Thread. In *Spider Ecophysiology*, (ed. W. Nentwig), pp. 303-315: Springer Berlin Heidelberg.

Opell, B. D. (1997). A comparison of capture thread and architectural features of Deinopoid and Araneoid orb-webs. *Journal of Arachnology* **25**, 295-306.

Opell, B. D. (1999). Changes in spinning anatomy and thread stickiness associated with the origin of orb-weaving spiders. *Biological Journal of the Linnean Society* **68**, 593-612.

Opell, B. D. and Hendricks, M. l. (2010). The role of granules within viscous capture threads of orb-weaving spiders. *Journal of Experimental Biology* **213**, 339-346.

Opell, B. D., Karinshak, S. E. and Sigler, M. A. (2011). Humidity affects the extensibility of an orb-weaving spider's viscous thread droplets. *Journal of Experimental Biology* **214**, 2988-2993.

Opell, B. D., Karinshak, S. E. and Sigler, M. A. (2013). Environmental response and adaptation of glycoprotein glue within the droplets of viscous prey capture threads from araneoid spider orb-webs. *Journal of Experimental Biology* **216**, 3023-3034.

Plateau, J. (1873). Statique expérimentale et théorique des liquides soumis aux seules forces moléculaires. **1**.

Rayleigh, J. W. S., Baron. (1892). Scientific papers. **3**, 585-596.

Sahni, V., Blackledge, T. A. and Dhinojwala, A. (2010). Viscoelastic solids explain spider web stickiness. *Nature Communications* **1**, 1-4.

Sahni, V., Blackledge, T. A. and Dhinojwala, A. (2011). Changes in the Adhesive Properties of Spider Aggregate Glue During the Evolution of Cobwebs. *Scientific Reports* **1**, 41.

Sahni, V., Blackledge, T. A. and Dhinojwala, A. (2011). A Review on Spider Silk Adhesion. *Journal of Adhesion* **87**, 595-614.

Sahni, V., Miyoshi, T., Chen, K., Jain, D., Blamires, S. J., Blackledge, T. A. and Dhinojwala, A. (2014). Direct Solvation of Glycoproteins by Salts in Spider Silk Glues Enhances Adhesion and Helps To Explain the Evolution of Modern Spider Orb Webs. *Biomacromolecules* **15**, 1225-1232.

Sensenig, A. T., Lorentz, K. A., Kelly, S. P. and Blackledge, T. A. (2012). Spider orb webs rely on radial threads to absorb prey kinetic energy. *Journal of The Royal Society Interface*.

Swanson, B. O., Blackledge, T. A., Beltrán, J. and Hayashi, C. Y. (2006). Variation in the material properties of spider dragline silk across species. *Appl. Phys. A* **82**, 213-218.

Swanson, B. O., Blackledge, T. A. and Hayashi, C. Y. (2007). Spider capture silk: performance implications of variation in an exceptional biomaterial. *Journal of Experimental Zoology Part A: Ecological Genetics and Physiology* **307A**, 654-666.

Townley, M. and Tillinghast, E. (2013). Aggregate Silk Gland Secretions of Araneoid Spiders. In *Spider Ecophysiology*, (ed. W. Nentwig), pp. 283-302: Springer Berlin Heidelberg.

Vollrath, F. (1988). Untangling the spider's web. *Trends in Ecology & Evolution* **3**, 331-335.

Vollrath, F. and Edmonds, D. (1989). Modulation of the mechanical properties of spider silk by coating with water. *Nature* **340**, 305-307.

Vollrath, F. and Tillinghast, E. K. (1991). Glycoprotein glue beneath a spider web's aqueous coat. *Naturwissenschaften* **78**, 557-559.

Vollrath, F., Fairbrother, W. J., Williams, R. J. P., Tillinghast, E. K., Bernstein, D. T., Gallagher, K. S. and Townley, M. A. (1990). Compounds in the droplets of the orb spider's viscid spiral. *Nature* **345**, 526-528.

Zschokke, S. and Vollrath, F. (1995). Unfreezing the Behavior of Two Orb Spiders. *Physiology and Behavior* **58**, 1167-1173.

2. Temperature mediates the effect of humidity on the viscoelasticity of glycoprotein glue within the droplets of an orb-weaving spider's prey capture threads

Sarah D. Stellwagen, Brent D. Opell, Kelly G. Short

Published in Journal of Experimental Biology *Stellwagen, S.D., Opell, B.D., and Short, K.G. (2014). Temperature mediates the effect of humidity on the viscoelasticity of glycoprotein glue within the droplets of an orb-weaving spider's prey capture threads. Journal of Experimental Biology 217, 1563-1569.*

Abstract

Sticky viscous prey capture threads retain insects that strike araneoid orb-webs. The threads' two axial fibers support a series of glue droplets, each featuring a core of adhesive viscoelastic glycoprotein covered by an aqueous solution. After sticking, the glue extends, summing the adhesion of multiple droplets, and dissipates some of the energy of a struggling prey. As a day progresses, threads experience a drop in humidity and an increase in temperature, environmental variables that have the potential to alter thread and web function. We hypothesize that thread droplets respond to these opposing environmental changes in a manner that stabilizes their performance and test this by examining threads spun by *Argiope aurantia*, a species that occupies exposed, weedy habitats. We confirmed that decreased humidity increases glycoprotein viscosity and found that increased temperature had the opposite effect. To evaluate the combined effect of temperature and humidity on a droplet's ability to transfer adhesive force and dissipate energy, we extended a droplet and measured both the deflection of the axial line supporting the droplet and the duration of its tensive load. The cumulative product of these two indices, which reflects the energy required to extend a droplet, was greatest under afternoon (hot and dry) conditions, less under morning (cool and humid), and least under hot & humid afternoon conditions. Although the opposing effects of temperature and humidity tend to stabilize glycoprotein performance, *A. aurantia* thread

droplets appear to function optimally during the afternoon, equipping this species to capture large orthopterans, which are most active at this time.

Keywords: *Argiope aurantia*, biomaterial, glycoprotein, hygroscopic, viscoelastic
** Journal of Experimental Biology requires the Methods section to follow the Discussion.*

INTRODUCTION

All animals produce glycoproteins, but few incorporate them as adhesive in traps that capture prey. Onychophorans squirt a sticky substance supported by proteinaceous threads onto nearby prey, however this material is not extruded prior to prey encounter (Betz and Kolsch, 2004). Marine gastropods in the genus *Dendropoma* deploy sticky mucus nets that gather suspended plankton and detritus (Kappner et al., 2000). Modern orb-weaving spiders incorporate viscoelastic glycoprotein glue in the capture spiral threads of their webs (Fig. 1). This system is unique in several ways; the adhesive is a critical part of an aerial filtering system and its production anticipates future prey. Unlike onycophoran adhesive, which is produced when needed, or gastropod mucus, which remains in an osmotically and thermally stable marine environment, spider thread glycoproteins must function over the course of a day where ambient temperature and humidity oscillate, often dramatically (Fig. 2).

Three spinning spigots on each of an orb-weaving spider's paired posterior lateral spinnerets produce its composite viscous capture threads. A single flagelliform spigot produces a supporting protein axial line (Sekiguchi, 1952), which is coated by material from two adjacent aggregate glands as it emerges (Apstein, 1889). The two coated lines from each spigot merge to produce a cylindrical, proto viscous thread (Warburton, 1890). Low molecular weight molecules and inorganic salts in the fluid surrounding the axial lines rapidly attracts atmospheric moisture, increasing the cylinder's volume and surface tension, setting the stage for Plateau-Rayleigh instability to form the cylinder into droplets (Plateau, 1873; Boys, 1889; Rayleigh, 1892; Edmonds and Vollrath, 1992). Within each droplet, an adhesive glycoprotein core forms and remains covered by a hygroscopic aqueous outer layer that also covers axial lines in the thread's inter-droplet region (Opell and Hendricks, 2009; Fig. 1C).

Thread adhesion is enhanced by the extensibility of both the glycoprotein cores within droplets (Sahni et al., 2010) and the axial lines (Opell et al., 2008). As force is applied to a thread that has contacted a surface, these droplets extend, permitting the axial line to sum their adhesive forces (Opell and Hendricks, 2007, 2009). The contribution of glycoprotein to this suspension bridge mechanism depends on a combination of viscosity that absorbs energy through hysteresis (Gosline et al., 1986) or dissipates energy upon droplet pull off (Sahni et al., 2010) and the reversible elastic deformations that retain prey in the web after interception (Sahni et al., 2010). These qualities, which contribute to the overall prey capture success of the web, have the potential to be altered by ambient conditions.

The hygroscopic aqueous material that coats the glycoprotein and axial lines of viscous threads absorbs atmospheric moisture and transfers this moisture to the glycoprotein glue (Opell et al., 2011b). Water absorbed by this outer layer during periods of high humidity (greater than ~60% RH), causes over-lubrication (over-hydration) of the glue in *Argiope aurantia* Lucas 1833, reducing adhesion (the energy required to pull a droplet from a surface) through the disruption of hydrogen bonding and electrostatic interactions of the glycoprotein molecules, as Sahni and colleagues (Sahni et al., 2011) also show for *Larinioides cornutus*. However, threads of the nocturnal *Neoscona crucifera*, found in humid habitats, do not exhibit an upper humidity threshold (Opell et al., 2013). This suggests the glycoprotein is an adaptable material, whose properties are selected to suit a species' habitat.

Argiope aurantia is an active daytime predator that prefers open, grassy habitats and, in our area, matures in late summer. Their webs are available to capture prey in the early morning as soon as enough webbing is produced for interception. Webs of adult females are usually recycled daily, however individuals may occasionally wait several days before replacing a web (Reed et al., 1969). Females continuously occupy the center of the web and only leave to capture prey, seek shelter during hazardous weather, and to deposit egg sacs. During the early morning, webs experience low, late summer and early autumn temperatures (15-20° C) and high relative humidities (90-100% RH). As the day progresses temperatures rise as high as 35-40° C, while RH often drops to 45% or below (Fig. 2). This normal cycling of temperature and humidity is sometimes interrupted by periods of rainy weather, resulting in unusually high daytime humidity (Fig. 2, August 5-7). Although *A. aurantia* forage from

morning to evening, the bulk of their prey is captured during the afternoon when large orthopterans are the most active and likely to be captured (Harwood, 1974).

As *A. aurantia* webs function over the course of a day when temperature and humidity vary greatly, the goal of this study is to examine the combined effect of these environmental factors on the properties of their glycoprotein adhesive. When temperature drops, viscous materials become stiffer, requiring either more force or more time to undergo deformation. Therefore, low temperatures may increase the viscosity of a spider web's adhesive droplets, resulting in stiffer glue and increased energy absorption during glycoprotein extension. However, the temperature increase that causes glycoprotein to become more pliable is usually accompanied by a decrease in humidity, which reduces glycoprotein hydration, extensibility, and the potential for over-lubrication. Therefore, we hypothesize that temperature and humidity act in an antagonistic fashion, which tends to stabilize glycoprotein function over the course of a day. We test this by measuring the performance of viscous droplets from the webs of *A. aurantia* under conditions that simulate cool and humid mornings, hot and dry afternoons, and hot and humid afternoons.

RESULTS

In contrast to previous studies that measured total droplet extension (Opell et al., 2011b, 2013), we focused on the time during which an extending thread droplet was under tension, reasoning that non-loaded glycoprotein filaments that occasionally persist after the filament is no longer under an observable tension, contributed neither to thread adhesion nor energy dissipation. We used angular deflection of a thread's axial line (Fig. 3) to quantify the tension on droplets that remained consolidated before extending (Pre-extension Phase in Fig. 4) and during extension (Droplet Extension Phase), with a 180° angle denoting a non-loaded condition. This angle also provided a means of comparing the impact of temperature and humidity on glycoprotein viscosity, as axial line deflection at the initiation of droplet extension is inversely proportional to glycoprotein viscosity. Plotting this angular index (Y axis) against the time in seconds at which each angle was measured produces a plot (Fig. 4), which is similar to a stress-strain curve, with the area under the line being proportional to the

energy required to extend a droplet. These curves provide a convenient way to compare droplet performance under the three experimental conditions.

Table 1 presents mean droplet dimensions (length, width, and volume) for droplets in the three treatment groups. The first set of values averages of the means of five droplets from each of the 13 individuals and includes the 2 extended droplets. The second set includes only the averages of each individual's 2 extended droplets. When log transformed, the droplet length, width, and volume for each treatment was normally distributed, however the trend for these dimensions to increase with humidity was not significant (ANOVA $P > 0.36$).

Table 2 compares the duration of Total Loaded Time (TLT), Pre-Extension (PE), and Droplet Extension (DE) phases and the axial line deflection angles at five intervals during DE for the three experimental conditions. The TLT for droplets exposed to afternoon conditions was 29.3s, which is 28% longer than morning conditions (22.9s) and 67% longer than hot & humid conditions (17.5s) (Student's t, $P = 0.0233$ and <0.0001, respectively). Thus, a 10° C rise in temperature increased TLT by 5.4s (24%) whereas a 35% decrease in RH increased TLT by 11.8s (40%). When an individual's mean droplet volume prior to extension was averaged across the three temperature/humidity treatments, droplet volume was directly related to the angle at the initiation of droplet pull off, inversely related to TLT, and unrelated to DE ($P = 0.0320$, 0.0317, and 0.5306, respectively). This indicates that as a droplet incorporates more atmospheric moisture the glycoprotein becomes more dilute, less force is required to initiate filament extension, and the filament more quickly attains a non-loaded length.

The pre-extension phase differed between the afternoon and hot & humid conditions, while the morning condition did not differ from either the afternoon or hot & humid conditions (Student's t, $P = 0.0085$, 0.1079, 0.2631 respectively). Under afternoon conditions, droplet pre-extension comprised 71% of the total loaded time (Fig. 5). This increased to 75% under morning conditions and 85% under hot & humid conditions. During the afternoon condition, the extension phase was longer than during the morning and hot & humid conditions, however the latter two conditions did not differ (Student's t, $P = 0.0219$, 0.0035, and 0.4729, respectively).

Axial line deflection at the initiation of droplet extension (DE time 0) decreases from hot & humid conditions to morning conditions to afternoon conditions (ANOVA, $P =$

0.0328), denoting a progressive increase in the tension on the glycoprotein core required to initiate filament extension as glycoprotein viscosity increased (Table 2, Fig. 6). This was associated with a progressive increase in the duration of the pre-extension phase (ANOVA, $P = 0.0287$), as more time was required to generate the increased tension on axial lines necessary to initiate droplet extension (Table 2). Under all three conditions, axial line deflection decreased during the DE phase (ANOVA or Wilcoxon, $P < 0.008$; Table 2, Fig. 6). As extension progressed, deflections at 25% and 50% under afternoon conditions differed from morning and hot & humid conditions, and at 75%, and 99% differed from hot & humid conditions, although morning and hot & humid conditions did not differ (Wilcoxon each pair; Table 2). The total change in angular deflection was remarkably similar among treatments (ANOVA, $P = 0.9432$; Table 2, Fig. 6), exhibiting only an offset in the initiating angle. Under afternoon conditions the rate of angular change was linear and under morning and hot & humid conditions most of the change occurred during the first half of loaded droplet extension.

As axial line deflection is proportionate to the tension on an extending droplet filament, the cumulative product of axial line deflection and the duration of loaded droplet extension is proportional to the energy required to extend a droplet. Plots of these values show that 25% more energy is required to extend a droplet under morning than hot & humid conditions, and 58% more energy is required to extend a droplet under afternoon conditions than under morning conditions (Fig. 6).

DISCUSSION

Viscous thread performance has been measured by the force required to pull a thread from a surface (Agnarsson and Blackledge, 2009; Opell and Hendricks, 2009) and by the energy required to do so (Sahni et al., 2010; Sahni et al., 2011). Our results allow us to gauge the affect of environmental conditions on both measures of droplet performance. Pre-extension time is directly related to the force required to initiate droplet extension and axial line deflection at the initiation of droplet extension is inversely related to this force. The area under the axial line deflection / loaded extension time curve represents the energy required to

complete loaded droplet extension (Fig. 6). As hypothesized, environmental conditions impact both measures of *A. aurantia* droplet performance. Like increased humidity, increased temperature reduced glycoprotein viscosity and, thereby, decreased the force required to initiate droplet extension, the duration of droplet extension times, the tension on extending droplet filaments, and the energy required to extend droplets.

Under hot and dry afternoon conditions, the greatest force was required to initiate droplet extension and the most energy required to extend droplets (Table 2, Fig. 6). Under cool and humid morning conditions, less force and less energy was required. Although the least force and energy was required under hot & humid afternoon conditions, these values were more similar to those of morning conditions than the latter was to afternoon conditions. Thus, under afternoon conditions, droplet extension has the potential to dissipate the greatest amount of energy from struggling prey (Fig. 6), suggesting the viscous glue droplets function optimally during this time. Although the ability to dissipate energy is lower under morning conditions (Fig. 6), lower temperatures help to stabilize droplet and thread function and facilitate prey capture during this time.

The effect of humidity, which has been documented previously (Opell et al., 2011b; Sahni et al., 2011; Opell et al., 2013), was greater than that of temperature. A 35% increase in RH produced a 14.2º increase in axial line deflection at the initiation of droplet extension, whereas a 10º C increase in temperature produced only a 6.1º increase in axial line deflection at the initiation of droplet extension (Table 2). This is also clearly seen in the progression of axial line deflection during the droplet extension phase (Fig. 6), where the difference between afternoon and hot & humid conditions is the result of a 35% RH difference and the difference between morning and hot & humid conditions is the result of a 10º C difference. Thus, decreasing humidity and increasing temperature experienced by webs during the afternoon affect viscous threads in opposite ways, but these changes are not strictly compensatory.

Spiders need time to assess, locate, and subdue prey intercepted by their webs. Large orb-weavers like *A. aurantia* rely extensively on large orthopteran prey captured during the afternoon (Harwood, 1974), and these prey can quickly escape from the web. A study examining the escape rates of insects in webs demonstrated that of the large, energetic insects that were intercepted by *A. aurantia* webs, 18% escaped in less than a second (Blackledge

and Zevenbergen, 2006). Consequently, the length of time that thread droplets can maintain a load while being extended is critical. Moreover, it is during this extension phase that that energy from a struggling prey is dissipated through hysteresis that occurs when droplets extend and contract.

The rate of droplet strain that we used (69.6 μm s^{-1}) was in the upper range of values used in other studies (1, 10, 50, and 100 μm s^{-1}; Sahni et al., 2010; Sahni et al., 2011). In both studies, conducted at a 25° C, increased strain rates increased the stress and strain on extending droplets. In the latter study, the maximum stress and strain acheived for each strain rate increased when humidity increased from 15% to 40%, and then decreased from 40% to 90%, however the relative response to each strain rate remained consistent. Therefore, we believe that similar to humidity, temperature acts to shift but not reorder the response of viscous droplets to strain rate, however the strain rate at which viscous threads have been selected to function has not been evaluated.

The molecular structure of spider glue glycoprotein from *Nephila clavipes* is thought to incorporate components that are similar to those of mucin glycoprotein (Tillinghast et al., 1993; Choresh et al., 2009), which is highly *O*-glycosylated (Rhodes and Ching, 1993). These carbohydrate side chains of glycoproteins are very hydrophilic and usually have all possible hydrogen bonds fulfilled either with water molecules or neighboring saccharides (Cambillau, 1995). One to three water molecules can act as bridges between saccharide and protein, establishing a network of viscous material in and around the glycoprotein (Cambillau, 1995). Opell and colleagues (Opell et al., 2013) suggested that over-lubrication in high humidity is due to water molecules providing alternate bonding sites, and disrupting secondary molecular structure of the glycoprotein glue. At optimum humidity, water molecules may keep some carbohydrate moieties ‘open’ by establishing bonds with them, while still allowing intramolecular structural stability. When a web intercepts an insect, these open carbohydrates may dissociate from the water to form bonds with polar cuticle and cuticular protrusions such as setae (Opell and Schwend, 2007). It may be that at lower temperatures, intramolecular hydrogen bonding within the glycoprotein becomes more stable, decreasing the bonding potential of water molecules with the carbohydrate side chains, and helping to stabilize the glycoprotein glue as its water content increases.

Orb-webs constructed by large spiders like *A. aurantia* have been selected to withstand the impacts of large, often fast-flying, highly profitable prey (Blackledge and Eliason, 2007; Sensenig et al., 2010; Harmer et al., 2011; Kelly et al., 2011; Sensenig et al., 2012). This is achieved principally through the energy absorbing toughness of the web's non-sticky radial lines, with viscous threads making only a minor contribution (Sensenig et al., 2012). Consequently, these viscous threads have been largely selected for prey retention (Blackledge and Eliason, 2007). The hygroscopicity that is resposible for viscous droplet formation continues to impact the performance of viscous treads over the course of a day and has the potential to adapt a species' web to its environment. A previous study (Opell et al., 2013) showed that the high hygroscopicity of *A. aurantia* threads adapts this species' threads to the low humidity of their exposed habitats. Our study suggests that these threads have also been selected to function optimally at times of the day when they have the greatest chance of intercepting large prey, with low afternoon humidity restoring some of the glycoprotein's viscosity lost to the typically higher temperature at this time of the day.

MATERIALS AND METHODS

Thread collection

We sampled the orb-webs constructed by 13 adult female *A. aurantia* found near Blacksburg, Montgomery County, VA, USA, from 31 August to 18 October 2012. Samples were collected between 05:30h and 09:30h and analyzed by 16:00h of the same day. One sector of each spider's web was collected on a 17 cm diameter aluminum ring with a bar across the center. The 5 mm wide ring and bar were covered with Scotch® double-sided tissue tape (Tape 4101T; 3M, St Paul, MN, USA) which adhered to web sectors, maintaining the threads at their native tension. When web sectors were collected, threads extending from the ring were cut with a scissor to avoid distorting the sample when the ring was withdrawn from the web. We placed web-sampling rings in a closed plastic container for transport to the laboratory. Each web location was marked with flagging tape to prevent an individual's web from being resampled.

From each spider's web sector we transferred two viscous thread strands to a microscope slide sampler used for each of the three temperature/humidity treatments. We

measured the extension of one droplet on each strand and the length (dimension parallel to axial line) and width of these two droplets plus three additional droplets per individual. An individual's extension and droplet volume measurements were averaged to give an operational sample size of 13 for each temperature/humidity treatment. Before collecting thread strands, we placed 4 mm wide brass bars that were covered with double-sided carbon tape (product 77816, Electron Microscopy Sciences, Hatfield, PA, USA) between the ring's rim and center bar along web radii. This further isolated and stabilized the web sample and ensured that the tension of viscous threads adjacent to the ones being collected was not altered. Forceps, which were blocked open at a distance to accommodate the supports on which thread strands would be suspended, were used to collect individual capture spiral threads and transfer them to a microscope slide sampler. Double-sided carbon tape on the forceps' tips held each thread strand securely when the thread was burned free using a hot wire probe. Five U-shaped brass struts were epoxied at 4.8 mm intervals to microscope slides with their free ends extending upward and covered with double-sided carbon tape (fig. 3 in Opell et al., 2011a). The forceps' tips were inserted into the U's of adjacent supports, allowing threads to be secured to the tops of their tape-covered supports.

To ensure that the probe used to extend droplets only contacted a single droplet at a time, we used a minuten insect pin moistened with distilled water to move away droplets that were adjacent to the test droplet located at the center of the thread strand. This process retained the aqueous coating of the strand's axial fibers, as demonstrated by the formation of small droplets similar to those often present between the large primary droplets of many viscous threads.

Humidity and temperature control

Thread samples were placed in a glass covered, aluminum observation chamber whose humidity was controlled as in previous studies (fig. 4 in Opell et al., 2011b) and monitored with a Fisher Scientific® Instant Digital Hygrometer. A Pletier thermo-electric unit mounted on the rear wall of this chamber and controlled by a thermostat permitted the temperature within the chamber to be controlled to ± 1° C. Small auxiliary heating or cooling blocks were placed on the observation window to prevent the condensation of water vapor on the glass's inner surface.

We chose 20° C to represent early to mid-morning temperatures and 30° C to represent mid-day and afternoon temperatures (Fig. 2). At humidities above 90%, threads tended to pull free from the tape on the slide; therefore morning humidity was simulated by 85% RH. Afternoon humidity was simulated by 50% RH, as a previous study suggests optimal humidity for *A. aurantia* is below 60% (Opell et al., 2013). Hot & humid conditions were simulated by 30° C and 85% RH. Although realistic, these values are probably a conservative portrayal of morning and afternoon environmental differences.

Droplet extension and volume

Prior to extension, we photographed an isolated suspended droplet and determined its volume as described below. A steel probe was then inserted through a port in the side of the test chamber and its 413 μm wide polished tip aligned and brought into contact with the focal droplet. To ensure full droplet adhesion, the probe was pressed against the droplet until the thread was deflected by a distance of 500 μm. A 60 fps video then recorded the probe's withdrawal at a velocity of 69.6 μm s^{-1} as a stepping motor moved the microscope stage, on which the chamber rested, pulling the droplet away from the stationary probe.

Dimensions from 5 droplets for each individual in each treatment replication were recorded, including the 2 droplets that were extended, and then averaged to determine how experimental conditions affected droplet volume. Only the values of extended droplets were used to determine if droplet size correlated with droplet performance. We used ImageJ (Rasband, 1997-2012) to measure droplet length (DL; dimension parallel to the axial fiber) and droplet width (DW), from which we calculated droplet volume (DV) using the following formula from a previous study (Opell and Schwend, 2007).

$$DV = (2\pi*DW*DL)/15$$

Droplet extension and axial line angle defection

The total loaded time (TLT) of droplet extension begins when the axial line is deflected from its initial non-loaded, 180° configuration and ends when the droplet returns to a non-loaded condition. TLT was divided into two phases; the pre-extension (PE) phase, during which a droplet exhibited tensive axial line deflection, but did not extend, thus

holding the axial line in contact with the probe, and the droplet extension (DE) phase, which began when a droplet filament started to form and ended when the axial line returned to its 180° configuration at the end of TLT (Fig. 4).

During DE we measured five axial line deflection angles: the angle at the start initiation of this phase, and the angles at 25%, 50%, 75%, and 99% of the total duration time of DE, using iMovie '11 (Apple Inc., 2010) and ImageJ programs. Subtracting the angle of axial line deflection from 180° produces an index that is directly proportional to the tension on the extending droplet filament.

Analysis

We analyzed the data for this study using JMP (SAS Institute, Cary, North Carolina) and considered comparisons with $P \leq 0.05$ as significant. Normally distributed values (as confirmed by Shapiro-Wilk W tests having $P \geq 0.05$) were compared using analysis of variance (ANOVA) and t-tests. If the data were not normal, they were log-transformed, and once again tested for normality, and their transformed values then compared using ANOVA tests. The Wilcoxon signed-rank test was used when values were not normally distributed.

ABBREVIATIONS

TLT: Total Loaded Time
PE: Pre-Extension
DE: Droplet Extension

ACKNOWLEDGEMENTS

Carlyle C. Brewster assisted with statistical analyses.

AUTHOR CONTRIBUTIONS

S.D.S. collected and prepared thread samples, performed droplet extensions and image measurements, analyzed data, and prepared the manuscript and figures. B.D.O. designed and constructed the instrumentation used in this study and contributed to data analysis and manuscript and figure preparation. K.G.S. assisted with thread collection, droplet extension, image measurements, and data entry.

COMPETING INTERESTS

No competing interests declared.

FUNDING

Funds from the State Council for Higher Education for Virginia provided the digital camera used in this study.

FIGURES

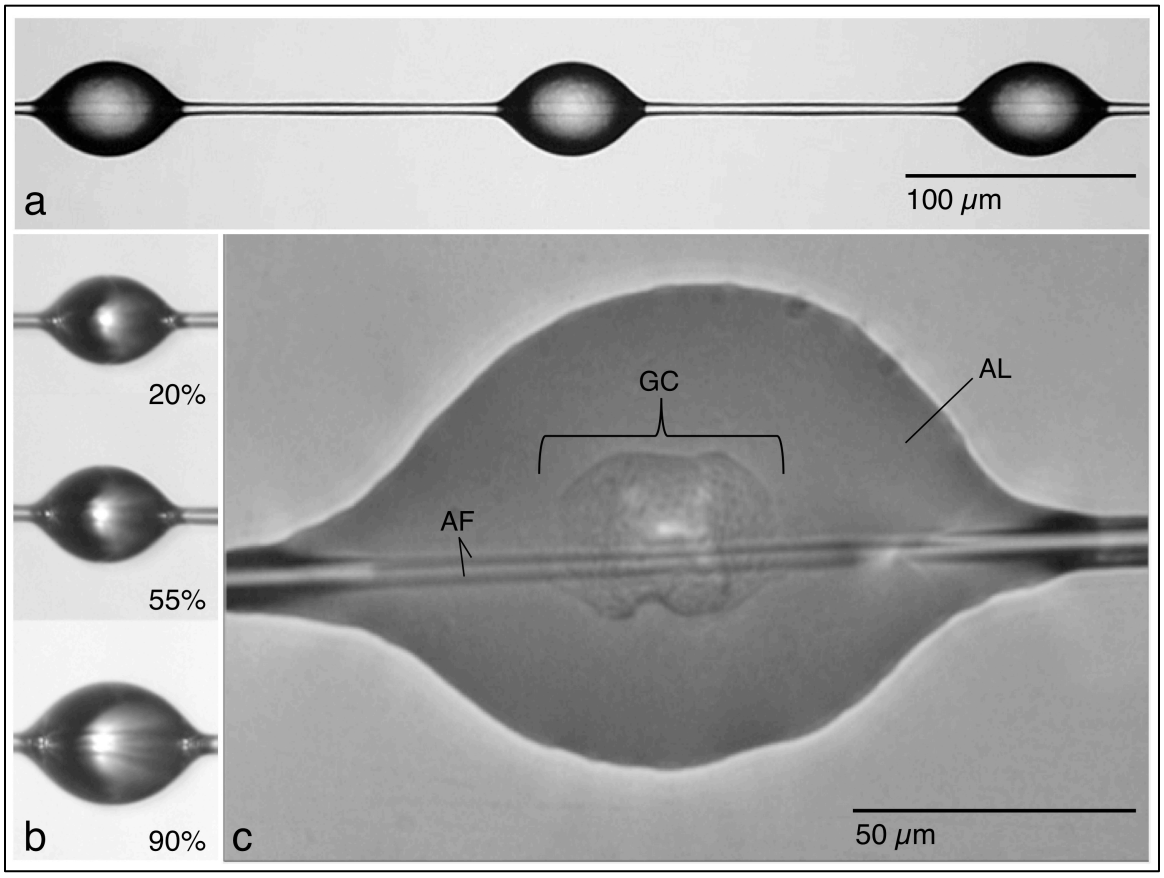

Figure 1. ***Argiope aurantia*** **viscous silk.** Glue droplets (a), a single droplet exposed to increasing humidity, demonstrating the hygroscopic properties of the aqueous material (b), and a flattened droplet showing the pair of supporting axial fibers (AF), outer aqueous layer (AL), and the inner glycoprotein core (GC).

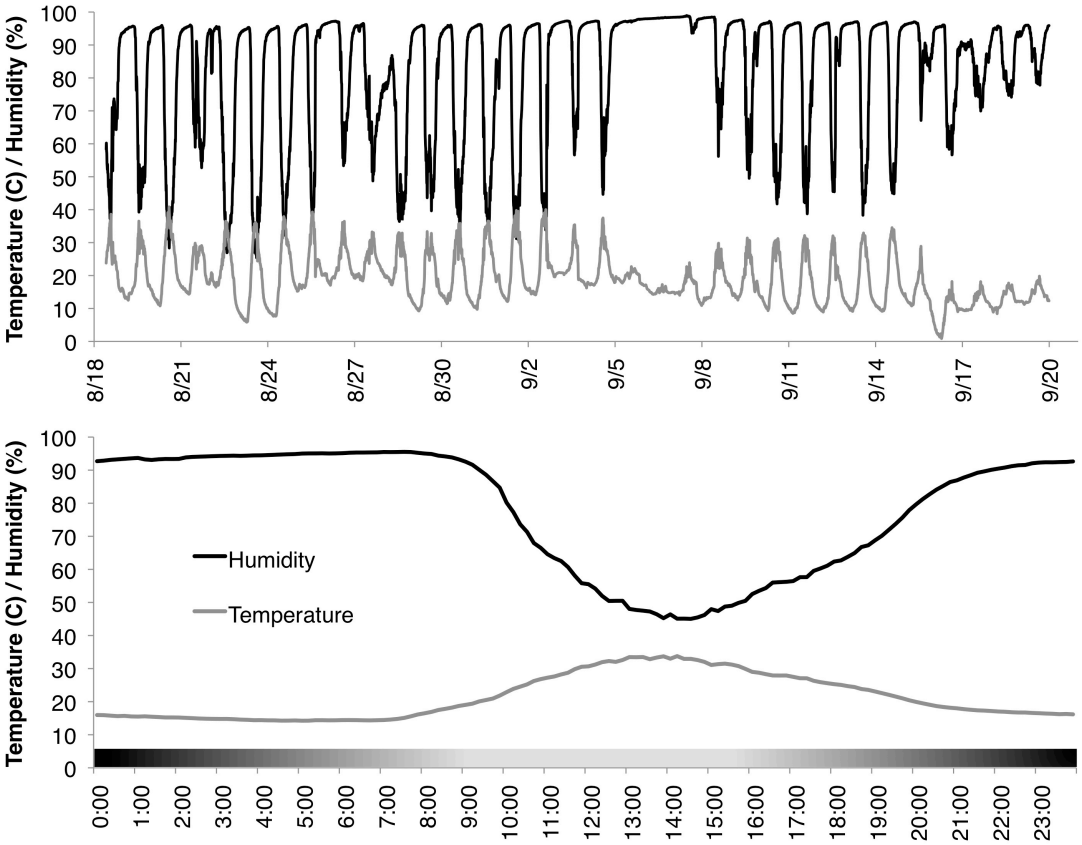

Figure 2. Humidity and temperature changes at the Heritage Park collecting site for *Argiope aurantia.* These data were collected August 18 - September 4, 2011 (a) and averaged over a 24-hour period from August 18 – Sept 6 (b).

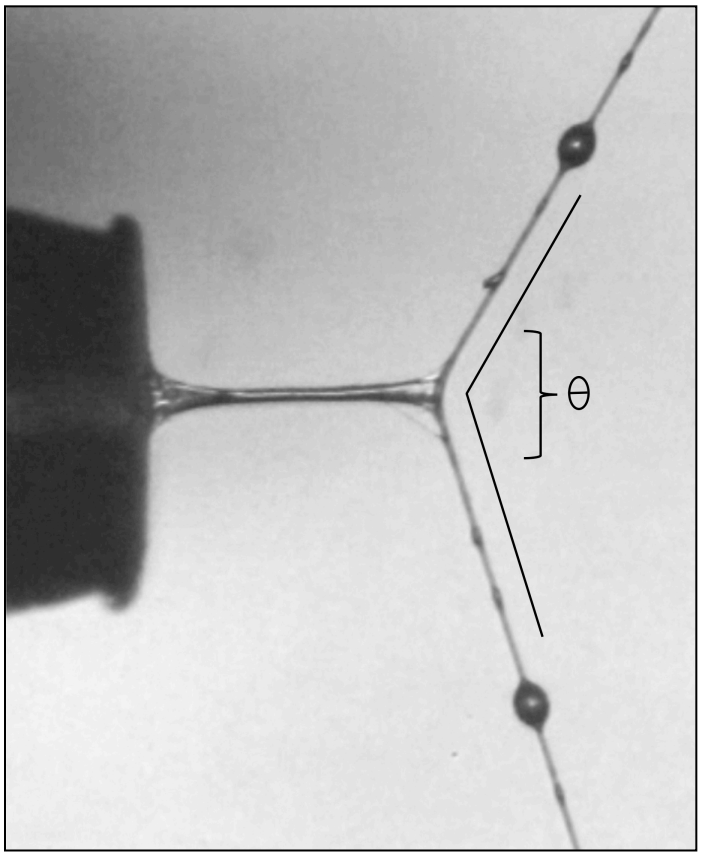

Figure 3. An extending droplet filament showing the angle of axial line deflection (θ).

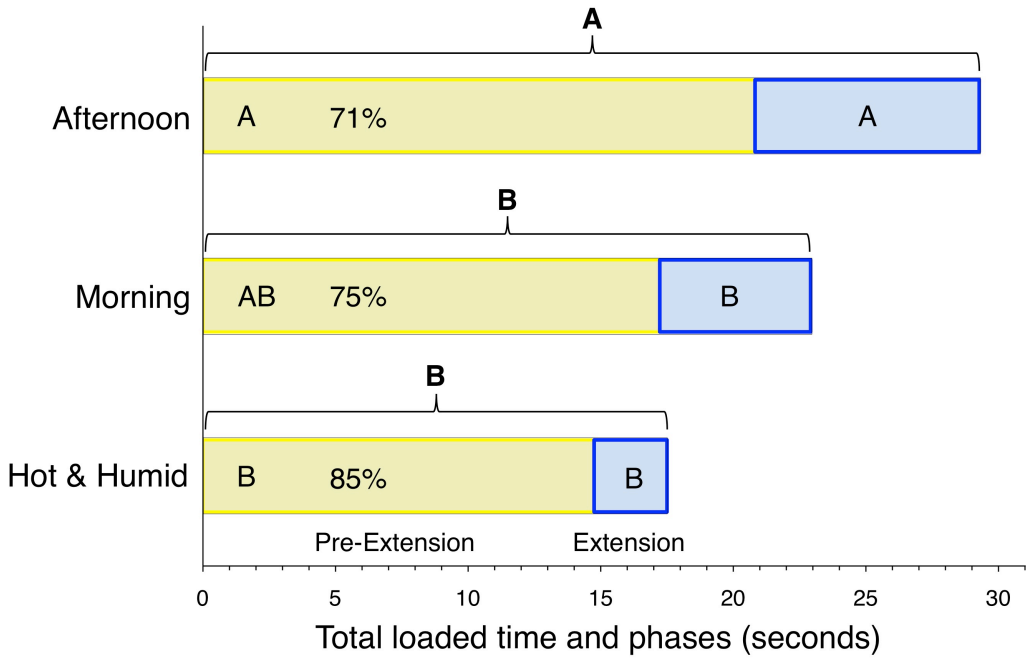

Figure 4. The phases of droplet loading, as indicated by axial line deflection. The pre-extension phase starts when the supporting axial line is 180° and finishes when the droplet begins to extend. The droplet extension phase begins when the droplet starts to extend and ends when the axial line resumes its 180° position. Before being plotted, angle values were subtracted from 180° to indicate an increase in line tension. The area under the curve represents the energy dissipated during droplet extension.

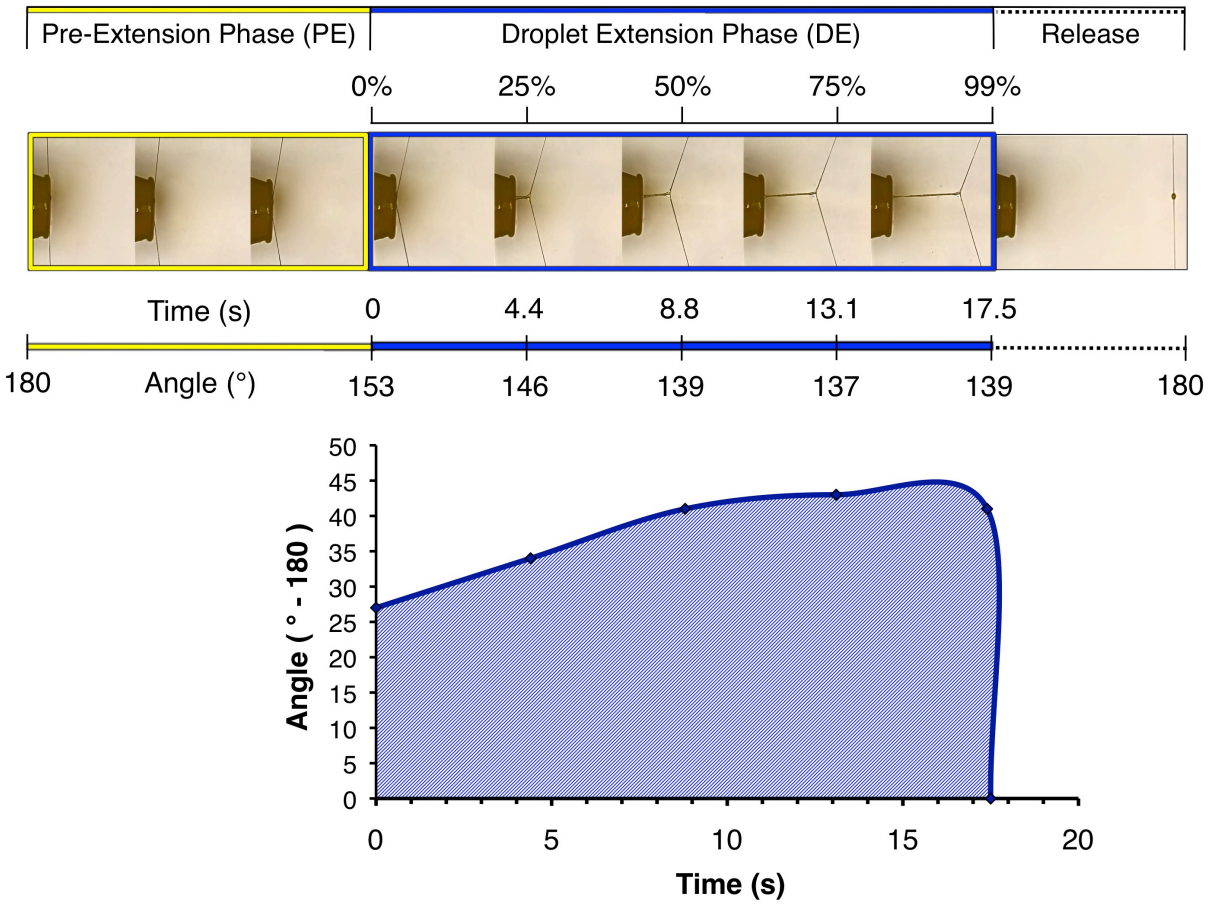

Figure 5. Total loaded time divided into pre-extension (yellow) and extension (blue) phases for the three treatment conditions. Percentages indicate the total loaded time during the pre-extension phase. Letters designate statistical ranking of total loaded time and individual phases, as documented in Table 2.

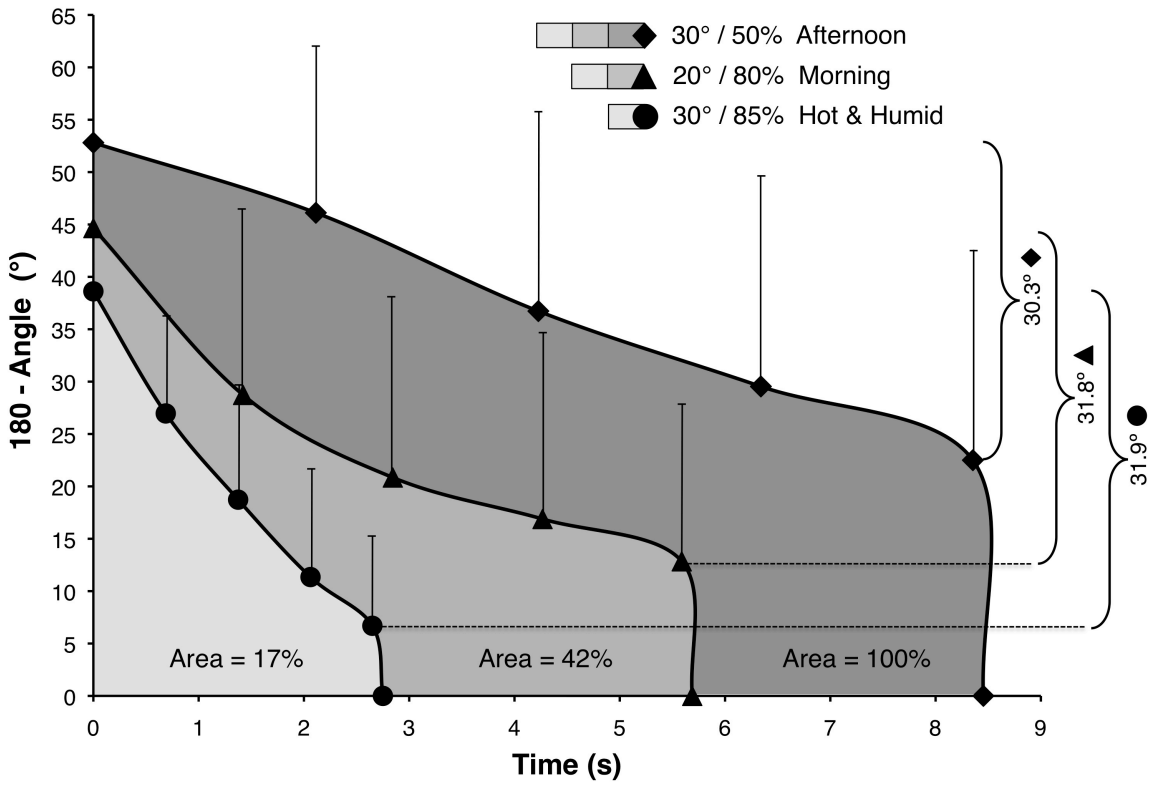

Figure 6. Axial line deflection at 0, 25, 50, 75, 99, and 100% of loaded droplet extension under each experimental condition. The range of values for each condition is shown at the right. As axial line deflection is proportionate to the tension on an extending droplet filament, the area under each curve represents the energy required to extend a droplet. Standard deviations are represented by the upper bars for the three treatments.

REFERENCES

Agnarsson, I. and Blackledge, T. A. (2009). Can a spider web be too sticky? Tensile mechanics constrains the evolution of capture spiral stickiness in orb-weaving spiders. *J. Zool.* **278**, 134-140.

Apstein, C. H. (1889). Bau und Function der Spinnendrusen der Araneida. *Archiv fur Naturgeschichte*, 29.

Betz, O. and Kolsch, G. (2004). The role of adhesion in prey capture and predator defence in arthropods. *Arthropod Struct. Dev.* **33**, 3-30.

Blackledge, T. A. and Zevenbergen, J. M. (2006). Mesh width influences prey retention in spider orb webs. *Ethology* **112**, 1194-1201.

Blackledge, T. A. and Eliason, C. M. (2007). Functionally independent components of prey capture are architecturally constrained in spider orb webs. *Biol. Lett.* **3**, 456-458.

Boys, C. V. (1889). Quartz Fibres. *Nature* **40**, 247-251.

Cambillau, C. (1995). The structural features of protein-carbohydrate interactions revealed by X-ray crystallography. In *Glycoproteins* (ed. J. V. Montreuil, J. F. G. Vliegenthart, and H. Schachter), pp 59-61. New York: Elsevier.

Choresh, O., Bayarmagnai, B. and Lewis, R. V. (2009). Spider Web Glue: Two Proteins Expressed from Opposite Strands of the Same DNA Sequence. *Biomacromolecules* **10**, 2852-2856.

Edmonds, D. and Vollrath, F. (1992). The contribution of atmospheric water vapour to the formation and efficiency of a spider's web. *Pro. R. Soc. Lond.* **248**, 145-148.

Gosline, J. M., DeMont, M. E. and Denny, M. W. (1986). The structure and properties of spider silk. *Endeavour* **10**, 37-43.

Harmer, A. M. T., Blackledge, T. A., Madin, J. S. M. and Herberstein, M. E. (2011). High-performance spider webs: integrating biomechanics, ecology and behaviour. *J. R. Soc. Interface* **8**, 457-471.

Harwood, R. H. (1974). Predatory Behavior of Argiope aurantia (Lucas). *Am. Midl. Nat.* **91**, 130-139.

Kappner, I., Al-Moghrabi, S. M. and Richter, C. (2000). Mucus-net feeding by the vermetid gastropod Dendropoma maxima in coral reefs. *Mar. Ecol. Prog. Ser.* **204**, 309-313.

Kelly, S. P., Sensenig, A., Lorentz, K. A. and Blackledge, T. A. (2011). Damping capacity is evolutionarily conserved in the radial silk of orb-weaving spiders. *Zoology* **114**, 233-238.

Opell, B. D. and Schwend, H. S. (2007). The effect of insect surface features on the adhesion of viscous capture threads spun by orb-weaving spiders. *J. Exp. Biol.* **210**, 2352-2360.

Opell, B. D. and Hendricks, M. L. (2007). Adhesive recruitment by the viscous capture threads of araneoid orb-weaving spiders. *J. Exp. Biol.* **210**, 553-560.

Opell, B. D. and Hendricks, M. L. (2009). The adhesive delivery system of viscous prey capture threads spun by orb-weaving spiders. *J. Exp. Biol.* **212**, 3026-3034.

Opell, B. D., Tran, A. M. and Karinshak, S. E. (2011a). Adhesive compatibility of cribellar and viscous prey capture threads and its implication for the evolution of orb-weaving spiders. *J. Exp. Zool.* **315**, 376–384.

Opell, B. D., Karinshak, S. E. and Sigler, M. A. (2011b). Humidity affects the extensibility of an orb-weaving spider's viscous thread droplets. *J. Exp. Biol.* **214**, 2988-2993.

Opell, B. D., Karinshak, S. E. and Sigler, M. A. (2013). Environmental response and adaptation of glycoprotein glue within the droplets of viscous prey capture threads from araneoid spider orb-webs. *J. Exp. Biol.* **216**, 3023-34.

Opell, B. D., Markley, B. J., Hannum, C. D. and Hendricks, M. L. (2008). The contribution of axial fiber extensibility to the adhesion of viscous capture threads spun by orb-weaving spiders. *J. Exp. Biol.* **211**, 2243-2251.

Plateau, J. (1873). Statique expérimentale et théorique des liquides soumis aux seules forces moléculaires. **1**.

Rayleigh, J. W. S., Baron. (1892). Scientific papers. **3**, 585-596.

Reed, C. F., Witt, P. N. and Scarboro, M. B. (1969). The orb web during the life of *Argiope aurantia* (Lucas). *Dev. Psychobiol.* **2**, 120-129.

Rhodes, J. M. and Ching, C. K. (1993). The Application of Lectins to the Study of Mucosal Glycoproteins. In *Glycoprotein Analysis in Biomedicine* (ed. E. F. Hounsell), pp. 247-262. New York: Humana Press.

Sahni, V., Blackledge, T. A. and Dhinojwala, A. (2010). Viscoelastic solids explain spider web stickiness. *Nat. Commun.* **1**, 1-4.

Sahni, V., Blackledge, T. A. and Dhinojwala, A. (2011). Changes in the Adhesive Properties of Spider Aggregate Glue During the Evolution of Cobwebs. *Sci. Rep.* **1**, 41.

Sekiguchi, K. (1952). On a new splnning gland found in geometric splders and its function. *Annot. Zool. Japonenses* **25**, 394-399.

Sensenig, A., Agnarsson, I. and Blackledge, T. A. (2010). Behavioural and biomaterial coevolution in spider orb webs. *J. Evolution. Biol.* **23**, 1839-1856.

Sensenig, A. T., Lorentz, K. A., Kelly, S. P. and Blackledge, T. A. (2012). Spider orb webs rely on radial threads to absorb prey kinetic energy. *J. R. Soc. Interface*.

Sensenig, A. T., Kelly, S. P., Lorentz, K. A., Lesher, B. and Blackledge, T. A. (2013). Mechanical performance of spider orb webs is tuned for high-speed prey. *J. Exp. Biol.* **216**, 3388-3394.

Tillinghast, E. K., Townley, M. A., Wight, T. N., Uhlenbruck, G. and Janssen, E. (1993). The adhesive glycoprotein of the orb web of *Argiope aurantia* (Araneae, Araneidae). *Mat. Res. Soc. Symp. P.* **292**, 9-23.

Warburton, C. (1890). The spinning apparatus of geometric spiders. *Q. J. Microsc. Sci.* **31**, 29-39.

TABLES

Table 1. Dimensions of suspended droplets for the three treatment groups (n=13 for each treatment; values were log transformed before analysis; mean ± 1 standard deviation).

	Afternoon 30°/50%	**Morning 20°/85%**	**Hot & Humid 30°/85%**	**ANOVA *P* value**
Droplet Volume (5 droplets)				
Droplet Length µm	57.1 ± 11.2	63.5 ± 14.3	63.6 ± 14.3	0.3641
Droplet Width µm	38.0 ± 8.1	42.7 ± 10.6	41.5 ± 10.3	0.4627
Droplet Volume μm^3	40253 ± 28787	57429 ± 43988	54836 ± 39251	0.4524
Droplet Volume (2 extended droplets)				
Droplet Length µm	57.9 ± 14.2	62.6 ± 14.0	61.6 ± 13.2	0.6029
Droplet Width µm	39.3 ± 10.6	42.9 ± 10.3	40.8 ± 8.9	0.6084
Droplet Volume μm^3	45546 ± 40076	57302 ± 44682	49854 ± 34950	0.5874

Table 2. Extension phase times and angle measurements for each of the three treatment group (n=13 for each treatment; mean ± 1 standard deviation).

	Afternoon 30°/50%	**Morning 20°/85%**	**Hot &Humid 30°/85%**	**ANOVA *P* value**
Extension Times (s)				
Total Load (TLT)	29.3 ± 6.7	22.9 ± 8.7	17.5 ± 4.4	0.0001
Student's t	A	B	B	
Pre-Extension (PE)	20.8 ± 5.4	17.2 ± 6.9	14.8 ± 4.0	0.0287
Student's t	A	AB	B	
Extension (DE)	8.5 ± 4.9	5.7 ± 5.8	2.75 ± 1.5	0.0094
Student's t (LOG transformed)	A	B	B	
Axial Line Deflections (°)				
Angle at Time 0	127.2 ± 13.3	135.3 ± 15.9	141.4 ± 9.8	0.0328
Student's t	A	AB	B	
				Wilcoxon *P* value
Angle at 25% (°)	133.9 ± 15.1	151.3 ± 17.6	153.0 ± 9.4	0.0053
Angle at 50% (°)	143.3 ± 18.7	159.2 ± 16.9	161.3 ± 10.4	0.0328
Wilcoxon Each Pair	A	B	B	
Angle at 75% (°)	150.5 ± 20.0	163.1 ± 17.5	168.7 ± 10.2	0.0407
Angle at 99% (°)	157.5 ± 19.5	167.2 ± 15.0	173.3 ± 8.5	0.0671
Wilcoxon Each Pair	A	AB	B	
				ANOVA *P* value
Angular Change ($T_{0\%}$-$T_{99\%}$)	30.3 ± 15.3	31.8 ± 14.8	31.9 ± 9.2	0.9432

3. THE IMPACT OF UVB RADIATION ON THE GLYCOPROTEIN GLUE OF ORB-WEAVING SPIDER CAPTURE THREAD

Sarah D. Stellwagen, Brent D. Opell, Mary E. Clouse

Accepted for publication by Journal of Experimental Biology, June 17, 2015. **In Press.**

Abstract

Many spider orb-webs are exposed to sunlight and the potentially damaging effects of Ultraviolet B (UVB) radiation. We examined the effect of UVB on the viscoelastic glycoprotein core of glue droplets deposited on the prey capture threads of these webs, hypothesizing that webs built by species that occupy sunny habitats are less susceptible to UVB damage than are webs built by species that prefer shaded forest habitats or by nocturnal species. Threads were tested shortly after being collected in the early morning and after being exposed to UVB energy equivalent to a day of summer sun and three times this amount. Droplets kept in a dark chamber allowed us to evaluate post-production changes. Droplet volume was unaffected by treatments, indicating that UVB did not damage the hygroscopic compounds in the aqueous layer that covers droplets. UVB exposure did not affect energies of droplet extension for species from exposed and partially to mostly shaded habitats (*Argiope aurantia*, *Leucauge venusta,* and *Verrucosa arenata*). However, UVB exposure reduced the energy of droplet extension in *Micrathena gracilis* from shaded forests and *Neoscona crucifera,* which forages at night. Only in *L. venusta* did energy of droplet extension increase after the dark treatment, suggesting endogenous molecular alignment. This study adds UVB irradiation to the list of factors (humidity, temperature, and strain rate) known to affect the performance of spider glycoprotein glue, factors that must be more fully understood if adhesives that mimic spider glycoprotein glue are to be produced.

Key Words: Adhesion, Biomaterials, Toughness, Silk, Ultraviolet

** Journal of Experimental Biology requires the Methods section to follow the Discussion.*

INTRODUCTION

Ultraviolet radiation (UVR) introduces free radical oxidative stress to organisms and biological materials, resulting in damaged cellular components including DNA and proteins (Tyrrell, 1995; Osaki and Osaki, 2011; Kaur et al., 2013; Matsuhira et al., 2013). Marine and terrestrial organisms have adapted to prevent and cope with such UVR exposure and damage. These adaptations can be behavioral, such as moving into the shade (Gleason et al., 2006; Ma et al., 2013), physiological, such as absorptive pigmentation like melanin (Singaravelan et al., 2008) and mycosporine-like amino acids (MAAs) (Kuffner, 2002; Hylander and Hansson, 2013), or biochemical such as molecular repair (Carlson and Smith, 1981; Connelly et al., 2009) and antioxidants (Swindells and Rhodes, 2004; Hudelson, 2011).

Some organisms, like the orb-weaving spider *Argiope aurantia* Lucas 1833, remain exposed to full sunlight during the day throughout the late summer and early fall (Harwood, 1974). These spiders produce aerial silk webs to catch and retain flying insects. Their webs consist of radial threads that support a spiral of capture silk, which incorporates adhesive glue droplets (Apstein, 1889; Sekiguchi, 1952; Sahni et al., 2014). Each transparent droplet is composed of an inner sticky, viscoelastic glycoprotein core (Sahni et al., 2010), covered by an aqueous, hygroscopic outer covering that maintains moisture levels (Fig. 1 A-C; Edmonds and Vollrath, 1992). Most species spin webs in the early morning hours, monitor them using a sit-and-wait strategy throughout the day, and recycle their silk when a new web is produced the next day (Reed et al., 1969).

Viscous capture thread originates from a pair of posterior lateral spinnerets on a spider's abdomen. A triad of spigots on each spinneret includes a central spigot that produces the flagelliform supporting axial strand while a pair of surrounding aggregate spigots secretes the glue. The coated strands from each spinneret then join to form a proto viscous thread. The glue first forms a continuous cylinder around the axial fibers, but after rapidly absorbing atmosphe ric moisture, swells to create surface tension that quickly separates the material into droplets (Fig. 1A; Plateau, 1873; Boys, 1889; Rayleigh, 1892; Edmonds and Vollrath, 1992). Each droplet is composed of a glycoprotein core (Opell and Hendricks 2010), which

confers stickiness (Sahni et al., 2010), surrounded by a hygroscopic aqueous layer that also extends into inter-droplet regions (Fig. 1). At the center of the glycoprotein core, a denser region termed a granule can often be seen in transmitted light images of flattened droplets (Opell & Hendricks, 2010). This granule is hypothesized to be a region where the glycoprotein is anchored to the axial lines, causing it to resist forces that would slide a droplet along these lines. The epi-illumination used in subsequent studies to more clearly reveal the outline of a droplet's glycoprotein core (e.g., Opell et al., 2013 and Stellwagen et al., 2014) makes it difficult to visualize these granules independently of the surrounding glycoprotein core within flattened droplets (Fig. 1C).

Inorganic and organic compounds in the hygroscopic aqueous solution are crucial for thread function. They attract atmospheric water, ensuring that both the axial lines and glycoprotein remain hydrated (Opell et al., 2011a, 2013). This maintains axial line supercontraction (Work, 1981; Work and Morosoff, 1982; Shao and Vollrath, 1999; Shao et al., 1999), and glycoprotein extensibility (Sahni et al., 2011; Opell et al., 2013). These compounds also solvate glycoproteins, enhancing their interactions with surfaces that a thread contacts (Sahni et al., 2014). A number of compounds within the aqueous material have been characterized (Townley and Tillinghast, 2013). Small inorganic compounds make up only 10 - 20% of a viscous thread's dry mass, with low molecular mass organic compounds (LMMC) comprising 40-70% (Fischer and Brander, 1960; Anderson and Tillinghast, 1980; Tillinghast and Christenson, 1984; Townley et al., 1991).

Spider thread adhesion has been characterized in two ways: the maximum force registered just before thread pull-off (e.g., Opell and Hendricks, 2009) and the cumulative energy (work) require to pull a thread from a surface (e.g., Sahni et al., 2011). Each index relies on the observation that adhesive forces of multiple droplets are summed as axial lines and droplets elongate under a load, much like the main cable and vertical suspenders effectively bear the load of a suspension bridge deck (Opell and Hendricks, 2007, 2009). Consequently, even modest degradation in performance at the level of individual droplets can result in a large loss of adhesion and energy dissipation as capture threads resist the struggles of an insect. By examining how droplets respond to ultraviolet radiation, we can understand the broader consequences of this potentially damaging environmental factor on the web's adhesive delivery system.

Two environmental factors are known to affect the capture spiral's glycoprotein: relative humidity (RH; Sahni et al., 2011; Opell et al., 2011a) and temperature (Stellwagen et al., 2014). Depending on the species, extensibility (how far a droplet stretches) and adhesion (energy required to pull a droplet from a surface) of the glue may continue to increase as RH approaches 100% (*Neoscona crucifera,* Lucas 1839; Opell et al., 2013), or may function optimally at intermediate levels (55% RH in *A. aurantia* and *Larinioides cornutus* (Clerck 1757); Sahni et al., 2011; Opell et al., 2013) and decrease at lower and higher humidity. Temperature affects the adhesive's viscosity, stiffening the glycoprotein when ambient conditions are cooler and reducing viscosity as temperature increases (Stellwagen et al., 2014). For species like *A. aurantia* that live in exposed habitats, this helps offset the effects of daily humidity oscillations, as low humidity, which increases viscosity, occurs at times of highest temperatures that have the opposite effect.

The effect of ultraviolet radiation, a third and potentially important environmental factor, on the extensibility of viscous droplets has not been examined. As some webs are exposed to full ambient UVR throughout the course of a day, it is possible that the most damaging component, ultraviolet B radiation (UVB, 280-315 nm), also affects droplet performance. Silkworm silk breaking extensibility is reduced by 67% and work reduced by 87% after just one hour of exposure to a combination of UVA and UVB (Aksakal et al., 2015 in press), however, this silk was treated to remove its sericin, a protective, amorphous, antioxidant glycoprotein. Sericin has been shown to block UVR damage in human (Dash et al., 2008) and mouse (Zhaorigetu et al., 2003) keratinocytes and suppress colon carcinogenesis when fed to mice (Sasaki et al., 2000). Historically considered a waste byproduct from silk manufacturing, sericin is now being used in a wide range of applications, including fabrics, biomedicine, and cosmetics (Zhang, 2002). It may be that compounds in the aqueous coating of the viscous droplets of orb-weavers' sticky silk spiral also function to protect the glycoprotein glue from direct or oxidative stress.

Alternatively, droplet performance may improve after exposure to UVR, as UVR induces cross-linking in proteins (Bhat and Karim, 2009; Hu et al., 2013). Non-adhesive spider silk continues to improve mechanically after several hours of natural UVA exposure and at twice the natural UVB exposure, however longer exposures eventually result in degradation (Osaki, 2004; Osaki and Osaki, 2011). Low UV doses may enhance silk

performance by further aligning proteins, similar to the "improvement phase", where molecule alignment is hypothesized to continue after a silk strand is extruded (Agnarsson et al., 2008). Our study included both dark aging and UVB exposure treatments, allowing us to separate and quantify these two effects on the performance of the viscous glue droplets.

Unlike *A. aurantia*, many orb-web spider species, including *Leucauge venusta* (Walckenaer, 1841) and *Verrucosa arenata* (Walckenaer, 1841), build webs in partially shaded areas (Zschokke et al., 2006; Bradley and Hickman, 2009), and others, like *Micrathena gracilis* (Walckenaer, 1805), prefer to construct their webs in shaded woody habitats where only an occasional sun fleck strikes their web (Biere and Uetz, 1981). Nocturnal species like *Neoscona crucifera* (Lucas, 1838) construct their webs a few hours after dusk (Adams, 2000). By investigating the effects of UVB radiation on the viscous glue droplets of these five araneoid orb-weavers (all of them members of the family Araneidae, except *L. venusta*, which is a member of the family Tetragnathidae), we tested the hypothesis that species which build their webs in open, sunny habitats produce droplets that are less susceptible to UVB damage than those which build their webs in more heavily shaded habitats or at night. We did this by measuring the duration of droplet extension and the angle of axial line deflection produced by extending droplets from fresh threads collected in the early morning (or evening in the case of *N. crucifera*) and compared these with measurements from droplets that were aged in the dark, droplets that were exposed for up to four hours to UVB levels typical of midday summer sun, and droplets that received approximately 3 times this amount of UVB exposure

We also photographed each thread droplet prior to extension, which permitted us to compare the effect of UVB on droplet volume. This is a critical part of the study, as LMMC in a droplet's aqueous layer are responsible for the droplet's hygroscopicity, and a droplet's water content affects glycoprotein extensibility (Opell et al., 2013). Inorganic compounds within the aqueous material are probably not susceptible to UVB damage, but the same may not be true for some of the LMMC. Thus, we also tested the hypothesis that UVB exposure affects the droplet volume of one or more study species.

RESULTS

UVB exposure had no clear or systematic effect on droplet volume (Table 1). The only treatment differences we observed were for *L. venusta* (1 hour UVB, mean = 1386.0 ± 748 μm^3 standard deviation; 3 hours UVB, mean = 1237.1 ± 435.7 μm^3; 4 hours dark, mean = 1591.2 ± 803.3 μm^3) and *V. arenata* (1 hour UVB, mean = 9472.4 ± 4684.9 μm^3; 4 hours dark, mean = 9584.5 ± 4244.4 μm^3)**,** where droplet volumes exceeded those of fresh threads. There were no differences for the other hourly treatments, or the extreme treatment for these species.

We brought individual suspended droplets in contact with a probe, then withdrew the probe at a constant rate, and compared the time a thread was under tension while a droplet extended (Fig. 2). The extension times reported in Table 2 provide an index of the extensibility of the glycoprotein within droplets. The hourly UVB irradiated and dark treatments for diurnal species are each presented as an average of the four, one-hour time interval means, as there was no statistical difference between these intervals. *P*-values for these combined averages represent the lowest value of the four comparisons. Values in parentheses next to significant *P*-v alues (in bold) indicate which of the four hourly treatment values differed from fresh threads. In the full sun species, *A. aurantia,* and partially shaded species, *L. venusta* and *V. arenata,* there were few effects of experimental treatments, and the instances of significance did not form a pattern that we considered meaningful. For example, the total loaded time (TLT), the time during which deflection of the axial line indicated tension on a droplet prior to and during extension, for *A. aurantia* after the 2-hour dark treatment was shorter than that of fresh threads (mean = 27.1 ± 8.4 s). However, no differences were seen for the 3 or 4-hour dark treatments, or for any of the normal UVB hourly or extreme treatments. In contrast, for both *M. gracilis* and *N. crucifera,* extreme UVB exposure decreased both TLT and the droplet extension phase (DE), the portion of TLT during which the droplet stretched. In *M. gracilis* there was a 7.1 second (20%) reduction in TLT and a 7.3 second (68%) reduction in DE. *Neoscona crucifera* showed an 11.8 second (23%) decrease in TLT, and a 9.7 second (37%) decrease in DE, while the pre-extension phase (PE) that preceded droplet extension remained relatively stable. Both TLT and DE are significantly shorter for *M. gracilis* after exposure to 3 hours UVB (Table 3), and DE is

significantly shorter after 3 hours dark. However, no differences were found after 4 hours of normal UVB or dark treatments.

Axial line deflection angles (Fig. 2, Appendix A) are an estimation of the force on droplets and were measured just prior to droplet extension (0% DE) and at 25%, 50%, 75%, and 99% of DE. By combining these angles with values for the diameter and Young's modulus of each species' paired axial lines, we computed the force on an extending droplet (Tables 4 & 5). Moderate (one hour) normal UVB exposure increased the force on extending *A. aurantia* droplets, although extreme exposure had a lesser and insignificant effect. This trend was also observed in *L. venusta*, where three-hour normal UVB and two-hour dark treatments increased the force on extending droplets. In contrast, for *M. gracilis*, both three-hour normal and extreme UVB treatments progressively decreased the force during the 50-99% extension intervals, with Extreme exposure having an average of 2.5 times the effect of the mean hourly exposure values. During the 50-99% intervals, the dark treatment reduced the force on *N. crucifera* droplets, and the extreme treatment reduced the force during the 50-99% intervals by an average of 23%, although this difference was not significant.

When the force on an extending droplet is plotted against extension time (Fig. 3) interspecific differences in droplet response to aging and UVB exposure appear. Extreme and combined hourly normal UVB exposures increased the force registered by extending *A. aurantia* droplets more than did the combined hourly dark treatments. Force on *L. venusta* droplets increased after both dark and UVB hourly treatments, but was little affected by the extreme UVB treatment. Neither aging nor UVB exposure had an effect on the performance of *V. arenata* droplets. However, extreme UVB greatly reduced the force registered by *M. gracilis* and slightly reduced that registered by *N. crucifera* droplets. Extreme UVB lengthened the extension times of *A. aurantia* droplets, but reduced the extension times of the other species.

The area under each of the force/extension time curves represents relative toughness and is an index of the energy required to extend a droplet (Fig. 3). The energy absorbed by *L. venusta* increases after 1 hour dark (111%; $P = 0.0440$) and remained higher after 2 hours dark (114%; $P = 0.0272$). *Verrucosa arenata* droplets remained remarkably stable, while energy absorption by *M. gracilis* droplets declined following normal UVB exposure, being reduced by 58% ($P = 0.0107$) after 3 hours UVB and 76% ($P = 0.0205$) after extreme UVB.

Neoscona crucifera droplets exhibited a 45% reduction ($P = 0.0251$) in energy absorption after the extreme UVB treatment.

DISCUSSION

The viscous capture spiral threads of orb-weaving spiders have been selected to retain insects that have intercepted a web (Blackledge and Eliason, 2007). This allows a spider time to locate prey in the web, evaluate the risk associated with its capture, and, finally, subdue it. As a viscous thread sums the adhesion of an estimated 20 droplets via the suspension bridge mechanism (Opell and Hendricks, 2007, 2009), small changes in individual droplet performance can have a large impact on thread performance. Even a few seconds decrease in prey retention time can mean a lost feeding opportunity for an orb-weaving spider (Blackledge and Zevenbergen, 2006). Moreover, the ability of the droplets to absorb the energy of struggling prey is crucial, and can be affected by environmental conditions such as humidity (Sahni et al., 2011; Opell et al., 2011a, 2013) and temperature (Stellwagen et al., 2014). This study demonstrated that, as hypothesized, the droplets of five spider species that ranged from full sun to nocturnal habitats were differentially affected by exposure to UVB radiation.

As gauged by droplet volume, UVB does not appear to impact the LMMC in droplets, supporting another observation that these compounds resist degradation (Opell et al., 2015 in press). Therefore, as all observations were made under the same humidity, any differences in droplet performance can be attributed to the direct effect of UVB on glycoprotein structure and not to changes in glycoprotein hydration mediated by LMMC. These LMMC also contribute more directly to thread adhesion by solvating and softening glycoproteins, and thus facilitate glycoprotein-surface interactions (Sahni et al., 2014). Therefore the stability of droplet volume also suggests that droplet adhesion was also unaffected by UVB exposure.

The viscous droplets of all five species continued to extend even after extreme UVB exposure, although only the performance of *V. arenata* droplets was wholly unaffected by aging or UVB irradiation. Droplets of *M. gracilis*, which are found within forests, and those of the nocturnal *N. crucifera,* exhibited significant reductions in performance after exposure to extreme UVB, with the relative toughness of the former dropping by three-quarters and of

the latter by almost half (Fig. 3). Interestingly, the droplets of *M. gracilis* show both a reduction in force and extension time, whereas those of *N. crucifera* maintain a similar force as fresh threads, but are reduced exclusively in extension time. Thus, our observations support the hypothesis that the glycoprotein within viscous droplets produced by shade dwelling and nocturnal species is more susceptible to UVB damage than species that live in exposed habitats. In contrast, normal and extreme UVB exposure increased the relative toughness of *A. aurantia*, a species found in exposed habitats, by increasing the force on extending droplets after normal UVB exposure, and both increasing force and the duration of droplet extension after extreme exposure. The relative toughness of *L. venusta* droplets, a species preferring partial shade, increased nearly twice as much during the dark treatment as during normal UVB treatments, while being little effected by extreme UVB. This suggests that the performance of *L. venusta* droplets is enhanced by a post-production improvement phase (Agnarsson et al., 2008) and that UVB exposure interferes with or reverses these changes. Additionally, L. *venusta* is a member of the family Tetragnathidae, while all other species used in this study are in the family Araneidae, suggesting phylogenetic differences in glue properties.

Although *N. crucifera* is a nocturnal species, extreme UVB exposure reduces the toughness of its droplets 30% less than it does those of the diurnal species *M. gracilis*. Though unexpected, this may be explained by observations that *Neoscona* species leave their webs up during the day, switching from a night-time monitoring position at the web's hub to a cryptic day-time position in vegetation adjacent to the web (Edwards, 1984). Their forest edge habitat would, thus, leave the webs exposed to UVB, which may explain their higher resistance to UVB than *M. gracilis*, whose webs are rarely exposed to even brief specks of sunlight. By collecting *N. crucifera* web samples in the evening and measuring them the following day, our procedures allowed for at least 10 hours of post-production curing of their threads before our treatments began, making it surprising that further aging during our tests had an apparent, though not a statistically significant, effect.

UVB irradiation mechanically strengthens the dragline silk of several diurnal spider species (Osaki, 2004; Osaki and Osaki, 2011), although the mechanism of change is undocumented. UVB irradiation also increases the viscosity of proteinaceous fish gelatin (Otoni et al., 2012), where it is thought that UVB produces free radicals, which link the

aromatic compounds in these materials (Fujimori, 1965). The capture spiral glycoprotein of *Araneus diadematus* Clerck 1758 includes aromatic amino acids (Andersen, 1970), suggesting that this may contribute to the increased toughness of droplets observed for *A. aurantia* following UVB exposure. However, this information is lacking for the species we studied, making it difficult to assess whether levels of these aromatic compounds could be responsible for observed differences.

Thread performance data exhibited high variance and although matched pair statistics reduced the impact of this variance, it made analysis challenging and probably accounts for such anomalies as the *M. gracilis* TLT fresh value differing from 3 hour but not from 4 hour UVB exposure values. The source of this inter-individual variance may lie in size, nutritional, or reproductive status differences among the mature females that produced the threads we studied. All the webs from which threads were collected appeared normal and did not show signs of spider senescence that has been reported for some orb-weavers (Eberhard, 1971) Differences in temperature and humidity at the time of web construction or thread position in the web may also affect droplets. However, we attempted to account for these issues by controlling room conditions and using threads from the outer 30% of a web.

Our study adds UVB irradiation to the list of factors known to affect the performance of spider glycoprotein glue, which includes humidity (Opell et al., 2011a, 2013), temperature (Stellwagen et al., 2014), and strain rate (Sahni et al., 2011). It is important to more fully understand these effects as material science moves toward producing environmentally non-toxic and energy conservative adhesives inspired by spider thread glycoprotein. Interspecific differences in the performance of viscous droplets in response to both humidity and UVB exposure offer a preview of the range of adhesives that might be modeled after orb-web spider glycoprotein glue. This glue is produced at ambient temperatures, is robust yet biodegradable, and, as this research demonstrates, can be very resistant to damaging UVB. In addition, this glue does not need the additional glandular processing of structural dragline silk, a requirement that has been the major obstruction to making synthetic silks on a commercial scale. Thus, a biomaterial modeled on spider glue may be both easier to produce and, through an understanding of the molecular differences that adapt the glue of different species to their habitats, easier to engineer for a range of applications.

MATERIALS AND METHODS

Study species and thread collection

Thread samples were collected from webs constructed by individual adult females of *A. aurantia* (n=13), *L. venusta* (n=12), *V. arenata* (n=12), and *M. gracilis* (n=12) on and near the Virginia Tech campus in Blacksburg, Montgomery County, VA, USA, from 09 August to 28 September 2013. Each sample was collected between 05:30h and 08:30h and all images and videos captured by 16:00h the same day. *Neoscona crucifera* (n=11) thread samples were collected from 21 August to 31 August 2014 between 21:30h and 23:00h and their study was completed by 16:00h on the following day. Webs from *N. crucifera* were exposed to only the extreme treatment, as hourly data from the diurnal species, collected in the previous year, did not appear useful in resolving the effects of short-term, low-level UVB exposure. A sector of each spider's web was collected on either a 15 x 52 cm aluminum rectangular frame or a 17 cm diameter aluminum ring with a bar across its center. The upper surfaces of these frames and rings were covered with Scotch® double-sided tissue tape (Tape 410M; 3M, St Paul, MN, USA), which adhered to web sectors, maintaining the threads at their native tension. Threads extending from the collecting frame were cut with a scissor to avoid distorting the sample when the frame was withdrawn from the web. We placed web-sampling frames in closed containers for transport to the laboratory. The location of each sampled web was marked with flagging tape to ensure that threads from an individual spider's web was included only once in the study.

To stabilize webs before transferring thread strands to microscope sampler slides, we placed 4 mm wide brass bars that were covered with double-sided carbon tape (product 77816, Electron Microscopy Sciences, Hatfield, PA, USA) across the frame's rim along web radii. This further isolated the web sample and ensured that the tension of viscous threads adjacent to the ones being collected was not altered. We used forceps, which were blocked open to accommodate the separation of the supports on sampler slide, to collect individual viscous threads and transfer them to a microscope slide sampler. Double-sided carbon tape on both the forceps' tips held each thread strand securely when the thread was pulled or burned free using a hot wire probe. Threads were placed on the tops of a sampler's U-shaped

brass struts, which were epoxied at 4.8 mm intervals to microscope slides and covered with double-sided carbon tape (fig. 3 in Opell et al., 2011b).

To ensure that the probe used to extend droplets contacted only a single droplet, we used a minuten insect pin moistened with distilled water to move away droplets that were adjacent to the test droplet located at the center of the thread strand. This process retained the aqueous coating of the strand's axial fibers, as demonstrated by the formation of small droplets similar to those often present between the large primary droplets of many viscous threads. Observations were made at 24°C and 55% RH and were established by turning electric humidifiers on and off, and adjusting the room's thermostat.

UVB Irradiance

A single 14.7 watt, 306 nm spectral peak UVB fluorescent tube (G15T8E; 440.4 mm length, 25.4 mm diameter; USHIO Inc., Cypress, CA, USA) was used to irradiate samples. The lamp hung diagonally from the top interior of a white surfaced ply board cabinet (52.5 x 37 x 48 cm). Airflow through the chamber was maintained by a small fan in the top of the chamber that drew air through three 7.5 cm diameter holes in the cabinet's lower sides and back.

We placed Microscope slide samplers with threads on a black felt covered Styrofoam block, which had a central hole to accommodate the sensor of the UVB meter used to measure thread exposure. Two slides with thread samples were placed on either side of a UVB meter's sensor probe to provide accurate readings of irradiance and cumulative UVB dosage throughout each trial. Irradiance was measured using a Solar Light Co., Inc. PMA2200 photometer radiometer equipped with a UVB detector (PMA2106-WP, Glenside, PA, USA) calibrated traceable to the National Institute of Standards and Technology (NIST) on 29 July 2013 with a spectral sensitivity from 280-320 nm, and peak sensitivity ~312 nm by the manufacturer.

To create a dark treatment cylinder for thread sampler slides, we epoxied two plastic 35 mm film development canisters together to create a 21 cm long, 9 cm diameter cylinder with light baffles at either end that permitted air flow. We placed this cylinder on the floor of the chamber at the same height as the platform on which exposed thread samples rested. The dark treatment cylinder and the UV cabinet maintained ambient room temperature and humidity within a standard deviation of ± 0.13C and ± 1.3% RH, and 0.08C and ± 1.7% RH,

respectively, as recorded every 30 seconds for 2 hours by Hobo® temperature/relative humidity data loggers (model U23-002; Onset Computer Corp., Bourne, MA).

For each of the following ten treatments, we tested two droplets from an individual's web sample: 1: Fresh threads measured immediately after UVB treatments and their controls had begun; 2-5: Threads kept in the dark canister within the UVB chamber for 1, 2, 3 and 4 hours; 6-9: Threads irradiated for 1, 2, 3 and 4 hours of light at ~2.5 W/m^2, a level typical of full sunlight received in this area in late summer from 10:00 to 14:00 and established by placing polyethylene plastic filters above the thread samplers; 10: Threads exposed to an extreme irradiance for 4 hours at ~ 7.5 W/m^2, the maximum level produced by the UVB lamp.

Droplet Extension and Volume

We photographed each isolated test droplet immediately prior to extension. All observations were made within a chamber that held microscope slide samplers and rested on the mechanical stage of a Mitutoyo FS60 inspection microscope (fig. 4 in Opell et al., 2011a). A steel probe was inserted through a port in the side of the test chamber and its 413 μm wide polished tip, previously cleaned with 95% ethanol on a Kimwipe, was aligned and brought into contact with the focal droplet and anchored to a stable mount. To ensure full droplet adhesion, the probe was pressed against the droplet until the thread was deflected by a distance of 500 μm. We then recorded a 60 fps video as the probe was withdrawn from the droplet at a velocity of 69.6 μm s^{-1} by a computer controlled stepping motor connected to the microscope stage's X axis by a flexible belt.

We used ImageJ (Rasband, 1997-2014) to measure droplet length (DL; dimension parallel to the support line) and droplet width (DW), and from these measurements computed droplet volume (DV) using the formula (Opell and Schwend, 2007; Liao et al., 2015):

$$DV = \frac{(2\pi \times DW^2 \times DL)}{15} \quad (1)$$

Droplet extension and axial line angle defection

The total loaded time (TLT) of droplet extension begins when the axial line is deflected from its initial non-loaded, 180° configuration and ends when the droplet returns to a non-loaded condition. We divided TLT into two phases; the pre-extension (PE) phase, during which a

droplet exhibited tensive axial line deflection, but did not extend, thus holding the axial line in contact with the probe, and the droplet extension (DE) phase, which began when a droplet filament started to form and ended when the axial line returned to its 180° configuration at the end of TLT (fig. 4 in Stellwagen et al., 2014). During DE we measured five axial line deflection angles: the angle at the initiation of this filament formation, and the angles at 25%, 50%, 75%, and 99% of the total duration time of DE, using iMovie '11 (Apple Inc., 2010) and ImageJ programs.

Force calculation

We used the diameter and Young's modulus of each species' axial fibers (Table 5) to estimate the force (F_{total}) on a droplet in three computational steps: 1. Determining the extension of the axial lines on either side of an extending droplet, 2. Converting this extension to force, and 3. Summing these force vectors to determine force exerted on a droplet filament (Fig. 4).

Each droplet was located near the center of a 4800 μm long support strand, however the entire thread was not captured in videos. Therefore, we used the supporting line's central deflection angle to calculate the change in length (ΔL) of each side (L_0 = 2400 μm) of the support thread according to the following formulas:

$$L = \frac{2400}{\sin(\theta \times 0.5)} \quad (2),$$

$$\Delta L = L - L_0 \quad (3)$$

Knowing the extensions of either side of the thread that supported a droplet, and the diameters and Young's modulus values for each species axial fibers, we calculated the force on each stretching thread on either side of a droplet (F_1, F_2) using the formula:

$$F_1, F_2 = \frac{EA_0\Delta L}{L_0} \quad (4),$$

where E is Young's Modulus and A_0 is two times the instantaneous cross sectional area of each of a strand's two cylindrical axial fibers. The Young's Moduli used in these calculations are appropriate for extensions less than ~50%, after which strain-hardening of the silk alters the properties of the silk (Sensenig et al., 2010). We calculated the average percent change in length of threads during droplet extension for each treatment to be substantially less than 50% (Appendix B). Instantaneous cross sectional area, which accounts for narrowing of axial fibers as they are stretched, was determined by multiplying reported cross sectional area (Table 5) by the ratio of the initial thread length to the final thread length.

To determine the total force exerted on a droplet filament, the angular deflection of a droplet's support line was again used to sum the force vectors of both sides of the support lines of a droplet, using the formula:

$$F_{total} = 2\cos(\theta \times 0.5)F_1 \quad (5)$$

Toughness or work is the area under a stress-strain curve, and because we generated stress-seconds of extension curves, we term this area under these curves relative toughness. This index of cumulative force on a droplet as it is extended was therefore equated to the area under a treatment's force / extension time plot (Fig. 3). To approximate this index for each treatment, we summed the products of force and DE at each DE interval (0, 25, 50, 75, and 99%), as described in the following formula, where F is the total force on an extending droplet and I is the droplet interval:

$$\frac{\left(F_I + F_{I+1}\right)}{2} \times \left(DE_{I+1} - DE_I\right) \quad (6)$$

Analysis

We used JMP (SAS Institute, Cary, North Carolina) to analyze data and considered comparisons with $P \leq 0.05$ as significant. All observations were normally distributed (as confirmed by Shapiro-Wilk W tests having $P \leq 0.05$). Each treatment value was compared to the fresh thread value, which served as the control. Droplet size and performance was very similar within an individual web sample but showed some inter-individual difference. To

address this we followed a repeated measures design, comparing values with matched pair t-tests. This approach results in any bias in the measurement of fresh droplets affecting each comparison. However, our best gauge of similarity of control and treatment droplets is droplet length and width, which are quite similar (Table 1).

ACKNOWLEDGEMENTS

Carlyle C. Brewster assisted with statistical analyses.

AUTHOR CONTRIBUTIONS

S.D.S. collected and prepared thread samples, performed droplet extensions and image measurements, analyzed data, and prepared the manuscript and figures. B.D.O. designed and constructed the instrumentation used in this study, collected and helped prepare thread samples, and contributed to data analysis, and manuscript and figure preparation. M.E.C. assisted with droplet extension, image measurements, and data entry.

COMPETING INTERESTS

No competing interests declared.

FUNDING

Funds from the State Council for Higher Education for Virginia provided the digital camera used in this study. This study was supported by National Science Foundation grant IOS-1257719.

FIGURES

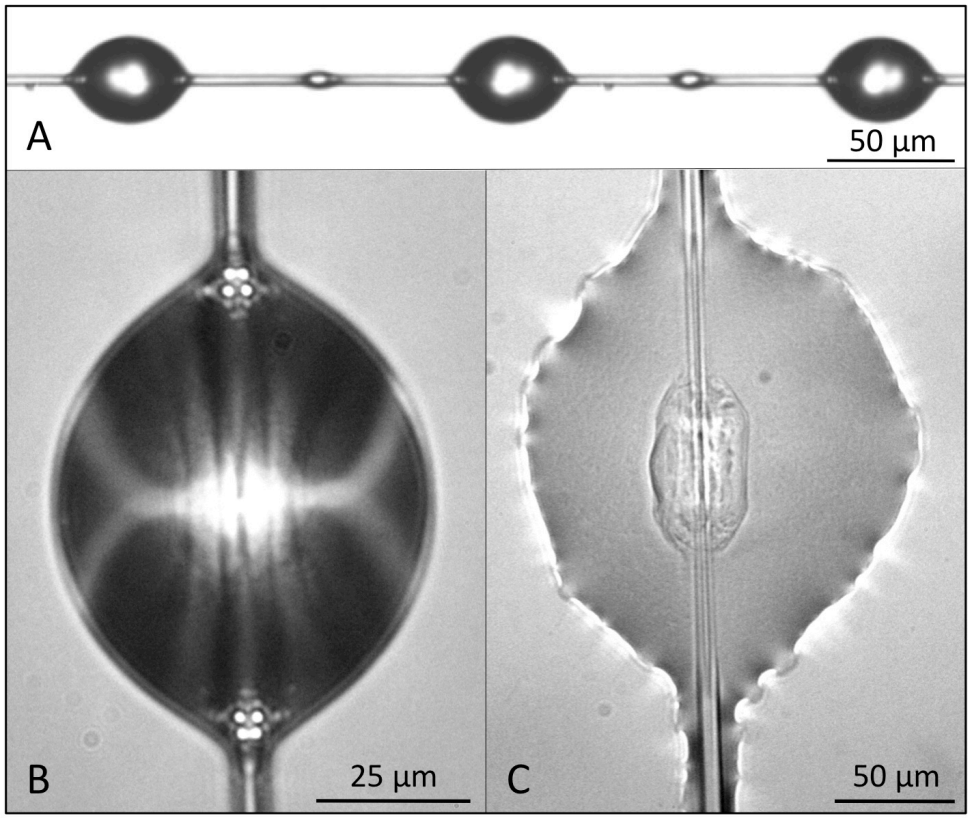

Figure 1: Viscous capture thread and droplets. *Micrathena gracilis* capture thread and droplets (A), a single suspended droplet (B) and a flattened droplet (C) of *Argiope aurantia* as viewed with epi-illumination. The outer aqueous layer and inner glycoprotein core are distinct when a droplet is flattened on a glass slide.

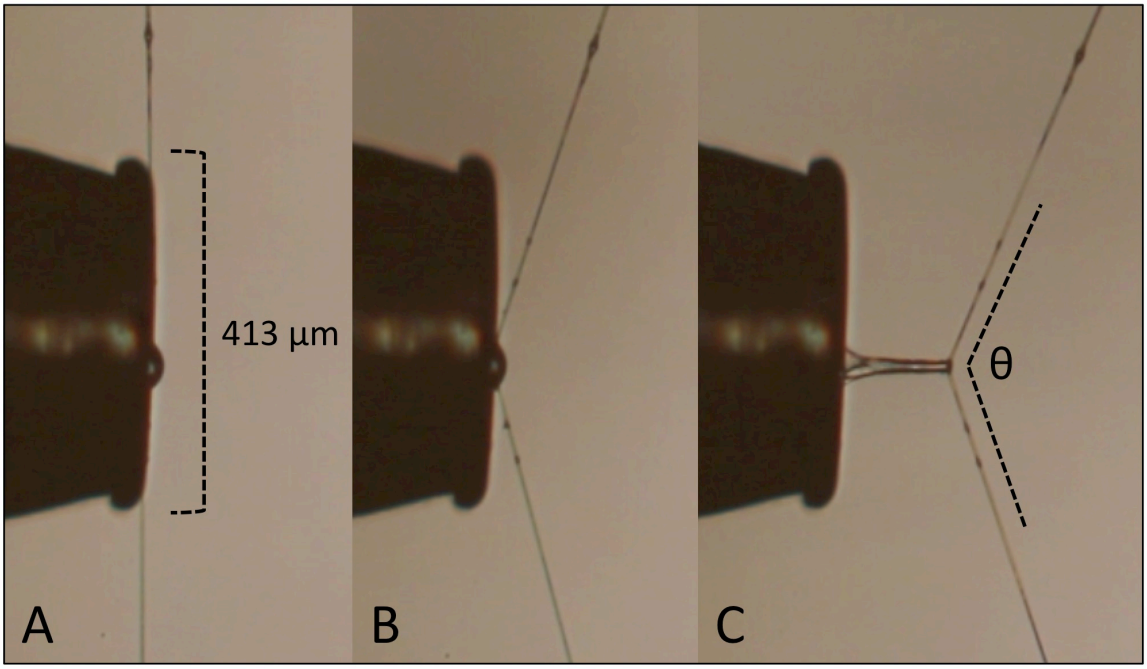

Figure 2. Droplet extension configurations. Droplet in the unloaded (A), pre-extension (B), and extension (C) phases. Angular deflection of the support line corresponds to the force on droplets in pre-extension and extension phases.

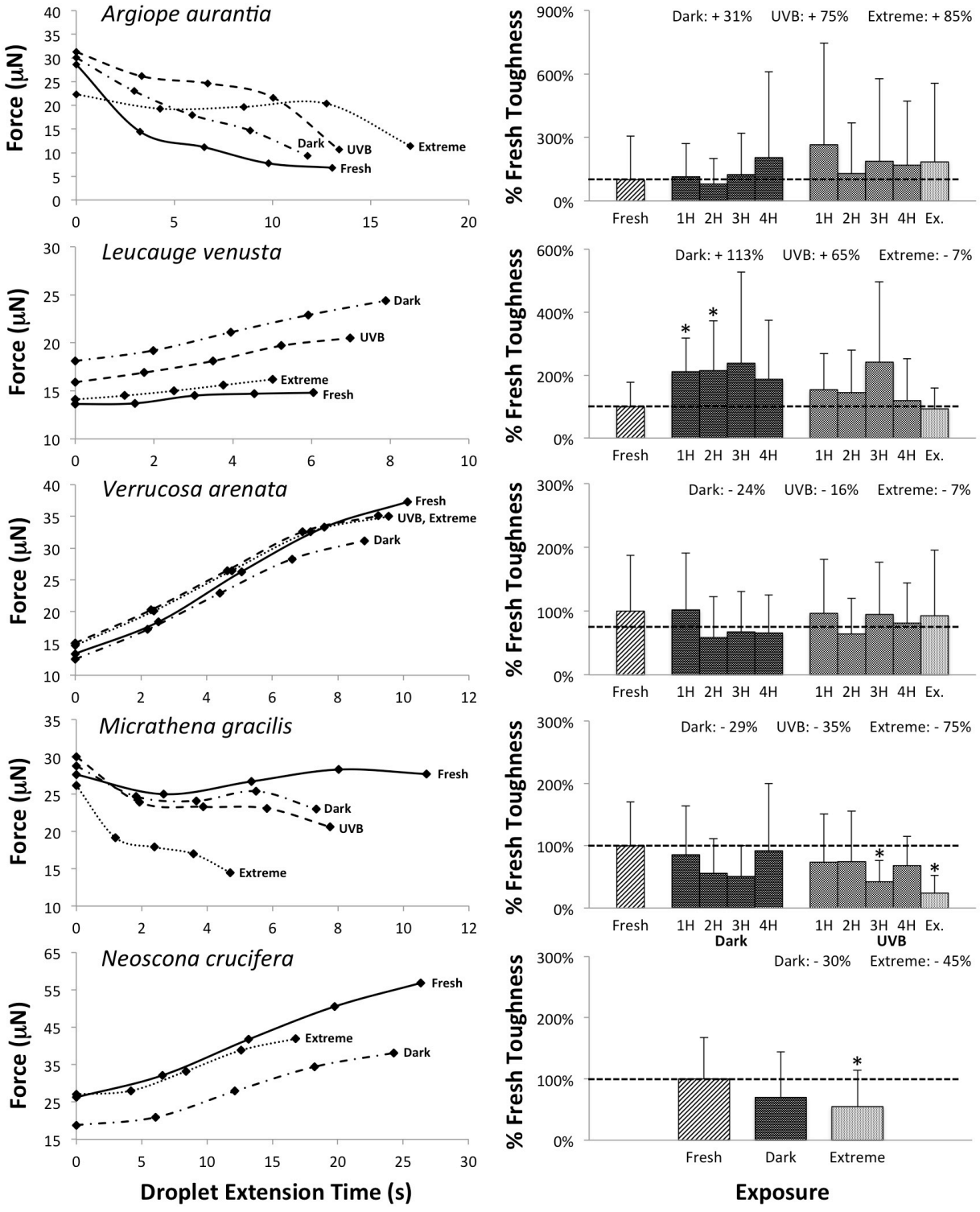

Figure 3. Force / extension time plots for viscous droplets and corresponding histograms of relative toughness for droplets in each treatment, as determined from areas under these curves. Points in force / extension time plots are mean values and are connected by smoothed lines. Relative toughness values are mean ± standard deviation with each significant difference from fresh threads, as determined by matched pair t-tests, being indicated by an asterisk.

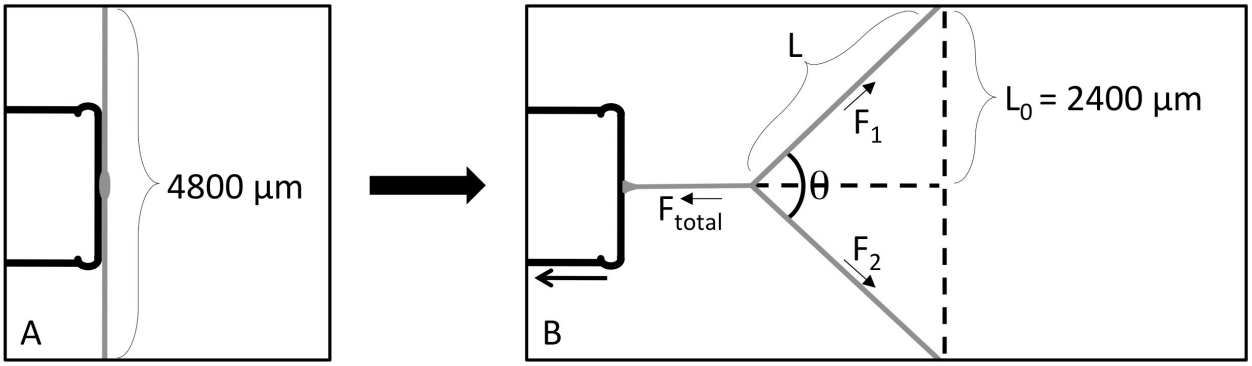

Figure 4. Computing force on an extending droplet from support line deflection. (A) The probe initially contacts the droplet in the center of a 4800 µm long strand of thread, at which point there is no force on the droplet, as indicated the support line's 180° configuration. (B) The droplet has extended as the thread and probe move apart, and the tension on the elongating droplet is visible in the deflection of the support line. Force on the droplet is calculated from the length of one half of a stretching thread (L), the original length of that half-thread (L_0), and the angle of axial deflection (θ). The force vectors of each side of the stretching thread (F_1, F_2), are summed to determine the force on a droplet (F_{total}).

REFERENCES

Adams, M. R. (2000). Choosing Hunting Sites: Web Site Preferences of the Orb Weaver Spider, Neoscona crucifera, Relative to Light Cues. *Journal of Insect Behavior* **13**, 299-305.

Agnarsson, I., Boutry, C. and Blackledge, T. A. (2008). Spider silk aging: initial improvement in a high performance material followed by slow degradation. *Journal of Experimental Zoology, Part A: Ecological Genetics and Physiology* **309A**, 494-504.

Aksakal, B., Koç, K., Yargı, Ö. and Tsobkallo, K. (2015 in press). Effect of UV-light on the uniaxial tensile properties and structure of uncoated and TiO2 coated Bombyx mori silk fibers. *Spectrochimica Acta Part A: Molecular and Biomolecular Spectroscopy*.

Andersen, S. O. (1970). Amino acid composition of spider silks. *Comparative biochemistry and physiology* **35**, 705.

Anderson, C. M. and Tillinghast, E. K. (1980). GABA and taurine derviatives on the adhesive spiral of the orb web of *Argiope* spiders, and their possible behavioral significance. *Physiological Entomology* **5**, 101-106.

Apstein, C. H. (1889). Bau und Function der Spinnendrusen der Araneida. *Archiv fur Natur-geschichte*, 29.

Bhat, R. and Karim, A. A. (2009). Ultraviolet irradiation improves gel strength of fish gelatin. *Food Chemistry* **113**, 1160-1164.

Biere, J. M. and Uetz, G. W. (1981). Web Orientation in the Spider Micrathena Gracilis (Araneae: Araneidae). *Ecology* **62**, 336-344.

Blackledge, T. A. and Zevenbergen, J. M. (2006). Mesh width influences prey retention in spider orb webs. *Ethology* **112**, 1194-1201.

Blackledge, T. A. and Eliason, C. M. (2007). Functionally independent components of prey capture are architecturally constrained in spider orb webs. *Biol. Lett.* **3**, 456-458.

Boys, C. V. (1889). Quartz Fibres. *Nature* **40**, 247-251.

Bradley, R. A. and Hickman, W. L. (2009). Spiders (Araneae) of the Glen Helen Nature Preserve, Green County, OH. . *The Ohio Journal of Science* **18**, 1-27.

Carlson, K. M. and Smith, K. C. (1981). Effect of the uvrD3 mutation on ultraviolet radiation-induced DNA-repair replication in Escherichia coli K12. *Mutation Research/Fundamental and Molecular Mechanisms of Mutagenesis* **84**, 257-262.

Connelly, S. J., Moeller, R. E., Sanchez, G. and Mitchell, D. L. (2009). Temperature Effects on Survival and DNA Repair in Four Freshwater cladoceran Daphnia Species Exposed to UV Radiation. *Photochemistry and Photobiology* **85**, 144-152.

Eberhard, W. G. (1971). Senile web patterns in *Uloborus diversus* (Araneae: Uloboridae). *Developmental Psychobiology* **4**, 249-254.

Edmonds, D. and Vollrath, F. (1992). The contribution of atmospheric water vapour to the formation and efficiency of a spider's web. *Proceedings of the Royal Society of London* **248**, 145-148.

Edwards, G. B. (1984). Large Florida orb-weavers of the genus Neoscona. *Entomology Circular, Florida Department of Agriculture and Consumer Services* **266**, 1-2.

Fischer, F. G. and Brander, J. (1960). Eine Analyse der Gespinste der Kreuzspinne. *Hoppe-Seylers's Zeitschrift fur Physiologische Chemie* **320**, 92-102.

Fujimori, E. (1965). Ultraviolet light-induced change in collagen macromolecules. *Biopolymers* **3**, 115-119.

Gleason, D., Edmunds, P. and Gates, R. (2006). Ultraviolet radiation effects on the behavior and recruitment of larvae from the reef coral Porites astreoides. *Marine Biology* **148**, 503-512.

Harwood, R. H. (1974). Predatory Behavior of *Argiope aurantia* (Lucas). *American Midland Naturalist* **91**, 130-139.

Hu, X., Raja, W. K., An, B., Tokareva, O., Cebe, P. and Kaplan, D. L. (2013). Stability of Silk and Collagen Protein Materials in Space. *Sci. Rep.* **3**.

Hudelson, K. (2011). Ultraviolet radiation tolerance in high elevation copepods from the Rocky Mountains of Colorado, USA, vol. 1520436, pp. 70. Ann Arbor: University of North Texas.

Hylander, S. and Hansson, L.-A. (2013). Vertical distribution and pigmentation of Antarctic zooplankton determined by a blend of UV radiation, predation and food availability. *Aquat Ecol* **47**, 467-480.

Kaur, J., Rajkhowa, R., Tsuzuki, T., Millington, K., Zhang, J. and Wang, X. (2013). Photoprotection by Silk Cocoons. *Biomacromolecules* **14**, 3660-3667.

Kuffner, I. B. (2002). Effects of ultraviolet radiation and water motion on the reef coral, *Porites compressa* Dana: a transplantation experiment. *Journal of Experimental Marine Biology and Ecology* **270**, 147-169.

Liao, C.-P., Blamires, S. J., Hendricks, M. L. and Opell, B. D. (2015). A re-evaluation of the formula to estimate the volume of orb web glue droplets. *Journal of Arachnology* **43**, 97-100.

Ma, Z., Li, W., Shen, A. and Gao, K. (2013). Behavioral responses of zooplankton to solar radiation changes: in situ evidence. *Hydrobiologia* **711**, 155-163.

Matsuhira, T., Yamamoto, K. and Osaki, S. (2013). Effects of UV irradiation on the molecular weight of spider silk. *Polym J* **45**, 1167-1169.

Opell, B. D. and Schwend, H. S. (2007). The effect of insect surface features on the adhesion of viscous capture threads spun by orb-weaving spiders. *Journal of Experimental Biology* **210**, 2352-2360.

Opell, B. D. and Hendricks, M. L. (2007). Adhesive recruitment by the viscous capture threads of araneoid orb-weaving spiders. *Journal of Experimental Biology* **210**, 553-560.

Opell, B. D. and Hendricks, M. L. (2009). The adhesive delivery system of viscous prey capture threads spun by orb-weaving spiders. *Journal of Experimental Biology* **212**, 3026-3034.

Opell, B. D. and Hendricks, M. l. (2010). The role of granules within viscous capture threads of orb-weaving spiders. *Journal of Experimental Biology* **213**, 339-346.

Opell, B. D., Karinshak, S. E. and Sigler, M. A. (2011a). Humidity affects the extensibility of an orb-weaving spider's viscous thread droplets. *Journal of Experimental Biology* **214**, 2988-2993.

Opell, B. D., Tran, A. M. and Karinshak, S. E. (2011b). Adhesive compatibility of cribellar and viscous prey capture threads and its implication for the evolution of orb-weaving spiders. *Journal of Experimental Zoology Part A: Ecological Genetics and Physiology* **315A**, 376-384.

Opell, B. D., Karinshak, S. E. and Sigler, M. A. (2013). Environmental response and adaptation of glycoprotein glue within the droplets of viscous prey capture threads from araneoid spider orb-webs. *Journal of Experimental Biology* **216**, 3023-3034.

Opell, B. D., Andrews, S. F., Karinshak, S. E. and Sigler, M. A. (2015 in press). The stability of hygroscopic compounds in orb-web spider viscous thread. *Journal of Arachnology* **43**.

Osaki, S. (2004). Ultraviolet Rays Mechanically Strengthen Spider's Silks. *Polymer Journal* **36**, 657-660.

Osaki, S. and Osaki, M. (2011). Evolution of spiders from nocturnal to diurnal gave spider silks mechanical resistance against UV irradiation. *Polymer Journal* **43**, 200-204.

Otoni, C. G., Avena-Bustillos, R. J., Chiou, B.-S., Bilbao-Sainz, C., Bechtel, P. J. and McHugh, T. H. (2012). Ultraviolet-B Radiation Induced Cross-linking Improves Physical Properties of Cold- and Warm-Water Fish Gelatin Gels and Films. *Journal of Food Science* **77**, E215-E223.

Plateau, J. (1873). Statique expérimentale et théorique des liquides soumis aux seules forces moléculaires. **1**: Gauthier-Villars.

Rayleigh, J. W. S., Baron. (1892). Scientific papers. **3**, 585-596.

Reed, C. F., Witt, P. N. and Scarboro, M. B. (1969). The orb web during the life of *Argiope aurantia*. *Developmental Psychobiology* **2**, 120-129.

Sahni, V., Blackledge, T. A. and Dhinojwala, A. (2010). Viscoelastic solids explain spider web stickiness. *Nature Communications* **1**, 1-4.

Sahni, V., Blackledge, T. A. and Dhinojwala, A. (2011). Changes in the Adhesive Properties of Spider Aggregate Glue During the Evolution of Cobwebs. *Scientific Reports* **1**, 41.

Sahni, V., Dhinojwala, A., Opell, B. and Blackledge, T. (2014). Prey Capture Adhesives Produced by Orb-Weaving Spiders. In *Biotechnology of Silk*, vol. 5 (eds. T. Asakura and T. Miller), pp. 203-217: Springer Netherlands.

Sekiguchi, K. (1952). On a new spinning gland found in geometric spiders and its function. *Annot Zool Japonenses* **25**, 394-399.

Sensenig, A., Agnarsson, I. and Blackledge, T. A. (2010). Behavioural and biomaterial coevolution in spider orb webs. *Journal of Evolutionary Biology* **23**, 1839-1856.

Shao, Z. and Vollrath, F. (1999). The effect of solvents on the contraction and mechanical properties of spider silk. *Polymer* **40**, 1799-1806.

Shao, Z., Vollrath, F., Sirichaisit, J. and Young, R. J. (1999). Analysis of spider silk in native and supercontracted states using Raman spectroscopy. *Polymer* **40**, 2493-2500.

Singaravelan, N., Grishkan, I., Beharav, A., Wakamatsu, K., Ito, S. and Nevo, E. (2008). Adaptive Melanin Response of the Soil Fungus *Aspergillus niger* to UV Radiation Stress at "Evolution Canyon", Mount Carmel, Israel. *PLoS ONE* **3**, e2993.

Stellwagen, S. D., Opell, B. D. and Short, K. G. (2014). Temperature mediates the effect of humidity on the viscoelasticity of glycoprotein glue within the droplets of an orb-weaving spider's prey capture threads. *Journal of Experimental Biology* **217**, 1563-1569.

Swindells, K. and Rhodes, L. E. (2004). Influence of oral antioxidants on ultraviolet radiation-induced skin damage in humans. *Photodermatology, Photoimmunology & Photomedicine* **20**, 297-304.

Tillinghast, E. K. and Christenson, T. (1984). Observations on the Chemical Composition of the Web of *Nephila clavipes* (Araneae, Araneidae). *Journal of Arachnology* **12**, 69-74.

Townley, M. and Tillinghast, E. (2013). Aggregate Silk Gland Secretions of Araneoid Spiders. In *Spider Ecophysiology*, (ed. W. Nentwig), pp. 283-302: Springer Berlin Heidelberg.

Townley, M. A., Bernstein, D. T., Gallagher, K. S. and Tillinghast, E. K. (1991). Comparative study of orb-web hygroscopicity and adhesive spiral composition in three araneid spiders. *Journal of Experimental Zoology* **259**, 154-165.

Tyrrell, R. M. (1995). Ultraviolet radiation and free radical damage to skin. *Biochemical Society Symposia* **61**, 47-53.

Work, R. W. (1981). A Comparative Study of the Supercontraction of Major Ampullate Silk Fibers of Orb-Web-Building Spiders (Araneae). *Journal of Arachnology* **9**, 299-308.

Work, R. W. and Morosoff, N. (1982). A physico-chemical study of the supercontraction of spider major ampullate silk fibers. *Textile Research Journal* **52**, 349-356.

Zschokke, S., Hénaut, Y., Benjamin, S. P. and García-Ballinas, J. A. (2006). Prey-capture strategies in sympatric web-building spiders. *Canadian Journal of Zoology* **84**, 964-973.

TABLES

Table 1: Dimensions of suspended droplets for all species and treatment groups. Significant *P*-values (<0.05) are in bold. Presented for the Normal UVB and Dark treatments are means obtained by averaging four, one-hour incremental treatment means (due to limited resolution). Individual comparisons were performed for these hourly treatments, and *P*-values presented are the lowest of the four comparisons; parenthesized values indicate which of the four hourly comparisons was significant, if applicable.

	Length μm	**Width** μm	**Volume** μm^3	**Matched Pair (Volume)**
A. aurantia				
Fresh	69.8 ± 9.7	52.4 ± 7.9	85409.4 ± 37734.7	
Dark	68.9 ± 13.5	54.2 ± 10.3	92922.9 ± 46753.4	$P \geq 0.0974$
Normal UVB	68.0 ± 12.6	53.1 ± 10.2	89481.4 ± 48948.9	$P \geq 0.3362$
Extreme UVB	65.0 ± 11.9	51.4 ± 9.4	79265.5 ± 40847.8	$P = 0.7462$
L. venusta				
Fresh	14.8 ± 2.0	12.6 ± 1.3	1030.0 ± 345.3	
Dark	15.4 ± 3.1	13.4 ± 2.8	1342.0 ± 859.2	**$P \geq 0.0043$ (4)**
Normal UVB	15.1 ± 2.5	13.4 ± 2.2	1257.6 ± 608.3	**$P \geq 0.0262, 0.0262$ (1, 3)**
Extreme UVB	14.8 ± 2.7	13.2 ± 2.3	1207.5 ± 664.8	$P = 0.3121$
V. arenata				
Fresh	29.4 ± 4.1	24.6 ± 3.6	8037.3 ± 3787.2	
Dark	30.3 ± 5.0	25.6 ± 3.8	9013.2 ± 4410.4	**$P \geq 0.0258$ (4)**
Normal UVB	30.4 ± 4.3	25.7 ± 3.5	9128.0 ± 3800.2	**$P \geq 0.0237$ (1)**
Extreme UVB	30.5 ± 4.6	25.9 ± 4.0	9214.9 ± 4139.6	$P = 0.1403$
M. gracilis				
Fresh	29.0 ± 3.3	24.2 ± 2.8	7429.2 ± 2852.6	
Dark	28.9 ± 3.9	24.5 ± 3.4	7725.4 ± 3419.5	$P \geq 0.1827$
Normal UVB	28.9 ± 3.6	24.5 ± 3.2	7688.4 ± 3048.8	$P \geq 0.1320$
Extreme UVB	27.5 ± 2.9	23.0 ± 2.7	6438.3 ± 2169.3	$P = 0.8763$
N. crucifera				
Fresh	32.6 ± 9.6	24.0 ± 7.3	10070.0 ± 8452.2	
Dark	31.3 ± 9.8	22.8 ± 7.2	8815.2 ± 6337.2	$P = 0.3682$
Extreme UVB	31.1 ± 9.4	22.3 ± 6.5	7992.8 ± 5650.0	$P = 0.2828$

Table 2: Extension phase times (seconds) for all species and treatments (mean ± 1 standard deviation). Significant *P*-values (<0.05) are in bold. Presented for the Normal UVB and Dark treatments are means obtained by averaging four, one-hour incremental treatment means (due to limited resolution). Individual comparisons were performed for these hourly treatments, and *P*-values presented are the lowest of the four comparisons; parenthesized values indicate which of the four hourly comparisons was significant, if applicable.

	Total Loaded Time	Matched Pair TLT	Pre-Extension	Matched Pair PE	Droplet Extension	Matched Pair DE
A. aurantia						
Fresh	30.7 ± 8.5		17.6 ± 6.4		13.1 ± 6.9	
Dark	29.5 ± 8.9	**P ≥ 0.0243 (2)**	17.4 ± 7.5	P ≥ 0.5492	11.8 ± 4.5	P ≥ 0.1088
Normal UVB	30.4 ± 10.5	P ≥ 0.4645	17.0 ± 9.0	P ≥ 0.2539	13.4 ± 5.5	P ≥ 0.8561
Extreme UVB	32.1 ± 7.7	P = 0.6780	15.1 ± 7.2	P = 0.1856	17.0 ± 6.3	P = 0.0781
L. venusta						
Fresh	31.0 ± 7.6		24.9 ± 7.8		6.1 ± 3.4	
Dark	36.5 ± 8.2	**P ≥ 0.0331(2)**	28.6 ± 7.4	P ≥ 0.1828	7.9 ± 5.2	P ≥ 0.1396
Normal UVB	33.6 ± 7.2	**P ≥ 0.0463 (3)**	26.6 ± 6.2	**P ≥ 0.0352 (3)**	7.0 ± 5.3	P ≥ 0.2748
Extreme UVB	30.3 ± 5.8	P = 0.7980	25.3 ± 5.1	P = 0.8805	5.0 ± 2.6	P = 0.3600
V. arenata						
Fresh	22.1 ± 7.5		12.0 ± 2.9		10.1 ± 5.1	
Dark	21.1 ± 6.7	P ≥ 0.4037	12.3 ± 3.7	P ≥ 0.4037	8.8 ± 4.1	P ≥ 0.1375
Normal UVB	22.2 ± 3.3	P ≥ 0.4743	13.0 ± 1.9	P ≥ 0.1161	9.2 ± 2.2	P ≥ 0.3272
Extreme UVB	22.9 ± 6.1	P = 0.7786	13.3 ± 2.3	P = 0.8257	9.6 ± 5.0	P = 0.4143
M. gracilis						
Fresh	36.3 ± 8.3		25.6 ± 6.7		10.7 ± 6.0	
Dark	32.5 ± 8.5	P ≥ 0.0557	25.7 ± 6.9	P ≥ 0.2024	6.7 ± 5.6	**P ≥ 0.0413 (3)**
Normal UVB	33.9 ± 8.4	**P ≥ 0.0209 (3)**	26.2 ± 7.7	P ≥ 0.1691	7.7 ± 5.2	**P ≥ 0.0397 (3)**
Extreme UVB	29.2 ± 5.1	**P = 0.0011**	25.8 ± 5.3	P = 0.9698	3.4 ± 3.2	**P = 0.0087**
N. crucifera						
Fresh	51.8 ± 13.4		25.4 ± 7.3		26.3 ± 11.3	
Dark	45.7 ± 17.9	P = 0.1803	21.4 ± 6.5	P = 0.0892	24.3 ± 15.5	P = 0.5325
Extreme UVB	40.5 ± 18.1	**P = 0.0061**	23.9 ± 9.1	P = 0.4551	16.6 ± 13.7	**P = 0.0024**

Table 3: *M. gracilis* extension phase times (seconds) for all treatments (mean ± 1 standard deviation). Significant *P*-values (<0.05) are in bold.

	TLT (s)	Matched Pair TLT	PE (s)	Matched Pair PE	DE (s)	Matched Pair DE
Fresh	36.3 ± 8.3		25.6 ± 6.7		10.7 ± 6.0	
Dark						
1 Hour	30.9 ± 8.1	P = 0.0845	22.7 ± 3.7	P = 0.2024	8.2 ± 7.3	P = 0.3628
2 Hours	31.7 ± 8.7	P = 0.2088	25.7 ± 8.2	P = 0.9896	6.0 ± 4.8	P = 0.0557
3 Hours	31.5 ± 7.2	P = 0.0557	25.4 ± 5.5	P = 0.8962	6.1 ± 3.8	**P = 0.0431**
4 Hours	35.7 ± 10.0	P = 0.8411	29.1 ± 8.2	P = 0.3028	6.6 ± 6.2	P = 0.1219
Normal UVB						
1 Hour	32.8 ± 7.5	P = 0.3411	24.0 ± 5.7	P = 0.5666	8.7 ± 4.8	P = 0.3879
2 Hours	35.9 ± 9.2	P = 0.9025	27.3 ± 9.4	P = 0.6117	8.6 ± 6.0	P = 0.3095
3 Hours	30.0 ± 8.4	**P = 0.0209**	23.5 ± 6.2	P = 0.2950	6.5 ± 4.3	**P = 0.0397**
4 Hours	36.8 ± 7.9	P = 0.8883	29.8 ± 8.2	P = 0.9698	7.0 ± 5.7	P = 0.1659
Extreme UVB	29.2 ± 5.1	**P = 0.0011**	25.8 ± 5.3	P = 0.9698	3.4 ± 3.2	**P = 0.0087**

Table 4: Force calculations (μN) at 0, 25, 50, 75, and 99% of the droplet extension time for all species and treatment groups (mean ± 1 standard deviation). Significant *P*-values (<0.05) are in bold. Presented for the Normal UVB and Dark treatments are means obtained by averaging four, one-hour incremental treatment means (due to limited resolution). Individual comparisons were performed for these hourly treatments, and *P*-values presented are the lowest of the four comparisons; parenthesized values indicate which of the four hourly comparisons was significant, if applicable.

	Force 0%	Matched Pair 0%	Force 25%	Matched Pair 25%	Force 50%	Matched Pair 50%	Force 75%	Matched Pair 75%	Force 99%	Matched Pair 99%
A. aurantia										
Fresh	28.7 ± 25.5		14.4 ± 19.2		11.2 ± 20.5		7.8 ± 21.9		6.8 ± 22.9	
Dark	30.1 ± 31.6	$P \geq 0.6585$	23.2 ± 34.8	$P \geq 0.0944$	18.1 ± 36.1	$P \geq 0.1774$	14.9 ± 33.4	$P \geq 0.1007$	9.4 ± 28.8	$P \geq 0.2626$
Normal UVB	31.1 ± 36.0	$P \geq 0.3770$	26.0 ± 38.9	**$P \geq 0.0090$ (1)**	24.6 ± 43.7	**$P \geq 0.0312$ (1)**	19.6 ± 40.2	**$P \geq 0.0346$ (1)**	10.5 ± 31.1	**$P \geq 0.0134$ (1)**
Extreme UVB	22.3 ± 25.2	$P = 0.2709$	19.3 ± 27.7	$P = 0.3481$	19.7 ± 33.7	$P = 0.1667$	20.3 ± 37.3	$P = 0.1054$	11.4 ± 26.8	$P = 0.1800$
L. venusta										
Fresh	13.6 ± 9.4		13.7 ± 9.3		14.5 ± 9.1		14.7 ± 8.7		14.8 ± 8.6	
Dark	18.1 ± 9.8	$P \geq 0.1036$	19.2± 10.0	**$P \geq 0.0437$ (2)**	21.1 ± 10.5	**$P \geq 0.0246$ (2)**	22.9 ± 10.9	**$P \geq 0.0064$ (2)**	24.4 ± 11.5	**$P \geq 0.0066$ (2)**
Normal UVB	15.9 ± 7.4	$P \geq 0.0530$	16.9 ± 7.5	**$P \geq 0.0271$ (3)**	18.1 ± 7.9	**$P \geq 0.0243$ (3)**	19.7 ± 8.6	**$P \geq 0.0212$ (3)**	20.5 ± 9.5	**$P \geq 0.0226$ (3)**
Extreme UVB	14.1 ± 5.9	$P = 0.8661$	14.5 ± 6.2	$P = 0.7884$	15.0 ± 6.4	$P = 0.8406$	15.6 ± 6.9	$P = 0.7593$	16.2 ± 7.2	$P = 0.6406$
V. arenata										
Fresh	13.4 ± 8.1		18.4 ± 11.8		26.3 ± 17.0		33.3 ± 22.8		37.3 ± 28.4	
Dark	12.5 ± 8.6	$P \geq 0.5983$	17.2 ± 11.4	$P \geq 0.5257$	22.9 ± 15.2	$P \geq 0.2967$	28.3 ± 19.3	$P \geq 0.2485$	31.2 ± 22.9	$P \geq 0.2329$
Normal UVB	15.1 ± 8.6	$P \geq 0.0969$	20.3 ± 11.4	$P \geq 0.1448$	26.5 ± 15.2	$P \geq 0.2661$	32.6 ± 19.2	$P \geq 0.2329$	35.1 ± 21.8	$P \geq 0.2419$
Extreme UVB	14.7 ± 6.9	$P = 0.5402$	20.1 ± 10.1	$P = 0.6213$	26.5 ± 14.8	$P = 0.7967$	32.6 ± 19.7	$P = 0.9208$	35.0 ± 22.9	$P = 0.9782$
M. gracilis										
Fresh	27.6 ± 14.7		25.0 ± 15.2		26.7 ±14.9		28.3 ± 15.0		27.7 ± 15.7	
Dark	28.8 ± 14.2	$P \geq 0.2409$	24.7 ± 13.9	$P \geq 0.2193$	25.1 ± 14.8	$P \geq 0.1836$	25.4 ± 15.5	$P \geq 0.0791$	23.0 ± 16.0	**$P \geq 0.0284$ (3)**
Normal UVB	30.0 ± 17.4	$P \geq 0.1460$	23.9 ± 15.1	$P \geq 0.0673$	23.3 ± 15.2	**$P \geq 0.0156$ (3)**	23.1 ± 15.4	**$P \geq 0.0075$ (3)**	20.6 ± 15.2	$P \geq$ **0.0048 (3)**
Extreme UVB	26.2 ± 11.0	$P = 0.6118$	19.2 ± 9.6	$P = 0.0961$	17.9 ± 9.6	**$P = 0.0357$**	17.0 ± 9.5	**$P = 0.0240$**	14.5 ± 8.8	**$P = 0.0177$**
N. crucifera										
Fresh	26.2 ± 15.9		32.1 ± 17.5		41.7 ± 20.8		50.5 ± 24.3		56.8 ± 27.5	
Dark	18.8 ± 15.3	$P = 0.1369$	20.9 ± 16.4	$P = 0.0594$	27.9± 19.7	**$P = 0.0395$**	34.4 ± 24.1	**$P = 0.0411$**	38.1 ± 26.3	**$P = 0.0254$**
Extreme UVB	27.0 ± 21.8	$P = 0.8556$	28.0 ± 21.4	$P = 0.3889$	33.2 ± 23.0	$P = 0.1360$	38.8 ± 25.1	$P = 0.0845$	41.9 ± 26.3	$P = 0.0516$

Table 5: Young's moduli used in the force calculations for each species, taken from supplementary table 4 in Sensenig et al. 2010.

	Spiral diameter (µm)	Young's modulus (GPa)
Argiope aurantia	4.8 ± 1.50	0.009 ± 0.011
Leucauge venusta	0.9 ± 0.26	0.058 ± 0.046
Verrucosa arenata	1.5 ± 0.64	0.098 ± 0.199
Micrathena gracilis	1.3 ± 0.30	0.052 ± 0.053
Neoscona crucifera	3.0 ± 1.18	0.010 ± 0.005

Appendix A: Axial deflection angle measurements at 0, 25, 50, 75, and 99% of the droplet extension time for all species and treatment groups (mean ± 1 standard deviation). Significant *P*-values (<0.05) are in bold. Presented for the Normal UVB and Dark treatments are means obtained by averaging four, one-hour incremental treatment means (due to limited resolution). Individual comparisons were performed for these hourly treatments, and *P*-values presented are the lowest of the four comparisons; parenthesized values indicate which of the four hourly comparisons was significant, if applicable.

	Axial Angle 0%	Matched Pair 0%	Axial Angle 25%	Matched Pair 25%	Axial Angle 50%	Matched Pair 50%	Axial Angle 75%	Matched Pair 75%	Axial Angle 99%	Matched Pair 99%
A. aurantia										
Fresh	135.7 ± 13.1		148.8 ± 14.8		155.7± 16.5		163.8 ± 16.2		168.7 ± 15.6	
Dark	133.9 ± 17.1	$P \geq 0.4927$	142.5 ± 20.6	**$P \geq 0.0323$ (4)**	150.9 ± 22.4	$P \geq 0.1107$	157.8 ± 23.1	$P \geq 0.0596$	165.4 ± 21.2	$P \geq 0.2201$
Normal UVB	135.9 ± 20.5	$P \geq 0.5235$	143.2 ± 23.0	$P \geq 0.0654$	150.4 ± 26.6	$P \geq 0.0868$	156.7 ± 26.4	**$P \geq 0.0284$ (1)**	164.5 ± 21.5	**$P \geq 0.0174$ (1)**
Extreme UVB	140.4 ± 17.8	$P = 0.3035$	147.5 ± 22.8	$P = 0.9906$	152.6 ± 26.9	$P = 0.5895$	155.9 ± 29.7	$P = 0.1844$	162.9 ± 23.0	$P = 0.1549$
L. venusta										
Fresh	116.8 ± 15.3		116.5 ± 15.2		114.9 ± 14.7		114.4 ± 14.6		114.6 ± 14.4	
Dark	109.6 ± 14.0	$P \geq 0.0665$	107.7 ± 13.9	**$P \geq 0.0293$ (2)**	104.9 ± 14.1	**$P \geq 0.0197$ (2)**	102.4 ± 14.3	**$P \geq 0.0052$ (2)**	100.9 ± 15.0	**$P \geq 0.0047$ (2)**
Normal UVB	112.5 ± 12.6	**$P \geq 0.0380$ (3)**	110.6 ± 12.1	$P \geq$ **0.0209 (3)**	108.6 ± 11.9	**$P \geq 0.0243$ (3)**	106.5 ± 12.3	**$P \geq 0.0239$ (3)**	105.6 ± 13.5	**$P \geq 0.0401/0.0256$ (1/3)**
Extreme UVB	115.5 ± 10.5	$P = 0.8080$	115.0 ± 10.7	$P = 0.7755$	113.8 ± 10.9	$P = 0.8354$	113.0 ± 11.7	$P = 0.7835$	112 .1 ± 12.0	$P = 0.6519$
V. arenata										
Fresh	143.1 ± 9.9		139.1 ± 11.7		134.1 ± 13.9		130.5 ± 15.6		129.3 ± 17.4	
Dark	145.0 ± 10.3	$P \geq 0.2784$	140.8 ± 11.6	$P \geq 0.3327$	136.8 ± 12.9	$P \geq 0.2785$	133.6 ±14.1	$P \geq 0.2381$	132.4 ± 15.4	$P \geq 0.2411$
Normal UVB	141.9 ± 5.9	$P \geq 0.3492$	137.5 ± 6.2	$P \geq 0.2841$	133.4 ± 7.0	$P \geq 0.4400$	130.1 ± 7.8	$P \geq 0.4035$	129.1 ± 8.3	$P \geq 0.4369$
Extreme UVB	141.5 ± 5.6	$P = 0.5368$	137.0 ± 7.2	$P = 0.5220$	132.0 ± 8.5	$P = 0.6063$	128.4 ± 9.8	$P = 0.6676$	127.2 ± 11.3	$P = 0.3650$
M. gracilis										
Fresh	114.8 ± 13.9		117.6 ± 14.5		115.7 ± 13.9		114.5 ± 13.9		116.0 ± 16.1	
Dark	114.3 ± 13.6	$P \geq 0.3015$	118.7 ± 14.2	$P \geq 0.1883$	117.1 ± 16.9	$P \geq 0.1883$	119.2 ± 16.8	$P \geq 0.0848$	123.7 ± 19.5	**$P \geq 0.0376$ (2)**
Normal UVB	113.4 ± 15.5	$P \geq 0.1519$	119.0 ± 15.3	$P \geq 0.1122$	120.2 ± 16.5	**$P \geq 0.0303$ (3)**	120.9 ± 17.3	**$P \geq 0.0194$ (3)**	125.1 ± 18.6	**$P \geq 0.0102$ (3)**
Extreme UVB	114.6 ± 11.4	$P = 0.9076$	123.4 ± 16.1	$P = 0.1851$	125.0 ± 16.7	$P = 0.0834$	127.2 ± 19.2	$P = 0.0680$	131 ± 19.6	$P = 0.0646$
N. crucifera										
Fresh	116.1 ± 14.1		111.0 ± 15.6		103.6 ± 16.5		97.9 ± 17.6		94.2 ± 18.5	
Dark	124.0 ± 15.1	$P = 0.0951$	122.0 ± 16.3	**$P = 0.0498$**	113.2 ± 16.3	**$P = 0.0328$**	110.0 ± 18.9	**$P = 0.0352$**	107.5 ± 20.3	**P =0.0257**
Extreme UVB	118.0 ± 19.2	$P = 0.6758$	117.5 ± 21.5	$P = 0.2312$	115.2 ± 21.5	$P = 0.1174$	109.0 ± 24.5	$P = 0.0906$	106.7 ± 25.3	$P = 0.2260$

Appendix B: Maximum mean percent axial line elongation as droplets extended during each treatment and the percent extension at which this value was expressed. For each species, maximum axial line extension occurred at the same percent extension.

	A. aurantia	***L. venusta***	***V. arenata***	***M. gracilis***	***N. crucifera***
Extension	0%	99%	99%	0%	99%
Fresh	10.6	21.1	12.7	21.2	41.8
Dark					
1 Hour	10.9	35.8	13.0	17.5	-
2 Hours	10.6	34.8	9.6	23.3	-
3 Hours	10.4	33.4	10.8	20.9	-
4 Hours	12.4	30.7	10.5	26.8	31.0
Normal UVB					
1 Hour	10.9	28.0	13.1	19.5	-
2 Hours	9.2	26.2	10.2	24.9	-
3 Hours	13.4	34.5	12.7	18.4	-
4 Hours	11.2	24.9	12.6	28.6	-
Extreme UVB	8.5	22.8	12.8	20.1	28.6

4. The impact of UVA on the glycoprotein glue of orb-weaving spider capture thread from diurnal and nocturnal species

Sarah D. Stellwagen, Brent D. Opell, Mary E. Clouse

Abstract

Diurnal orb-web weaving spiders build webs in the early morning and forage throughout the day while exposed to the full spectrum of ultraviolet radiation from the sun. Other spiders build their webs after dusk, and complete the bulk of their foraging by the following morning. We examined the effect of UVA on the viscoelastic glycoprotein core of glue droplets of orb-web capture spiral thread. We hypothesized that droplets from spiders that occupy sunny habitats will either be unaffected or will benefit from UVA exposure; whereas droplets from nocturnal species will be degraded. One set of threads from each web of a diurnal and a nocturnal spider species were exposed to two-thirds of peak incident UVA for four hours to test the effect of exposure, and another set kept in a dark chamber to assess the effect of post-production droplet aging. The droplet size and performance of droplets from these threads were compared to those of fresh threads. The dark treatment showed similar declines in performance to those exposed to UVA. After exposure to UVA, there was a reduction in the droplet extension time for the diurnal species (*Argiope trifasciata*) but this did not affect the overall energy absorption abilities of the droplets. Droplets from the nocturnal species, *Neoscona crucifera*, did not show any reduction in performance. This study suggests that ecologically relevant levels of UVA exposure do not affect the glycoptroptein within the droplets of orb-weaving spider capture silk.

KEY WORDS: Adhesion, Biomaterials, Toughness, Silk, Ultraviolet, UVA

** To maintain consistency with chapters 2 & 3, the materials section follows the discussion.*

INTRODUCTION

Ultraviolet radiation (UVR) comes in several forms, the least damaging of which is UVA, however more UVA enters the atmosphere than the other forms of UVR (Rizzo et al. 2011). Species of the genus *Argiope,* including *A. trifasciata* Forskaal 1775, are found in habitats where their webs are exposed to full sun. Others, such as *Neoscona crucifera* (Lucas, 1838)*,* are nocturnal and forage from the center of their webs at night, however they do leave their adjacent retreats to collect prey that become caught in the web during the day. Aerial webs of these species consist of radial threads that support a spiral of capture silk, which incorporates adhesive glue droplets to catch and retain flying insects (Apstein, 1889; Sekiguchi, 1952; Sahni et al., 2014). Each of these droplets contains an inner sticky, viscoelastic glycoprotein core (Sahni et al., 2010), surrounded by an aqueous outer covering that retains moisture (Edmonds and Vollrath, 1992). Low molecular weight compounds (LMMC) and inorganic salts in this aqueous coat confer hygroscopicity (Townley and Tillinghast, 2013).

Ultraviolet radiation induces cross-linking in proteins (Bhat and Karim, 2009; Hu et al., 2013), and we have shown that full sun diurnal species produce webs that are not only resistant to degradation, but relative toughness may actually be enhanced by UVB (Stellwagen et al. 2015, in press). Non-adhesive spider silk continues to improve mechanically after several hours of natural UVA exposure, however longer exposures do eventually result in degradation (Osaki, 2004; Osaki and Osaki, 2011). Low UV doses may enhance silk performance by further aligning proteins, similar to the "improvement phase", where molecule alignment is hypothesized to continue after a silk strand is extruded (Agnarsson et al., 2008). UVA at ~700 W/m^2 reduces the molecular weight of spider dragline silk from *Nephila clavipes* Linnaeus 1767 over 30% the first hour, and more than 80% after 5 hours, however this radiation intensity is over 20x natural incident UVA striking spider webs in the summer (Matsuhira et al., 2013). Osaki and Osaki, (2011) demonstrated that ecologically relevant doses of UVA actually serve to mechanically strengthen dragline silk of *Argiope bruennichii,* while weakening that of *Neoscona nautica*.

We investigated the effects of UVA radiation on the viscous glue droplets of *A. trifasciata* and *N. crucifera* (family Araneidae), as a compliment to our previous UVB study and previous studies suggesting that UVA acts to enhance spider silk. We tested the hypothesis that droplets from the webs of the diurnal species, *A. trifasciata,* are more likely to be enhanced by UVA exposure than those of *N. crucifera,* which builds its webs at night. We did this by measuring the

duration of droplet extension and the angle of axial line deflection produced by extending droplets from fresh threads collected in the early morning or late evening, depending on species. We compared these values with those from droplets that were aged in the dark and droplets that were exposed to four hours of UVA at a fluence rate of ~13 W/m^2, which is approximately 2/3 of the maximum incident UVA at peak daylight hours. We also photographed each thread droplet prior to extension, which permitted us to compare the effect of UVA on droplet volume. This allowed us to test the hypothesis that UVA exposure affects the droplet volume by degrading or enhancing the LMMC in a droplet's aqueous layer

RESULTS

UVA exposure had no effect on droplet volume for either species or treatment (Table 1). The extension times reported in Table 2 provide an index of the extensibility of the glycoprotein within droplets. For the full sun species, *A. trifasciata,* droplet extension time was reduced from 8.5 seconds to 6 seconds after UVA exposure, while *N. crucifera* extension times were unaffected.

When the force on an extending droplet is plotted against extension time, interspecific differences in droplet response to aging and UVA exposure become clearer. The area under each of these force/extension time curves represents relative toughness and is an index of the energy required to extend a droplet (Table 3, Fig. 1). Compared with fresh threads, the energy absorbed by *A. trifasciata* and *N. crucifera* decreases 55% and 43%, respectively, after dark treatments and 45% and 31%, respectively, after UVA exposure. Neither treatment difference is significant and, although both treatment values are less than the control, there is no evidence to suggest that that UVA exposure degraded droplet performance more than aging.

DISCUSSION

Retention time is important for prey capture success, and a reduction of only a few seconds can mean a lost feeding opportunity for an orb-weaving spider (Blackledge and Zevenbergen, 2006). This study hypothesized that droplets from webs of the diurnal, full sun species *A. trifasciata* would be more likely to be positively affected by UVA than those from the nocturnal species *N. crucifera*, or at least would be more resistant to UVA exposure. However,

droplets from *A. trifasciata* webs showed a reduction in droplet extension time after exposure to UVA, even though this did not affect the overall energy absorption of the threads. Interestingly, the relative toughness of webs from both species decreased more after dark exposure than after UVA exposure, although these differences were not statistically significant. It may be that the chemical cross-linking mechanism hypothesized to strengthen dragline silk (Craig et al., 1994) either does not affect the glycoprotein, or that higher doses of UVA not typically experienced by spider threads are needed to see this affect. Similar to UVB, UVA does not appear to impact the LMMC in droplets, which supports the observation that these compounds resist degradation (Opell et al., 2015 in press). Thus, our study suggests that ecologically relevant doses of UVA have little impact on spider capture spiral thread.

MATERIALS AND METHODS

Study species and thread collection

Thread samples from webs constructed by 13 adult female *A. trifasciata* were collected on and near the Virginia Tech campus in Blacksburg, Montgomery County, VA, USA, from 15 August to 25 September 2014. Each sample was collected between 05:30h and 08:30h and all images and videos captured by 16:00h the same day. Threads from eleven adult female *Neoscona crucifera* webs were collected from 01 September to 13 September 2014 between 21:30h and 23:00h and their study was completed by 16:00h on the following day. Except for differences in irradiance described below, all methods and analyses are those described by Stellwagen et al. (2015, in press).

UVB Irradiance

Two 15.0 watt, 352 nm spectral peak UVA fluorescent tube (F15T8BL; 440.4 mm length, 25.4 mm diameter; USHIO Inc., Cypress, CA, USA) were used to irradiate samples. Irradiance was measured using a Solar Light Co., Inc. PMA2200 photometer radiometer equipped with a UVA detector (PMA2110, Glenside, PA, USA) calibrated traceable to the National Institute of Standards and Technology (NIST) on 18 August 2014 with a spectral sensitivity from 320-400 nm. Threads were irradiated for 4 hours at ~13 W/m^2 (the maximum level produced by the UVA lamps), which is two-thirds the maximum level full sunlight received in this area in late summer.

Analysis

We used JMP (SAS Institute, Cary, North Carolina) to analyze data and considered comparisons with $P \leq 0.05$ as significant. All observations were normally distributed (as confirmed by Shapiro-Wilk W tests having $P \leq 0.05$). Each treatment value was compared to the fresh thread value, which served as the control. Droplet size and performance was very similar within an individual web sample but showed some inter-individual difference. To address this we followed a repeated measures design, comparing values with matched pair t-tests. This approach results in any bias in the measurement of fresh droplets affecting each comparison. However, our best gauge of similarity of control and treatment droplets is droplet length and width, which are quite similar (Table 1).

ACKNOWLEDGEMENTS

Carlyle C. Brewster assisted with statistical analyses.

AUTHOR CONTRIBUTIONS

S.D.S. collected and prepared thread samples, performed droplet extensions and image measurements, analyzed data, and prepared the manuscript and figures. B.D.O. designed and constructed the instrumentation used in this study, collected and helped prepare thread samples, and contributed to data analysis, and manuscript and figure preparation. M.E.C. assisted with droplet extension, image measurements, and data entry.

COMPETING INTERESTS

No competing interests declared.

FUNDING

Funds from the State Council for Higher Education for Virginia provided the digital camera used in this study. This study was supported by National Science Foundation grant IOS-1257719.

FIGURES

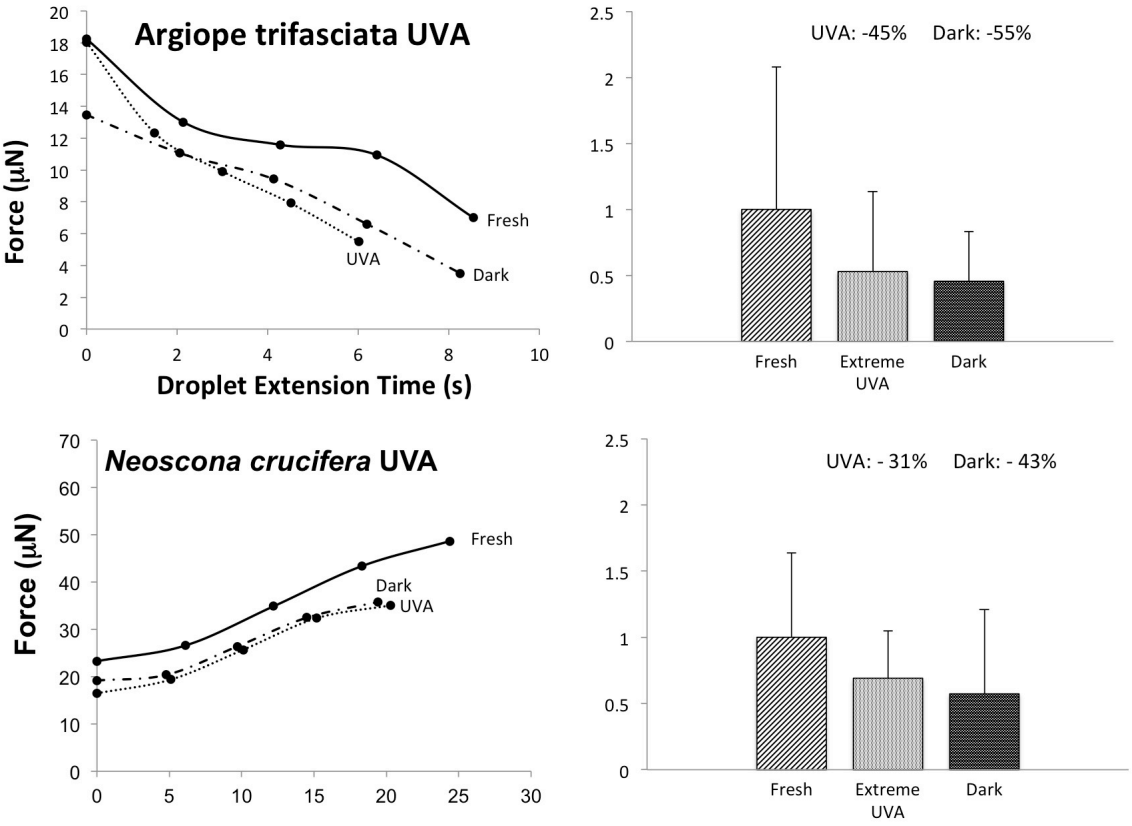

Figure 1. Force / extension time plots for viscous droplets and corresponding histograms of relative toughness for droplets in each treatment, as determined from areas under these curves. Points in force / extension time plots are mean values and are connected by smoothed lines. Relative toughness values are mean ± standard deviation.

REFERENCES

Agnarsson, I., Boutry, C. and Blackledge, T. A. (2008). Spider silk aging: initial improvement in a high performance material followed by slow degradation. *Journal of Experimental Zoology, Part A: Ecological Genetics and Physiology* **309A**, 494-504.

Apstein, C. H. (1889). Bau und Function der Spinnendrusen der Araneida. *Archiv fur Natur-geschichte*, 29.

Bhat, R. and Karim, A. A. (2009). Ultraviolet irradiation improves gel strength of fish gelatin. *Food Chemistry* **113**, 1160-1164.

Blackledge, T. A. and Zevenbergen, J. M. (2006). Mesh Width Influences Prey Retention in Spider Orb Webs. *Ethology* **112**, 1194-1201.

Craig, C. L., Bernard, G. D. and Coddington, J. (1994). Evolutionary shifts in the spectra properties of spider silks. *Evolution* **48**, 287-296.

Edmonds, D. T. and Vollrath, F. (1992). The Contribution of Atmospheric Water Vapour to the Formation and Efficiency of a Spider's Capture Web. *Proceedings of the Royal Society B: Biological Sciences* **248**, 145-148.

Hu, X., Raja, W. K., An, B., Tokareva, O., Cebe, P. and Kaplan, D. L. (2013). Stability of Silk and Collagen Protein Materials in Space. *Sci. Rep.* **3**.

Matsuhira, T., Yamamoto, K. and Osaki, S. (2013). Effects of UV irradiation on the molecular weight of spider silk. *Polym J* **45**, 1167-1169.

Opell, B. D., Andrews, S. F., Karinshak, S. E. and Sigler, M. A. (2015 in press). The stability of hygroscopic compounds in orb-web spider viscous thread. *Journal of Arachnology* **43**.**Osaki, S.** (2004). Ultraviolet Rays Mechanically Strengthen Spider's Silks. *Polym J* **36**, 657-660.

Osaki, S. and Osaki, M. (2011). Evolution of spiders from nocturnal to diurnal gave spider silks mechanical resistance against UV irradiation. *Polymer Journal* **43**, 200-204.

Rizzo, J. L., Dunn, J., Rees, A. and Runger, T. M. (2011). No Formation of DNA Double-Strand Breaks and No Activation of Recombination Repair with UVA. *J Invest Dermatol* **131**, 1139-1148.

Sahni, V., Blackledge, T. A. and Dhinojwala, A. (2010). Viscoelastic solids explain spider web stickiness. *Nature Communications* **1**, 1-4.

Sahni, V., Dhinojwala, A., Opell, B. and Blackledge, T. (2014). Prey Capture Adhesives Produced by Orb-Weaving Spiders. In *Biotechnology of Silk*, vol. 5 eds. T. Asakura and T. Miller), pp. 203-217: Springer Netherlands.

Sekiguchi, K. (1952). On a new spinning gland found in geometric spiders and its function. *Annot Zool Japonenses* **25**, 394-399.

Townley, M. and Tillinghast, E. (2013). Aggregate Silk Gland Secretions of Araneoid Spiders. In *Spider Ecophysiology*, (ed. W. Nentwig), pp. 283-302: Springer Berlin Heidelberg.

TABLES

Table 1: Dimensions of suspended droplets for both species and treatments (n=13; mean ± 1 standard deviation).

	Length μm	**Width** μm	**Volume** μm^3	**Matched Pair (Volume)**
A. trifasciata				
Fresh	47.7 ± 8.0	33.5 ± 6.2	24,707 ± 13,183	
Dark	48.1 ± 7.3	34.6 ± 6.1	26,006 ± 12,071	$P = 0.4901$
UVA	48.1 ± 7.3	33.6 ± 6.1	24,760 ± 12,031	$P = 0.9812$
N. crucifera				
Fresh	32.0 ± 10.8	23.4 ± 7.8	10,211 ± 11,940	
Dark	30.9 ± 9.0	22.8 ± 6.8	8,690 ± 8,142	$P = 0.2492$
UVA	31.3 ± 9.5	23.1 ± 6.8	9,237 ± 9,513	$P = 0.2931$

Table 2: Extension phase times (seconds) for both species and treatments (n=13; mean ± 1 standard deviation).

	Total Loaded Time	**Pre-Extension**	**Droplet Extension**	**Matched Pair DE**
A. trifasciata				
Fresh	32.5 ± 8.2	24.0 ± 7.3	8.5 ± 6.3	
Dark	28.4 ± 5.9	20.2 ± 7.7	8.3 ± 6.2	$P = 0.8457$
UVA	29.5 ± 7.1	23.5 ± 7.7	6.0 ± 5.2	$\mathbf{P = 0.0015}$
N. crucifera				
Fresh	28.2 ± 11.0	23.7 ± 11.3	24.2 ± 10.6	
Dark	41.4 ± 5.7	22.0 ± 7.9	19.4 ± 7.8	$P = 0.1363$
UVA	40.2 ± 11.4	20.0 ± 6.8	20.3 ± 12.7	$P = 0.2849$

Table 3. Relative toughness and LOG relative toughness for each species and treatment (n=13; mean ± 1 standard deviation).

	Toughness	Log Toughness	
A. trifasciata			**Wilcoxon**
Fresh	99.1 ± 106.8	3.5 ± 1.4	
Dark	45.2 ± 37.1	2.9 ± 1.7	$P = 0.6519$
UVA	52.5 ± 60.1	3.3 ± 1.2	
N. crucifera			**Matched Pair**
Fresh	819 ± 524	6.4 ± 0.73	
Dark	469 ± 242	6.0 ± 0.5	$P = 0.1496$
UVA	566 ± 627	5.8 ± 1.1	$P = 0.1083$

5. Capture spiral glue distributions across orb-webs of *Argiope trafasciata* (Araneae: Araneidae)

Sarah D. Stellwagen, Brent D. Opell, Mary E. Clouse

In preparation for submission.

Abstract

Orb-weaving spiders complete their webs by spinning a sticky capture spiral that will retain insects that strike the web. Many species exhibit top-bottom asymmetry with the lower half of the web presenting more capture area, which a spider is able to use effectively, because running speeds are faster when spiders move downwards. This study expands the understanding of web asymmetry by examining an additional level of web flexibility: intra-web differences in the glycoprotein and aqueous volumes and in the extensibility characteristics of adhesive capture spiral droplets of *Argiope trifasciata* orb-webs. We characterized these features for droplets collected from the top, top middle, inner, bottom middle, and bottom of webs and examined their relationship to microhabitat conditions measured for this species. The most notable differences in droplets were seen between those from the top and bottom of the web. Bottom threads are the first to be spun, are the largest and have a 2:1 ratio of aqueous to glycoprotein volume, whereas droplets at the top threads, which are spun shortly after bottom strands, are half the size of the bottom droplets with a 3:1 ratio of aqueous to glycoprotein volume. However, as the spiral moves inwards, droplets from the middle regions of the top and bottom sectors are larger than those from the top, supporting the hypothesis that a spider has some control over the total amount of glue being extruded onto the axial threads. During the early morning hours, when webs are spun, there are no microhabitat temperature or humidity gradients that would differentially affect viscous droplet formation. However, greater humidity in the region of the lower third of an orb-web has the potential to increase the volume and water content of droplets in this web region, increasing the extensibility of the glycoprotein cores of these droplets.

KEY WORDS: Adhesion, Biomaterials, Toughness, Silk, Asymmetry, Orb-Web, Spider

** To maintain consistency with chapters 2 & 3, the materials section follows the discussion.*

INTRODUCTION

Orb-weaving spiders construct aerial webs that perform three tasks: prey interception, energy dissipation, and retention (Chacón and Eberhard, 1980), and two silk types permit a web to accomplish these tasks. Major ampullate silk forms both the outer structural silk frame and the radial threads that it supports. Radii originate from the center of the web and extend outwards like the spokes of a wheel, and are responsible for dissipating most of the kinetic energy of intercepted prey (Sensenig et al., 2012). Radial threads also support a second type of thread, the spirally arrayed viscous prey capture thread. This thread is formed of axial lines covered by viscoelastic, adhesive glue (Apstein, 1889; Sekiguchi, 1952; Sahni et al., 2014) and performs the final act of retaining prey. Web architecture can be modified in ways that appear to optimize prey capture and many spiders adjust the top-bottom symmetry of their webs (Masters and Moffat, 1983), web capture area, radial thread density, and capture spiral spacing (Chacón and Eberhard, 1980; Eberhard, 1986).

Spiders complete their webs by adding the capture silk, beginning from the bottom of the web's frame, and spiraling their way towards the center. Many orb-webs, especially those of larger, heavier spiders, exhibit a bottom-biased asymmetry, where the bottom sector of the web below the hub is larger and has either more capture spirals, the result of several switchbacks, or greater spacing between spirals (Eberhard, 1986). Many studies have documented the prey capture benefits of this asymmetry, by showing that spiders can harness gravity to increase downwards running speeds, and that a downward facing resting position reduces time spent orienting towards prey in the larger lower portion of the web (Masters and Moffat, 1983; Herberstein and Heiling, 1999; Maciejewski, 2010; Zschokke and Nakata, 2010; Gregorič et al., 2013). Some species exhibit the reverse of both asymmetry and resting position, however upward-biased spiders tend to be small, and thus exhibit less difference in up-down running speeds (Nakata and Zschokke, 2010). An exception to this generalization is *Verrucosa arenata* (Walckenaer, 1841), a large spider (7-14 mm, 0.05-0.46 g) that rests facing upwards, but still exhibits bottom-biased asymmetry (Rao et al., 2011). However, this

study also demonstrated that *V. arenata* does not exhibit differences in up-down running speeds.

Orb-web asymmetry is the product of selection that optimizes the use of silk resources for prey capture. By differentially allocating resources to separate regions of a web, the contribution of each region to whole-web function can be balanced and improved. This whole web design flexibility also extends to the contributions of threads that form the web, with radial major ampullate threads performing most of the web's energy absorption and viscous capture spiral threads most of the prey retention function. Because the viscous glue droplets responsible for prey retention are themselves an integral part of the capture spiral silk, this material is selected in the context of spiral patterns. Differences in size, distribution, and performance have the potential to add yet another level of specialization to differences in web symmetry. Little is known about a spider's ability to alter the way in which these droplets contribute to prey capture. The principal focus of this study is to examine this flexibility in spider resource allocation and understand its consequences in the context of an orb-web's microhabitat.

Web size, or the total area within a web's frame lines, varies widely depending on species or individual. Larger webs require either more capture silk or greater spiral spacing, and both parameters must be adjusted in order optimize resource use and prey capture (Eberhard, 1986). Spiders are considered to be generalist predators, however the amount and size of prey captured by webs has been shown to be important. The 'Rare Large Prey Hypothesis' explains that though spiders capture mainly smaller prey, the rare capture of large prey constitutes an essential role in a spider's development and reproductive success (Venner and Casas, 2005). The validity of this hypothesis as extended to all orb-weaving spiders has been called into question, and the trade-offs of web architecture for species-specific or individual-specific optimal resource acquisition has been offered as a more comprehensive perspective on orb-web structure and function (Eberhard, 2013).

Most research examining orb-web architecture has focused on how spiders alter the number, density, and patterns of the different silk components for prey capture (e.g. (Chacón and Eberhard, 1980; Masters and Moffat, 1983; Eberhard, 1986). Only two studies have examined the distributions of the adhesive glue droplets that coat the capture spirals of orb-webs. Edmonds and Vollrath (1992) observed differences in droplet size between the top and

the bottom of orb-webs, although did not quantify these differences. This study also demonstrated that when viscous thread cylinders form under high humidity droplets are larger and more widely spaced than under low humidity. Opell et al. (2009) examined inner-outer web differences in lateral regions of orb-webs, avoiding the subject of asymmetry, and found that droplets from the outer spiral threads were stickier, despite similarities in droplet volume and number of droplets per millimeter.

Assessing intra-web differences in viscous thread size and performance requires an understanding of the thread's composition. Viscous capture glue is spun from a triad of spigots located on each of the abdominal posterior lateral spinnerets. Two aggregate spigots secrete the viscous glue directly onto the supporting axial thread produced from a central flagelliform spigot. This glue initially surrounds the thread, however the hygroscopic nature of the material rapidly absorbs atmospheric moisture, resulting in surface tension that breaks the cylinder into evenly spaced droplets (Boys, 1889; Rayleigh, 1892; Edmonds and Vollrath, 1992). The center of each droplet is composed of an adhesive glycoprotein (Opell and Hendricks, 2010) responsible for sticking to prey (Sahni et al., 2010), and surrounded by a hygroscopic aqueous material that retains moisture and lubricates the glycoprotein core. The aqueous region of the droplets contains small inorganic and low molecular weight compounds that are responsible for the hygroscopic nature of this material (Townley and Tillinghast, 2013). Changes in humidity affect the performance of the droplets by increasing or decreasing the water content and therefore performance of the glycoprotein (Opell et al., 2011; Sahni et al., 2011). For some species, higher humidity improves droplet extensibility (stretching distance) and adhesion (energy required to pull a droplet free from a surface) while others perform best under mid-range humidity (Sahni et al., 2011; Opell et al., 2013). Additionally, temperature affects the viscosity of the droplets by stiffening the glue when it is cooler, and softening it when temperatures increase (Stellwagen et al., 2014).

Three factors have the potential to affect intra-web differences in droplet volume: 1. Spiders use muscular valves to regulate flow of silk from their spinnerets and, therefore, have the potential to control the volume of viscous material as capture thread is spun (Foelix, 2011), 2. Spiders expend silk reserves during web construction (Peters, 1937; Witt et al., 1968; Eberhard, 1972; Eberhard, 1986), suggesting that droplets might become progressively smaller during this process, and 3. Ambient humidity influences droplet size and distribution

(Edmonds and Vollrath, 1992), suggesting that humidity gradients present when a web is spun will influence droplet size. Although factors 1 and 2 are not completely independent because dwindling resources may influence how a spider chooses to allocate the remainder of the glue, our experimental design permits us to determine which and how these factors determine droplet size. If there is no humidity gradient when a web is spun, the last factor can be eliminated. A strict resource availability explanation predicts that a decrease in droplet volume across the web in the following order: bottom, top, middle, inner. Conspicuous deviation from this pattern, particularly strong contrasts between top and bottom droplet features, would support a significant impact of resource allocation by a spider.

The main goal of this study is to expand understanding of the capture system and its relationship to asymmetrical architecture typical of large orb-webs constructed by spiders like *Argiope trifasciata* Forsskål 1775. We do this by determining whether there are intraweb differences in distribution and performance of droplets from the bottom, top, middle of the top and bottom sections, and the innermost spirals (Fig. 1), and by testing the hypothesis that these differences are physiologically controlled. An alternative hypothesis is that humidity gradients between upper and lower web sectors are responsible for any differences observed in droplet size, distribution, and performance. Thus, a second goal of this study is to characterize the microhabitat of *A. trifasciata* during web construction and foraging. *Argiope trifasciata* was chosen for this study because we observed that their webs exhibit a bottom-biased asymmetry, with capture spiral construction beginning at the bottom, where a spider places several switchbacks of capture thread before making complete spirals, and a final spiral that defines the border of the free zone near the web's hub. Their webs are positioned such that the lower portion is tucked down into open, weedy vegetation, while the top is slightly above vegetation height, creating the potential for a top-bottom microclimate gradient.

RESULTS

Asymmetrical capture spiral patterns are the result of differential selective pressures at the tops and bottoms of orb-webs. Our results show that the webs of *A. trifasciata* used in this study exhibited architectural asymmetry, i.e. longer bottom sectors that contain more capture spirals than the tops (Table 1). These results show that droplet size

and performance also differ across the web, in ways that appear to functionally reinforce this asymmetry (Fig. 2).

Mean droplet dimensions (length, width, and volume) for suspended droplets used to visualize glycoprotein volume are presented in Table 2. Bottom droplets were larger than droplets from all other regions ($P < 0.0184$), top droplets were smaller than top middle droplets ($P = 0.0355$), and inner droplets had the smallest volumes of all droplets, and were significantly smaller than bottom-middle droplets ($P = 0.0177$). Table 3 presents mean droplet dimensions (length, width, and volume) for suspended droplets from each web region that were photographed just prior to extension, as well as the mean distance between droplets distributed on threads from these regions. Droplet volume followed a similar pattern to those that were flattened, however, due to slight variations in length and width, the top droplets used for extension had the smallest volume, which was similar than the volume of the inner droplets used for flattening, and vice versa. Droplets from the bottom capture threads were again larger than droplets from any other region ($P < 0.0368$), whereas those from the top threads had the smallest average volume, and were smaller than top-middle droplets ($P = 0.0029$), but were most similar to the inner droplets. The top middle, inner, and bottom middle droplets did not differ. The average distance between droplets did not differ significantly between web regions, however the bottom droplets were ~30μm further apart than the top or top middle droplets.

Dimensions of flattened droplets are presented in Table 4. Bottom droplets had larger glycoprotein volumes than droplets from any other region ($P < 0.0212$). Droplets from the top, top middle, and inner sectors of the web did not differ, however inner droplet glycoprotein volumes were smaller than the bottom middle droplets ($P = 0.0310$) and droplets from the top and bottom regions were the most similar and did not differ. Bottom droplets had the largest aqueous volume, however it only differed from inner droplets ($P = 0.0361$) and top droplets ($P = 0.0075$), but not than top or bottom middle droplets. Inner droplet aqueous material was less than bottom middle droplets ($P = 0.0361$), but did not differ from that of droplets in the upper sector of the web. Droplets from the middle of the upper and lower sectors of the web had the most similar aqueous volumes, while bottom droplets had the largest average aqueous and glycoprotein volumes.

We believe that the ratio of aqueous to glycoprotein volume serves as an index of the degree of water-saturation within the glycoprotein core, where higher indices are associated with less viscous or more highly lubricated glycoproteins (Table 5). Bottom droplets have twice as much aqueous material as glycoprotein ($P < 0.0395$), whereas the inner droplets have four times as much aqueous material as glycoprotein, more than that of top droplets ($P = 0.0472$). Top, top middle, and bottom middle droplets had approximately three times as much aqueous material as glycoprotein, and did not differ from one another.

Using videos of droplets extending, we measured both droplet extension time (DE), which is a measure of droplet viscosity (Table 6), as well as the axial defection angle (Appendix A) during this extension, from which we calculated force measurements (Table 7). Combining force and droplet extension time, we can gauge the relative toughness of the droplets from the different regions of the web (Table 8). Bottom droplets had nearly twice the DE of any other region ($P < 0.0348$) except the top-middle, but still extended 37% longer than this region's droplets. Droplets from the top middle and bottom middle sectors had the largest relative toughness, more than droplets from the top ($P = 0.0109$, $P = 0.0197$), inner ($P = 0.0285$, $P = 0.0037$), or bottom ($P = 0.0070$, $P = 0.0012$), and did not differ from each other.

Parameter data collected both from webs used in extension trials and from webs in the field are presented in Table 1. Webs used in extension trials had top sectors that were shorter in length (measured from the top-most spiral to the inner-most spiral of the top sector) than the bottom sector (measured from the inner-most spiral of the lower sector to the bottom-most spiral), and had fewer spirals than the bottom sector. Parameters from an additional 13 webs were recorded in the field and showed a similar pattern to those used for extension trials. Additionally, the mean height of the bottom of the web (measured from the ground to the bottom frame line) was lower than the mean height of the top of the web (measured from the ground to the top frame line).

Microhabitat humidity and temperature data are presented in Table 9. While not all sites revealed a humidity gradient, and there was no evidence of a temperature gradient, data collected from the site where we have observed the most *A. trifasciata,* the Pig Barn, showed ~6% humidity difference between the vegetation height and 30 cm below

vegetation height. This corresponds to a humidity gradient that would be observed between the bottom of the web and the upper two thirds of the web (Figure 1, Table 1).

DISCUSSION

Selective pressures adapt the structural features of a species' orb-web, such as web area and spiral spacing, in unique ways (Stowe, 1978). The bottom often has more capture area than the top (Masters and Moffat, 1983; Herberstein and Heiling, 1999). Our study documents asymmetry in *A. trifasciata* and details top-bottom and inner-outer spiral differences in viscoelastic glycoprotein glue droplet characteristics. Additionally, we connect microhabitat humidity gradients to differences in droplet size and performance, showing that differences in humidity across the web may influence how a spider allocates resources.

There are striking differences in the size, glycoprotein volume, aqueous volume, and performance of viscous droplets across an *A. trifasciata* web. The most notable are that droplets at the bottom of the web, which are the first to form are the largest and have a 2:1 ratio of aqueous to glycoprotein volume, whereas droplets at the top are half the size of the bottom droplets with a 3:1 ratio of aqueous to glycoprotein volume, despite being the second droplets deposited. However, as the spiral moves inwards, droplets from the middle regions of the top and bottom sectors are larger than those from the top, but maintain the same ratio of aqueous to glycoprotein volume as the top droplets. Droplets from the innermost spirals tend to be small and similar in size as the top, but have four times more aqueous than glycoprotein volume, the highest ratio of droplets from any region of the web. These differences support the hypothesis that a spider has some control over the total amount of glue being extruded onto the axial threads, which may include valvular control and pulling rate. The aqueous and glycoprotein materials are produced and contained within the same gland, and therefore spiders are unlikely to have control over the ratio of these materials. This may also apply to the LMMC and salts in the aqueous material, although as silk dope moves down a spinning gland's ducts ions are added to and withdrawn from the material (Foelix, 2011). Evidence suggests that during orb-web construction, spiders completely exhaust their glycoprotein stores (Peters, 1937; Witt et al., 1968; Eberhard, 1972; Eberhard,

1986). This could influence a spider's controlled resource allocation and, thus, account for the non-linear decline in total droplet volume that we observed.

The material properties of the droplets suggest that the ratio of aqueous to glycoprotein volume confers functional consequences, with more aqueous material improving glycoprotein function (Table 5, Fig. 3). Bottom droplets, which have the least aqueous volume, also absorb the least amount of energy per glycoprotein volume. Their possibly lower viscosity, as suggested by the lower force/glycoprotein, permits them to extend further, but greatly reduces the work required to extend droplets. Inner spiral droplets have the greatest proportion of aqueous material, are the most viscous, and exhibit the greatest relative toughness. However, our data do not allow us to determine if the ratio, *sensu sticto*, is responsible for differences in glycoprotein performance. It may be that the aqueous material that is extruded at the beginning starts with a combination of salts and LMMC that shifts as the gland empties.

When considering whole web function, it appears that spiders strategically place droplets within in the web. Microhabitat data do not support the hypothesis that humidity gradients during the time when webs are built are responsible for differences in droplet size. The toughness per glycoprotein volume is high in top droplets and low in bottom droplets (Fig. 3), but the larger glycoprotein volumes of bottom droplets mediates this difference, conferring more relative toughness to droplets in the bottom spirals (Fig. 4). However, the greatest relative toughness occurred in the center of the top and bottom web regions. This may indicate that spiders have allocated resources in a way that optimizes performance of the central web region, which is near the spider's resting position at the web's hub. This also suggests that the lower region of the web, which establishes web asymmetry, is of low quality and serves as a "last ditch" area for securing insects that would otherwise escape from the web.

Differences in microhabitat across webs also have the potential to impact the variation observed in droplet performance. During the time when these spiders are actively foraging, temperature differs little across a web, but humidity is approximately 6% higher at the bottom of the web than a third of the way up the web's top to bottom diameter (Table 9). The bottom droplets may therefore have access to more moisture that could further improve their function beyond simply increasing their size, as salts and LMMC in the aqueous

material attract more moisture and transfer it to the glycoprotein (Opell et al., 2013). While data for *A. trifasciata* is currently lacking, this difference in humidity for it's sister species, *Argiope aurantia*, would confer ~8 MJ/m^3 difference in toughness per droplet (Fig. 5). Accounting for droplet and spiral spacing this amounts to an additional 30% increase in toughness in the bottom web region.

Studies of asymmetry from orb-webs with classic architecture have largely ignored prey tumbling, which describes prey that struggle free from some sticky spirals only to become re-entangled in others from lower parts of the web, even though up to 30% of prey have been documented to tumble free and escape from orb-webs (Eberhard, 1989; Zschokke et al., 2006). While it's clear that a downwards orientation and larger lower web section is an efficient strategy for coping with the effects of gravity as it relates to spider running speed, increasing the size of this portion of the web may also be beneficial to the spider, as tumbling prey are faced with additional sticky silk. Differentiation of glue resource deposition across the web may therefore be, in part, a response to tumbling. The top droplets are small, and, as prey tumbling after intersecting this web region would have many more threads to intercept as they tumble, spiders may conserve resources by limiting the deposition of glue near the uppermost areas of the web. Additionally, the middle portions of the web also support the toughest per volume droplets, which, at least for the top sector, would help secure prey tumbling from the upper most threads. It follows, then, that prey striking the middle of the lower sector of the web would tumble towards the less tough glue at the bottom. However, if spiders are responding to tumbling while conserving resources by reducing the size of the top droplets, it may be that droplets of the additional silk threads added to the bottom web that creates asymmetry, though less tough, present more glue material for capture. Additionally, active orthoperans are a significant proportion of *A. trifasciata* diet (Levi, 1968; Olive, 1980) and active prey tumble at higher rates and escape the most frequently, (Zschokke et al., 2006).

This research demonstrates that the viscous glue droplets of the orb-web capture spiral contribute another level of adaptability for prey capture. The flexibility of silk resource allocation allows optimization for specific tasks, and the size, distribution, and performance of the droplets complements the differences that underlie web symmetry. Microhabitat gradients may interact with observed differences, optimizing web sector performance. Most

of this study's findings address behavioral and functional aspects of orb-web architecture and viscous capture thread. However, the observation that the ratio of aqueous to glycoprotein volume differs across the web and that this could influence the material properties of glycoprotein has important implications for material science. The LMMC within viscous droplets are known to play a critical role beyond conferring droplet hygroscopicity, as they solvate glycoproteins, enhancing their interactions with surfaces that a droplet contacts (Sahni et al., 2014). Thus, the aqueous to glycoprotein ratio may correlate not only with glycoprotein viscosity and extensibility, but also with glycoprotein interactivity. This observation will aid in the design and improvement of the next generation of biomimetic materials as engineers seek to develop capture spiral-inspired adhesives.

MATERIALS AND METHODS

Collecting and preparing threads

Thread samples were collected from webs constructed by individual adult females of *A. trifasciata* (n=12) on the Virginia Tech campus in Blacksburg, Montgomery County, VA, USA, from 15 September 2014 to 03 October 2014. We did not collect the spiders or measure their size, but marked their web's position with flagging tape to avoid resampling a web. Each sample was collected between 05:30h and 08:30h and all images and videos captured by 16:00h the same day. The complete upper and lowers sectors of each spider's web were collected on a 15 x 52 cm aluminum rectangular frame. The upper surfaces of these frames were covered with Scotch® double-sided 3M™ High Performance Double Coated Tape (Tape 9086; 3M, St Paul, MN, USA), which adhered to web sectors, maintaining the threads at their native tension. Threads extending from the collecting frame were cut with a pair of scissors to avoid distorting the sample when the frame was withdrawn from the web. The frame was oriented to collect the complete top and bottoms of the web, as well as several inner spirals from the sides of the web. We placed web-sampling frames in closed containers for transport to the laboratory. The location of each sampled web was marked with flagging tape to ensure that threads from an individual spider's web was included only once in the study.

Using the collected web sectors, we determined the total length of each web, from the top frame thread to the bottom frame thread, the length of the top and bottom sections, measured from the top frame line to the inner most spiral of the respective section, the number of spirals in the top and bottom sections, and the distance from the center of the hub to the inner most spiral of the top and bottom sections.

We used forceps, which were blocked open to accommodate the separation of the supports on sampler slides, to collect individual viscous threads and transfer them to a microscope slide sampler. Double-sided carbon tape on both the forceps' tips held each thread strand securely when the thread was pulled or burned free using a hot wire probe. Threads were placed on the tops of a sampler's U-shaped brass struts, which were epoxied at 4.8 mm intervals to microscope slides and covered with double-sided carbon tape (fig. 3 in (Opell et al., 2011b).

Capture spiral threads were collected from 5 places on each web (Fig. 1): 1. The top most threads just beneath the upper frame thread, 2. The middle of the web's top section, determined by dividing the total number of spirals in the top section in half, 3. The inner most threads located around the hub of the web, 4. The middle of the web's bottom section and 5. The bottom most spiral threads just above the bottom frame line.

Determining Glycoprotein Volume

For each individual's web we determined the volume of glycoprotein in the core of three droplets from each of the five web positions. As described more fully in Opell et al., 2013, viscous droplets were flattened to permit visualization of the inner glycoprotein material, however the epi-illumination of this microscope system does not resolve the glycoprotein granule anchor at the center of the larger surrounding glycoprotein material (Opell and Hendricks, 2010). Just prior to flattening, three droplets from each web sector were photographed in a suspended state. Next, in contrast to Opell et al. 2013, we simply placed a 22 mm glass cover slip over the droplets to be visualized, as this study was conducted at a constant temperature and humidity, and the test chamber was therefore left open. Cover slips were cleaned with a Kimwipe ® and 95% ethanol before use. After placing the cover slip over the threads, the eraser of a pencil was used to gently press the cover slip to

ensure flattening was even, and the three droplets were again photographed in their flattened condition.

Extending droplets

To ensure that the probe used to extend droplets only contacted a single droplet at a time, we used a minuten insect pin moistened with distilled water to move away droplets that were adjacent to the test droplet located at the center of the thread strand. This process retained the aqueous coating of the strand's axial fibers, as demonstrated by the formation of small droplets similar to those often present between the large primary droplets of many viscous threads.

We photographed each isolated test droplet immediately prior to extension. All observations were made at 23°C and 55% RH. A steel probe was inserted through a port in the side of the test chamber and its 413 μm wide polished tip, previously cleaned with 95% ethanol on a Kimwipe, was aligned and brought into contact with the focal droplet and anchored to a stable mount. To ensure full droplet adhesion, the probe was pressed against the droplet until the thread was deflected by a distance of 500 μm. We then recorded a 60 fps video as the probe was withdrawn from the droplet at a velocity of 69.6 μm s^{-1} by a computer controlled stepping motor connected to the microscope stage's X axis by a flexible belt.

Determining droplet volume

We used ImageJ (Rasband, 1997-2014) to measure droplet length (DL; dimension parallel to the support line) and droplet width (DW), and from these measurements computed droplet volume (DV) using the formula (Opell and Schwend, 2007; Liao et al., 2015):

$$DV = \frac{(2\pi \times DW^2 \times DL)}{15} \quad (1)$$

Characterizing droplet extension

The total loaded time (TLT) of droplet extension begins when the axial line is deflected from its initial non-loaded, 180° configuration and ends when the droplet returns to a non-loaded condition. We divided TLT into two phases; the pre-extension (PE) phase, during which the

axial thread exhibited tensile deflection, but the droplet did not extend, thus holding the axial line in contact with the probe, and the droplet extension (DE) phase, which began when a droplet filament started to form and ended when the axial line returned to its 180° configuration at the end of TLT (fig. 4 in Stellwagen et al., 2014). During DE we measured five axial line deflection angles: the angle at the initiation of this filament formation, and the angles at 25%, 50%, 75%, and 99% of the total duration time of DE, using iMovie '11 (Apple Inc., 2010) and ImageJ programs.

Determining the force on droplet filaments

We used the diameter and Young's modulus of *A. trifasciata* axial fibers (from Sensenig et al. 2010) to estimated the force (F_{total}) on a droplet in three computational steps: 1. Determining the extension of the axial lines on either side of an extending droplet, 2. Converting this extension to force, and 3. Summing these force vectors to determine force exerted on a droplet filament.

Each droplet was located near the center of a 4800 μm long support strand, however the entire thread was not captured in videos. Therefore, we used the central deflection angle of the supporting line to calculate the change in length (ΔL) of each side (L_0 = 2400 μm) of the support thread according to the following formulas:

$$L = \frac{2400}{\sin(\theta \times 0.5)} \quad (2),$$

$$\Delta L = L - L_0 \quad (3).$$

Knowing the extensions of either side of the thread that supported a droplet, and the diameters and Young's modulus values for each species axial fibers, we calculated the force on each stretching thread on either side of a droplet (F_1, F_2) using the formula:

$$F_1, F_2 = \frac{EA_0\Delta L}{L_0} \quad (4),$$

where E is Young's Modulus and A_0 is two times the instantaneous cross sectional area of the two cylindrical axial fibers of each strand. Instantaneous cross sectional area, which accounts for narrowing of axial fibers as they are stretched, was determined by multiplying reported cross sectional area (from Sensenig et al. 2010) by the ratio of the initial thread length to the final thread length. To determine the total force exerted on a droplet filament, the angular deflection of a droplet's support line was again used to sum the force vectors of both sides of the support lines of a droplet, using the formula:

$$F_{total} = 2\cos(\theta \times 0.5)F_1 \tag{5}$$

Toughness, an index of cumulative force on a droplet as it is extended, was equated to the area under a force / extension time plot for a treatment. To approximate this index for each treatment, we summed the products of force and DE at each DE interval (0, 25, 50, 75, and 99%), as described in the following formula, where F is the total force on an extending droplet and I is the droplet interval:

$$\frac{\left(F_I + F_{I+1}\right)}{2} \times \left(DE_{I+1} - DE_I\right) \tag{6}$$

Measuring web placement and microhabitat

We measured 5 web parameters from 13 adult female *A. trafasciata* in the field, 7 from between rows of hay bales, and 6 from surrounding weedy habitats: 1. Distance from the ground to the bottom of the web, and from ground to the top of the web (as the webs were often slightly tilted), 2. Length of the top-to-bottom spiral diameter, 3. Length of each individual top and bottom web sector, from the outer-most to inner-most spiral, 4. Number of spirals in the top and bottom sections, and 5. Height of the vegetation surrounding the webs.

To assess gradients in temperature and humidity we placed HOBO® data loggers (U23 Pro v2, Onset Computer Corporation, Bourne, MA) at four sites where *A. trafasciata* webs were observed. At each site, five data loggers were arranged on vertical pole to gather data from: 1. Ground level, 2: Level with the top of the vegetation, 3-4: Two equal intervals between the ground and top of the vegetation, and 5: A distance above the vegetation equal to each of the subintervals between the top of the vegetation and ground level. Logger poles

collected data for 7-9 days at each site, and recorded the temperature and humidity every 15 minutes.

Analysis

For droplet comparisons, each sampling unit was an individual spider's web. When multiple measurements were taken, such as those used in determining glycoprotein volume, these were averaged for an individual and the average used in subsequent statistical analysis. For each of the five positions within a web, the values for droplet size, glycoprotein volume, aqueous volume, and droplet performance were averaged. For temperature and humidity recordings, we averaged values at each 15-minute time interval over the course of the 7-9 day period, the time during which the logger poles were recording at a particular site. We used JMP (SAS Institute, Cary, North Carolina) to analyze data and considered individual comparisons with $P \leq 0.05$ as significant. All observations were normally distributed (as confirmed by Shapiro-Wilk W tests having $P \leq 0.05$). Droplet size and performance were each very similar within an individual web sample but showed some inter-individual difference. To address this we followed a repeated measures design, comparing values with matched pair t-tests. If the data were not normal, they were log-transformed, and again tested for normality, and their transformed values then compared using matched pair t-tests. The Wilcoxon signed-rank test was used when values were not normally distributed.

ACKNOWLEDGEMENTS

Carlyle C. Brewster assisted with statistical analyses.

AUTHOR CONTRIBUTIONS

S.D.S. collected and prepared thread samples, performed droplet extensions and image measurements, analyzed data, and prepared the manuscript and figures. B.D.O. designed and constructed the instrumentation used in this study, collected and helped prepare thread samples, and contributed to data analysis, and manuscript and figure preparation. M.E.C. assisted with droplet extension, image measurements, and data entry.

COMPETING INTERESTS

No competing interests declared.

FUNDING

Funds from the State Council for Higher Education for Virginia provided the digital camera used in this study. This study was supported by National Science Foundation grant IOS-1257719.

FIGURES

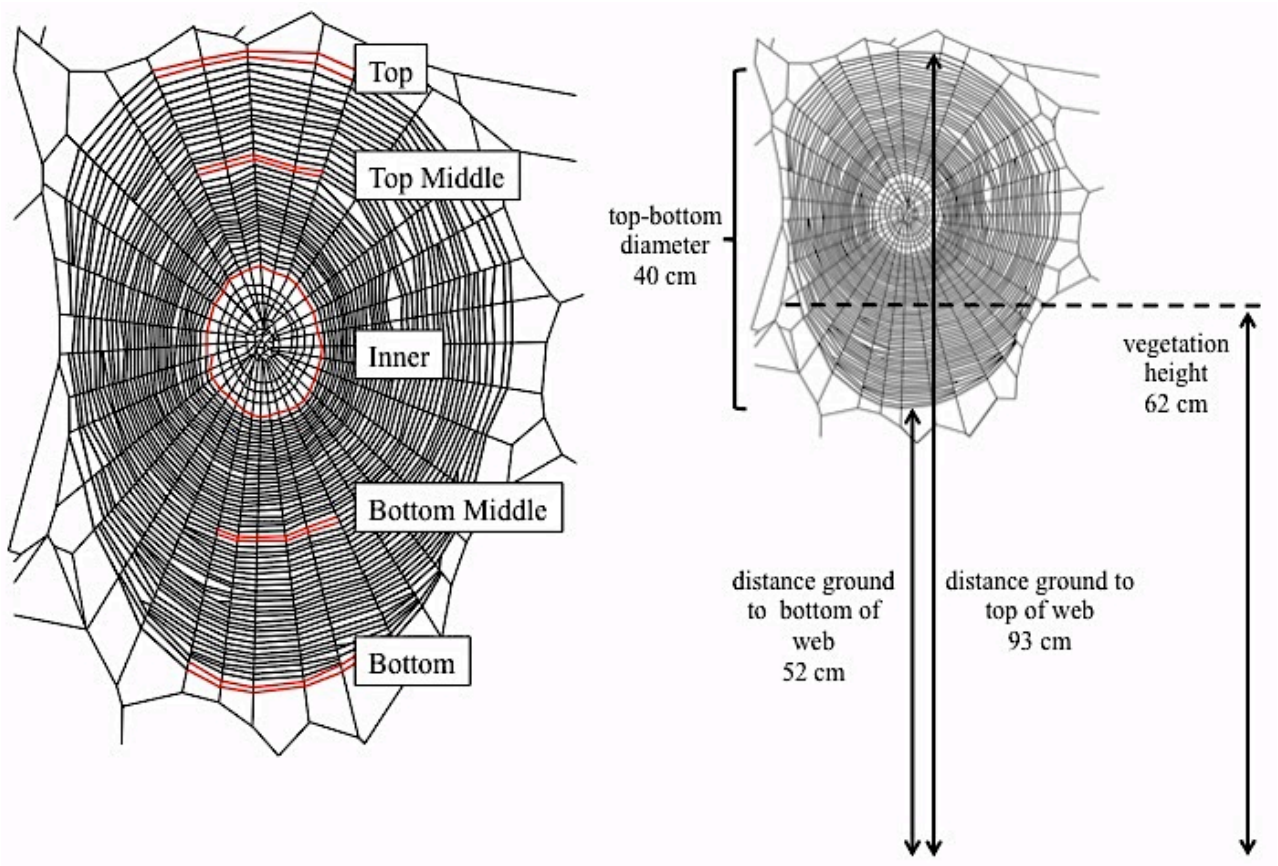

Figure 1. Orb-web showing placement of sampled threads, and an orb-web with corresponding heights measured in the field.

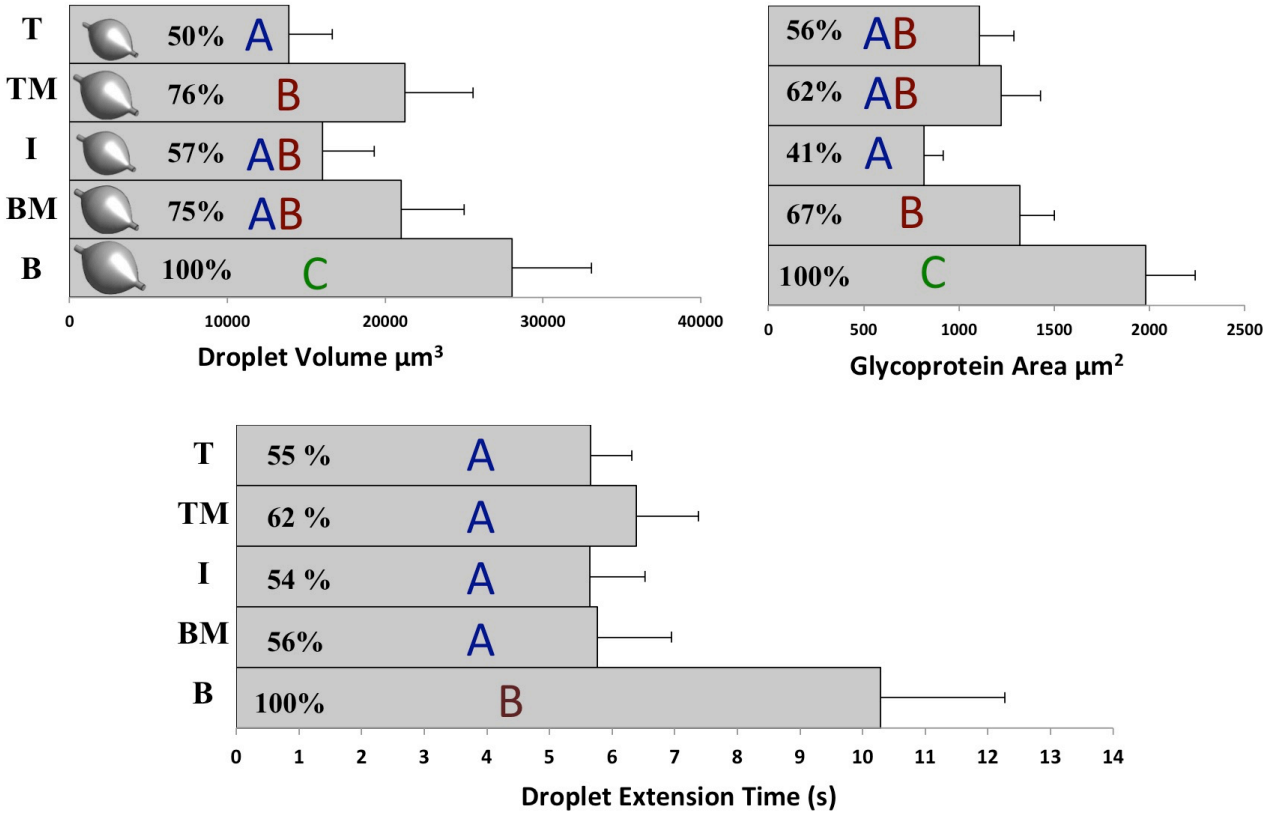

Figure 2. Histograms showing the relationship of Droplet Volume, Glycoprotein Area, and Droplet Extension Time in the five areas of the web. T = Top, TM = Top Middle, I = Inner, BM = Bottom Middle, B = Bottom.

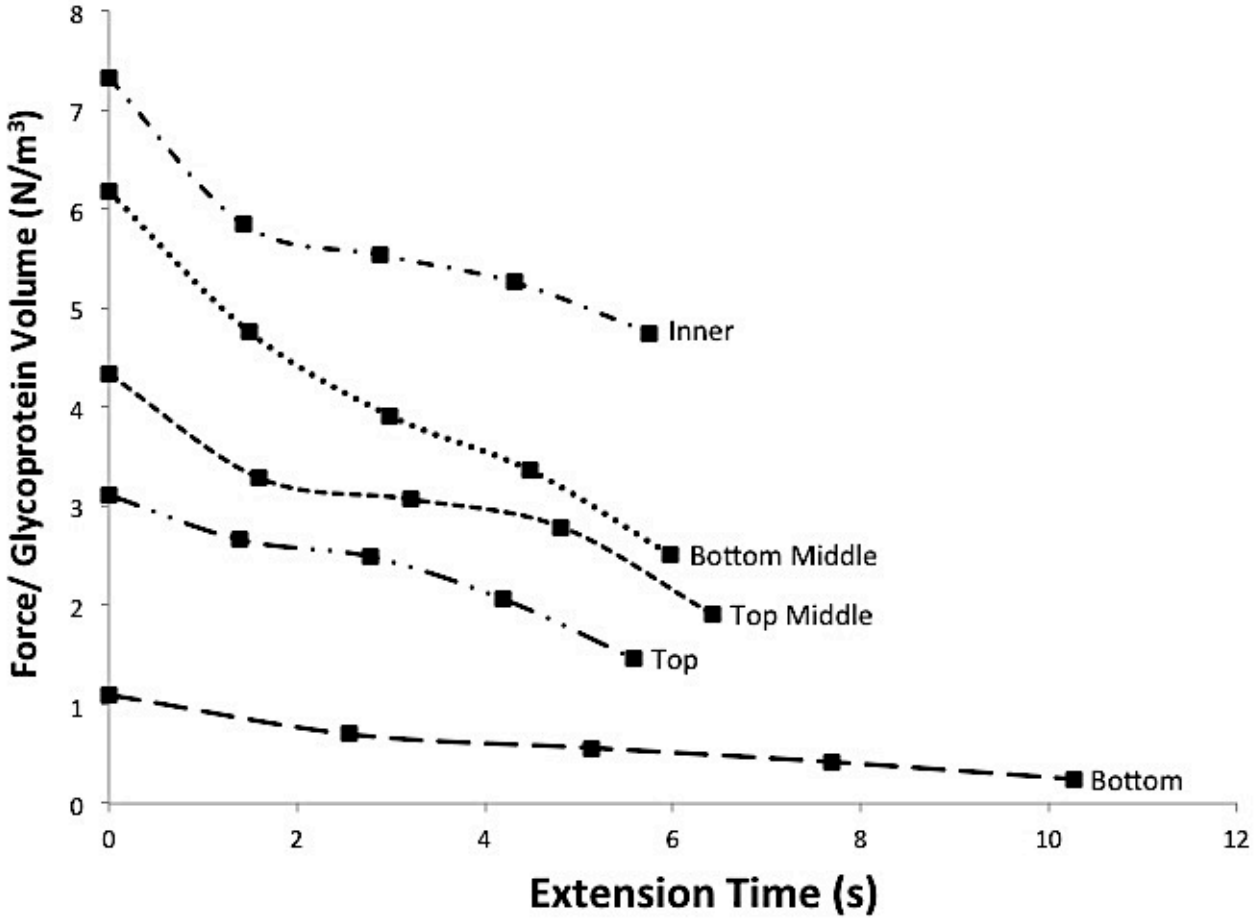

Figure 3. Droplet force / droplet glycoprotein volume plotted against droplet extension time. The area under each curve represents toughness per glycoprotein volume.

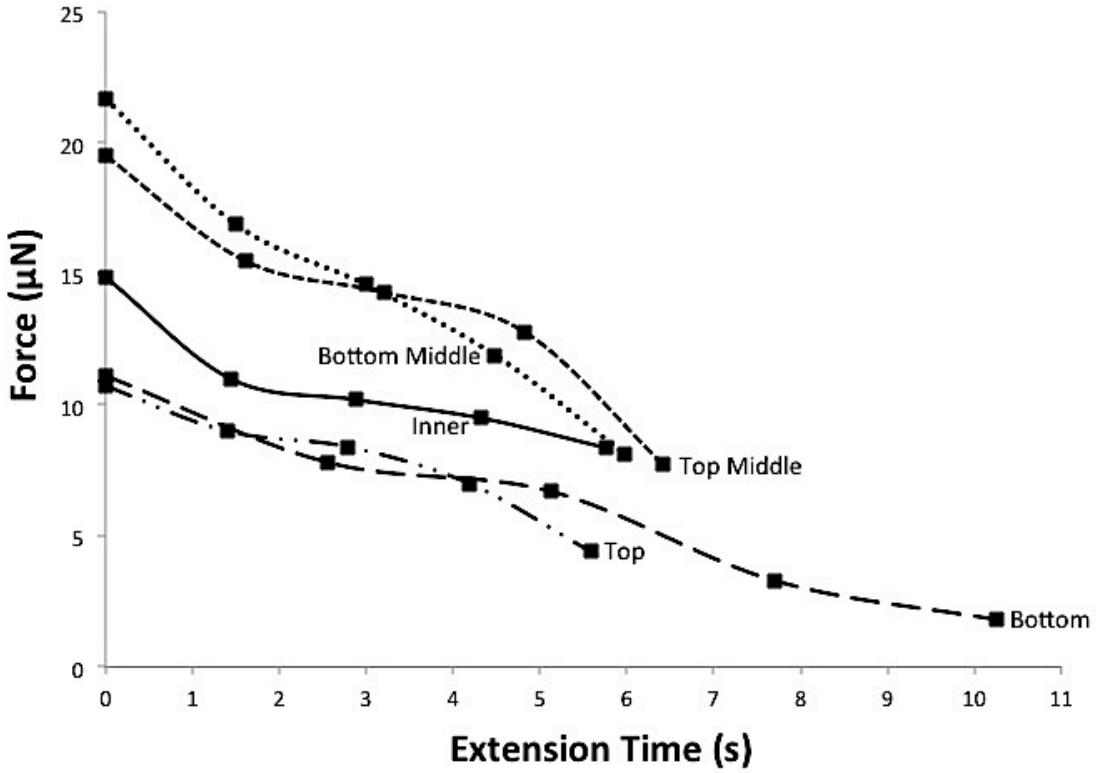

Figure 4. Droplet force plotted against droplet extension time. The area under each curve represents the relative toughness of individual droplets from each area of the web.

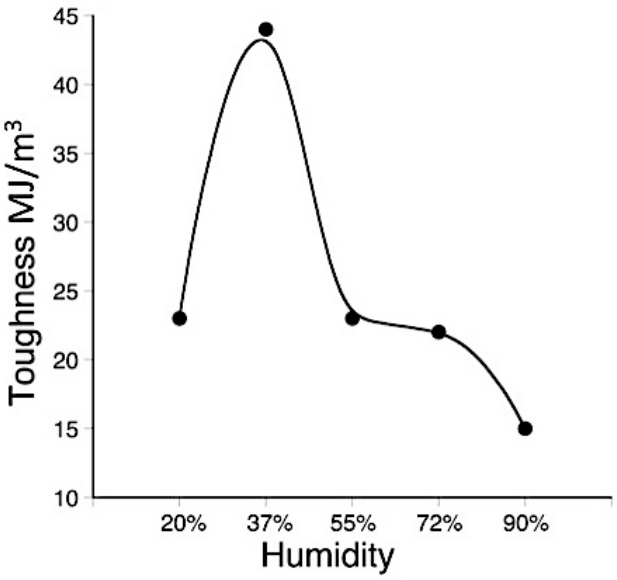

Figure 5. Change in *A. aurantia* toughness across 5 humidities, computed from axial line deflection, Young's modulus, and axial diameters of flagelliform fibers taken from supplementary table 4 in Sensenig et al. 2010. Values are based on fresh (wet) viscous threads and droplets. (Opell and Andrews in prep).

REFERENCES

Apstein, C. H. (1889). Bau und Function der Spinnendrusen der Araneida. *Archiv fur Naturgeschichte*, 29.

Boys, C. V. (1889). Quartz Fibres. *Nature* **40**, 247-251.

Chacón, P. and Eberhard, W. G. (1980). Factors affecting numbers and kinds of prey caught in artificial spider webs with considerations of how orb-webs trap prey. *Bulletin of the British Arachnological Society* **5**, 29-38.

Eberhard, W. G. (1972). The web of Uloborus diversus (Araneae: Uloboridae). *Journal of Zoology* **166**, 417-465.

Eberhard, W. G. (1986). Effect of orb-web geometry on prey interception and retention. In *Spiders: Webs, Behavior, and Evolution*, (ed. W. A. Shear), pp. 70-100. Stanford: Stanford University Press.

Eberhard, W. G. (1989). Effects of orb-web orientation and spider size on prey retention. *Bulletin of the British Arachnological Society* **8**, 45-48.

Eberhard, W. G. (2013). The rare large prey hypothesis for orb web evolution: a critique. *Journal of Arachnology* **41**, 76-80.

Edmonds, D. and Vollrath, F. (1992). The contribution of atmospheric water vapour to the formation and efficiency of a spider's web. *Proceedings of the Royal Society of London* **248**, 145-148.

Foelix, R. F. (2011). Biology of spiders. Oxford: Oxford University Press.

Gregorič, M., Kiesbüy, H., Quiñones Lebrón, S., Rozman, A., Agnarsson, I. and Kuntner, M. (2013). Optimal foraging, not biogenetic law, predicts spider orb web allometry. *Naturwissenschaften* **100**, 263-268.

Herberstein, M. E. and Heiling, A. M. (1999). Asymmetry in spider orb webs: A result of physical constraints? *Animal Behaviour* **58**, 1241-1246.

Levi, H. W. (1968). The spider genera *Gea* and *Argiope* in America (Araneae: Araneidae). *Bulletin of the Museum of Comparative Zoology* **136**, 319-352.

Liao, C.-P., Blamires, S. J., Hendricks, M. L. and Opell, B. D. (2015). A re-evaluation of the formula to estimate the volume of orb web glue droplets. *Journal of Arachnology* **43**, 97-100.

Maciejewski, W. (2010). An analysis of the orientation of an orb-web spider. *Journal of Theoretical Biology* **265**, 604-608.

Masters, W. M. and Moffat, A. J. M. (1983). A Functional Explanation of Top-Bottom Asymmetry in Vertical Orbwebs. *Animal Behaviour* **31**, 1043-1046.

Nakata, K. and Zschokke, S. (2010). Upside-down spiders build upside-down orb webs: web asymmetry, spider orientation and running speed in Cyclosa. *Proceedings of the Royal Society B: Biological Sciences* **277**, 3019-3025.

Olive, C. W. (1980). Foraging Specialization in Orb-Weaving Spiders. *Ecology* **61**, 1133-1144.

Opell, B.D. and Andrews, S.F. In preparation. Evolutionary and environmental plasticity in the material properties of orb spider glycoprotein glue.

Opell, B. D. and Schwend, H. S. (2007). The effect of insect surface features on the adhesion of viscous capture threads spun by orb-weaving spiders. *Journal of Experimental Biology* **210**, 2352-2360.

Opell, B. D. and Hendricks, M. l. (2010). The role of granules within viscous capture threads of orb-weaving spiders. *Journal of Experimental Biology* **213**, 339-346.

Opell, B. D., Karinshak, S. E. and Sigler, M. A. (2011). Humidity affects the extensibility of an orb-weaving spider's viscous thread droplets. *Journal of Experimental Biology* **214**, 2988-2993.

Opell, B. D., Tran, A. M. and Karinshak, S. E. (2011b). Adhesive compatibility of cribellar and viscous prey capture threads and its implication for the evolution of orb-weaving spiders. *Journal of Experimental Zoology Part A: Ecological Genetics and Physiology* **315A**, 376-384.

Opell, B. D., Karinshak, S. E. and Sigler, M. A. (2013). Environmental response and adaptation of glycoprotein glue within the droplets of viscous prey capture threads from araneoid spider orb-webs. *Journal of Experimental Biology* **216**, 3023-3034.

Opell, B. D., Lipkey, G. K., Hendricks, M. L. and Vito, S. T. (2009). Daily and Seasonal Changes in the Stickiness of Viscous Capture Threads in Argiope aurantia and Argiope trifasciata Orb-webs. . *Journal of Experimental Zoology* **311A**, 217–225.

Opell, B. D. and Andrews, S. F. in preparation. Evolutionary and environmental plasticity in the material properties of orb spider glycoprotein glue.

Peters, H. (1937). Studien am netz der kreuzspinne (Aranea Diadema.). *Z. Morph. u. Okol. Tiere* **32**, 613-649.

Rao, D., Fernandez, O. C., Castañeda-Barbosa, E. and Díaz-Fleischer, F. (2011). Reverse positional orientation in a neotropical orb-web spider, Verrucosa arenata. *Naturwissenschaften* **98**, 699-703.

Rayleigh, J. W. S., Baron. (1892). Scientific papers. **3**, 585-596.

Sahni, V., Blackledge, T. A. and Dhinojwala, A. (2010). Viscoelastic solids explain spider web stickiness. *Nature Communications* **1**, 1-4.

Sahni, V., Blackledge, T. A. and Dhinojwala, A. (2011). Changes in the Adhesive Properties of Spider Aggregate Glue During the Evolution of Cobwebs. *Scientific Reports* **1**, 41.

Sahni, V., Dhinojwala, A., Opell, B. and Blackledge, T. (2014). Prey Capture Adhesives Produced by Orb-Weaving Spiders. In *Biotechnology of Silk*, vol. 5 eds. T. Asakura and T. Miller), pp. 203-217: Springer Netherlands.

Sekiguchi, K. (1952). On a new spinning gland found in geometric spiders and its function. *Annot Zool Japonenses* **25**, 394-399.

Sensenig, A., Agnarsson, I. and Blackledge, T. A. (2010). Behavioural and biomaterial coevolution in spider orb webs. *Journal of Evolutionary Biology* **23**, 1839-1856.

Sensenig, A. T., Lorentz, K. A., Kelly, S. P. and Blackledge, T. A. (2012). Spider orb webs rely on radial threads to absorb prey kinetic energy. *Journal of The Royal Society Interface*.

Stellwagen, S. D., Opell, B. D. and Short, K. G. (2014). Temperature mediates the effect of humidity on the viscoelasticity of glycoprotein glue within the droplets of an orb-weaving spider's prey capture threads. *Journal of Experimental Biology* **217**, 1563-1569.

Stowe, M. K. (1978). Observations of Two Nocturnal Orbweavers That Build Specialized Webs: Scoloderus cordatus and Wixia ectypa (Araneae: Araneidae). *Journal of Arachnology* **6**, 141-146.

Tillinghast, E. K. and Christenson, T. (1984). Observations on the Chemical Composition of the Web of *Nephila clavipes* (Araneae, Araneidae). *Journal of Arachnology* **12**, 69-74.

Venner, S. and Casas, J. (2005). Spider webs designed for rare but life-saving catches. *Proceedings. Biological sciences / The Royal Society* **272**, 1587-1592.

Witt, P. N., Reed, C. F. and Peakall, D. B. (1968). A spider's web: problems in regulatory biology. Berlin; Heidelberg; New York - Book: Springer-Verlag.

Zschokke, S. and Nakata, K. (2010). Spider orientation and hub position in orb webs. *Naturwissenschaften* **97**, 43-52.

Zschokke, S., Hénaut, Y., Benjamin, S. P. and García-Ballinas, J. A. (2006). Prey-capture strategies in sympatric web-building spiders. *Canadian Journal of Zoology* **84**, 964-973.

TABLES

Table 1. Parameter data from webs used for extension trials and webs in the field (mean ± 1 standard deviation).

	Mean ± s.d.	Matched Pair, One tailed t-test
Webs used in extension trials n=12		
Total Web Diameter (Top Frame Line to Bottom Frame Line) cm	37.2 ± 8.1	
Top Length (Inner spiral of top sector to top-most spiral) cm	12.2 ± 2.9	***P* = 0.0497**
Bottom Length cm	15.5 ± 5.2	
# Spirals Top	34.7 ± 7.7	***P* = 0.0130**
# Spirals Bottom	42.8 ± 7.6	
Webs measured in the field n=13		
Height, Ground to Bottom Frame Line	52.4 ± 15.5	***P* < 0.0001**
Height, Ground to Top Frame Line	93.1 ± 16.1	
Total Web Diameter (Top to Bottom) cm	42.5 ± 9.3	
Top Length cm	14.7 ± 3.9	***P* = 0.0014**
Bottom Length cm	17.3 ± 4.2	
# Spirals Top	35.6 ± 4.2	***P* < 0.0001**
# Spirals Bottom	43.2 ± 3.8	
Vegetation Height	62.7 ± 17.2	

Table 2: Dimensions of suspended droplets before flattening (n=12, mean ± standard deviation).

	Length μm	Width μm	Volume μm^3	Matched Pair (Volume, LOG transformed)	Droplet Spacing μm (Distance/Drop)
Top	39.5 ± 8.2	26.8 ± 6.0	13,874 ± 9,652	A	149 ± 46
Top Middle	45.3 ± 9.8	31.3 ± 7.0	21,239 ± 14,980	B	149 ± 40
Inner	41.3 ± 9.6	28.2 ± 6.5	16,028 ± 11,003	AB	179 ± 40
Bottom Middle	46.1 ± 9.8	31.0 ± 6.5	21,033 ± 13,770	AB	171 ± 47
Bottom	50.7 ± 9.5	34.2 ± 6.6	28,015 ± 17,540	C	181 ± 53
ANOVA			**(LOG) *P* = 0.0430**		***P* = 0.4923**

Table 3: Dimensions of suspended droplets before extension (n=12, mean ± standard deviation).

	Length μm	Width μm	Volume μm^3	Matched Pair (Volume, LOG transformed)
Top	43.0 ± 10.4	28.9 ± 7.0	17,612 ± 13,520	AB
Top Middle	46.4 ± 9.3	31.6 ± 6.7	21,911 ± 15,490	CD
Inner	40.5 ± 8.1	27.2 ± 5.3	13,827 ± 7,690	A C
Bottom Middle	47.3 ± 8.3	31.5 ± 5.9	21,531 ± 12,400	B D
Bottom	53.7 ± 10.7	36.0 ± 7.5	32,644 ± 20,134	E
ANOVA			**(LOG) *P* = 0.0142**	

Table 4: Dimensions and calculated volumes of flattened droplets (n=12, mean ± 1 standard deviation).

	Total Droplet Flattened Area μm^2	Flattened Droplet Thickness μm	Glycoprotein Area μm^2	Glycoprotein Volume μm^3	Matched Pair (Glyco. Vol)	Aqueous Volume μm^3	Matched Pair (Aqu. Vol.)	Aqueous Volume / Glycoprotein Volume	Matched Pair (A.V./G.V.)
Top	4,238 ± 1,963	3.8 ± 1.1	1,105 ± 638	4,707 ± 4,301	AB	12,906 ± 9,592	AB	3.2 ± 1.1	A
Top Middle	4,826 ± 1,780	4.2 ± 1.3	1,219 ± 659	5,748 ± 4,600	AB	16,745 ± 13,404	CD	3.3 ± 1.3	AB
Inner	3,897 ± 1,503	3.5 ± 1.1	815 ± 353	3,075 ± 1,941	A	10,741 ± 5,938	A D	4.0 ± 1.5	B
Bottom Middle	4,882 ± 1,658	4.2 ± 1.1	1,320 ± 603	5,987 ± 3,879	B	15,423 ± 9,500	BC	3.0 ± 1.2	AB
Bottom	6,296 ± 2,644	4.9 ± 1.4	1,981 ± 857	10,666 ± 7,458	C	19,721 ± 12,693	C	2.1 ± 0.7	C
ANOVA (LOG transformed)									

Table 5. Relative toughness per glycoprotein volume and LOG relative toughness for each web region (n=12, mean ± 1 standard deviation).

	Toughness (N/m^3)	LOG Toughness	Matched Pair
Top	3.2 ± 6.3	1.20 ± 1.21	AB D
Top Middle	18.6 ± 14.5	2.23 ± 0.69	C
Inner	31.9 ± 45.4	1.72 ± 1.74	A C
Bottom Middle	14.3 ± 22.4	2.27 ± 0.96	C
Bottom	7.9 ± 3.1	0.52 ± 0.96	D
ANOVA		***P* = 0.0051**	

Table 6. Extension phase times (seconds) for each web section (n=12, mean ± 1 standard deviation).

	TLT	PE	DE	Matched Pair DE
Top	24.5 ± 6.7	18.8 ± 7.3	5.7 ± 2.3	A
Top Middle	32.9 ± 7.4	25.5 ± 8.7	6.4 ± 3.4	AB
Inner	27.8 ± 8.6	22.2 ± 7.3	5.6 ± 3.4	A
Bottom Middle	32.5 ± 5.1	26.8 ± 4.2	5.8 ± 4.1	A
Bottom	29.6 ± 6.0	19.3 ± 7.5	10.3 ± 6.9	B
ANOVA			***P* = 0.0468**	

Table 7. Force on extending droplets for each web region and time interval (n=12, mean ± 1 standard deviation).

	Force 0%	Wilcoxon Each Pair	Force 25%	Wilcoxon Each Pair	Force 50%	Wilcoxon Each Pair	Force 75%	Wilcoxon Each Pair	Force 99%	Wilcoxon Each Pair
Top	10.7 ± 8.2	A	9.0 ± 8.5	A	8.4 ± 7.8	A C	7.0 ± 6.5	AB	4.4 ± 3.6	AB
Top Middle	19.5 ± 15.3	AB	15.5 ± 13.3	AB	14.3 ± 12.4	AB	12.8 ± 11.8	A	7.71 ± 7.9	A
Inner	14.9 ± 11.7	AB	11.0 ± 10.5	AB	10.2 ± 10.5	A C	9.5 ± 10.6	AB	8.37 ± 10.5	A
Bottom Middle	21.7 ± 7.7	B	16.9 ± 8.2	B	14.6 ± 7.6	B	11.9 ± 8.1	A	8.13 ± 8.2	A
Bottom	11.1 ± 9.4	A	7.8 ± 8.1	A	6.7 ± 8.2	C	3.3 ± 3.8	B	1.8 ± 3.1	B
Wilcoxon	***P* =0.0205**		***P* =0.0399**		***P* =0.0357**		***P* =0.0107**		***P* =0.0197**	

Table 8. Relative toughness and LOG relative toughness for each web region (n=12, mean ± 1 standard deviation).

	Toughness	LOG Toughness	Matched Pair
Top	38.3 ± 46.9	2.47 ± 1.54	A
Top Middle	69.4 ± 41.8	3.76 ± 0.72	B
Inner	70.6 ± 86.3	2.64 ± 1.64	A
Bottom Middle	77.3 ± 81.7	3.77 ± 0.93	B
Bottom	40.9 ± 44.7	2.78 ± 1.09	A
ANOVA		***P* = 0.0251**	

Table 9. Microhabitat humidity and temperature data logged in *A. trifasciata* habitats in late summer 2014. Loggers were placed 1: One interval above vegetation, 2: Vegetation Level, 3: One interval below vegetation level, 4: Two intervals below vegetation level, 5: Ground level.

	Longitude Latitude	Dates	Mean Humidity % (0500/1300)	Mean Temperature °C (0500/1300)	Logger Interval Spacing
Pig Barn Woods	37°12'37.2"N 80°25'46.5"W	8/12 - 8/21	1: 99.9/71.9 2: 99.9/71.4 3: 99.9/69.3 4: 99.9/70.5 5: 100/83.1	1: 14.3/22.9 2: 14.6/23.1 3: 14.2/23.8 4: 14.2/ 23.6 5: 14.4/23.5	35 cm
ESL #1	37°13'10.0"N 80°25'50.4"W	8/2 - 8/11	1: 98.0/69.7 2: 97.9/68.4 3: 98.0/68.4 4: 97.8/70.2 5: 95.1/100	1: 17.4/26.4 2: 17.2/26.6 3: 16.8/27.1 4: 16.9/27.1 5: 17.2/25.2	42 cm
ESL #2	37°13'09.3"N 80°25'48.4"W	8/12 - 8/22	1: 99.7/76.3 2: 99.8/75.2 3: 99.8/75.6 4: 98.6/75.2 5: 100/90.4	1: 14.2/21.5 2: 14.1/22.3 3: 13.8/22.6 4: 14.0/22.6 5: 14.4/20.6	43 cm
Pig Barn	37°12'47.8"N 80°26'25.5"W	8/22 - 8/31	1: 99.2/54.1 2: 98.9/49.8 3: 98.9/55.2 4: 98.2/60.7 5: 99.8/77.1	1: 15.6/30.2 2: 15.3/31.8 3: 15.4/32.5 4: 15.5/30.8 5: 16.1/30.4	30 cm

Appendix A. Axial angles for all species and treatments (n=12, mean ± 1 standard deviation).

	Axial Angle 0%	Matched Pair	Axial Angle 25%	Matched Pair	Axial Angle 50%	Matched Pair	Axial Angle 75%	Matched Pair	Axial Angle 99%	Matched Pair
Top	132.6 ± 18.3	A	137.8 ± 19.2	A	139.8 ± 19.7	A	143.3 ± 19.5	ABC	149.6 ± 17.2	A
Top Middle	117.5 ± 17.4	BC	123.9 ± 17.4	BC	125.7 ± 17.1	BC	129.3 ± 18.1	A C	139.1 ± 17.5	A
Inner	126.2 ± 17.2	A C	134.7 ± 18.1	A C	138.0 ± 19.6	A C	141.5 ± 21.2	C	146.2 ± 22.6	A
Bottom Middle	112.2 ± 10.2	B	119.4 ± 12.8	B	124.0 ± 13.0	B	130.0 ± 14.0	A	139.6 ± 16.3	A
Bottom	131.5 ± 16.3	A	142.2 ± 16.7	A	145.9 ± 16.8	A	153.9 ± 14.1	B	161.1 ± 13.2	B
ANOVA	***P* = 0.0101**		***P* = 0.0083**		***P* = 0.0119**		***P* = 0.0059**		***P* = 0.0222**	

6. Conclusion

Sarah D. Stellwagen

Spider orb-webs consist of many functional components that are integrated to capture prey. This has allowed each element to be optimized for a specific role. The radial threads function to absorb and dissipate kinetic energy from intercepted prey (Sensenig et al., 2012), while the capture spiral threads dissipate and retain prey after initial interception (Sahni et al., 2011). These two components are supported by frame threads, and together, form a web that functions to intercept prey, dissipate energy, and retain prey (Chacón and Eberhard, 1980; Blackledge et al., 2011). The focus of this dissertation was to investigate the selective pressures that influence one element of this system, the adhesive glue droplets supported by the capture spiral thread, which together, are responsible for prey retention, and to answer questions from an ecological perspective that are also important for materials science. First, I examined the effects of abiotic factors temperature and ultraviolet radiation on the performance of the glue droplets. Second, I documented the characteristics and distributions of the glue droplets across orb-webs, which provided insight into how the ratio of the glue's materials affects droplet performance. The outcome of this research is not only important for understanding spider and spider silk evolution, but also provides materials engineers with important data needed to produce diverse and effective adhesives based on capture spiral glue.

Efforts to produce synthetic spider dragline silk with similar properties have thus far been largely unsuccessful, at least on a commercial scale (Slotta et al., 2012). The transformation of liquid silk dope within a spider's internal gland reservoir into the solid silk fiber that emerges from the spinneret occurs along ductwork that involves a set of complicated chemical processes not yet replicable in the lab. The glycoprotein glue from capture spiral thread of orb-webs, however, is amorphous within the aggregate gland, and remains amorphous after deposition, suggesting little internal processing after the material is initially produced within the gland.

Synthetic glues come in a variety of formulas with properties tailored for specific applications. Pressure sensitive tapes do not require heat or chemicals for bonding to occur

and are used commercially and in homes. Chemical cement adhesives tend to be irreversible and harden into a strong, solid material. In addition to being water soluble and biodegradable, capture spiral glue is also incredibly tough. These characteristics - potential ease of production, environmentally friendly application, and pertinent material properties - make this substance a good candidate for a biologically inspired adhesive. Additionally, the diversity of glue function from orb-weaving spiders of different habitats constitutes a vast cache of unique properties to formulate different glues based on specific needs (e.g. desert versus tropical applications). My research has answered important questions that will be invaluable for the design and production of biomimetic spider glues.

I focused on examining how environmental factors influence capture spiral glue droplet performance, and how differences in the size and performance of the droplets across the web are related to web architecture and microhabitat temperature and humidity gradients (Fig. 1). My first experiment demonstrated how temperature mediates the effect of humidity, an important glycoprotein pressure that can dramatically affect droplet performance on species-specific scale. As humidity fluctuates throughout a day, so does temperature, and the opposing consequences of these two environmental factors on the glue's performance help stabilize its function. I also examined the effect of ultraviolet radiation on the glycoprotein glue, an important abiotic factor known to affect biological organisms and materials in a variety of ways, both positive and negative. Some silk products are enhanced by UVR, but little was previously known about how UVR influences the glycoprotein of capture spiral silk or its adhesive component. This research showed that viscous thread droplets from a range of species, those that receive full sun exposure to those that receive little to no sun exposure, all resist degradation from relevant daily doses of UVB. Evidence also suggests that the glue of full sun species might actually be enhanced by UVB, while that of shaded species can absorb a limited dose of UVB before rapidly degrading. Furthermore, UVA exposure equivalent to that experienced over the course of a day does not appear to affect glycoprotein performance.

Finally, I showed that the glue droplets of the capture threads of *Argiope trifasciata* are differentially distributed in size and performance from the top to bottom and inner to outer spirals of the web. This research also exposed how a larger percentage of aqueous material within droplets results in tougher glycoprotein. These results are important for understanding selection pressures that shape webs for prey capture, as this adds to the list of

web adjustable components whose variation results in functional differences across the web. Furthermore, this research resulted in novel information about the role of the aqueous material for droplet performance.

The experiments conducted for this dissertation contribute to our understanding of spider orb-webs from an individual component, whole-web function, and materials science perspective. It provides a comprehensive look at the role of capture spiral adhesive in the context of web environment, and yields valuable information for asking further questions about the web system, the integration of its components, and focus for discovering functional mechanisms. How do the differences in droplet size and performance across the web affect prey capture, and how does the evolution of this glue component affect the function of other web elements? What are the molecular mechanisms responsible for droplets' responses to temperature and UVR resistance and enhancement? Could these properties be selectively incorporated into synthetic adhesives? Finally, this work illustrates the importance of the capture spiral droplet plasticity in the context of spider habitat diversity.

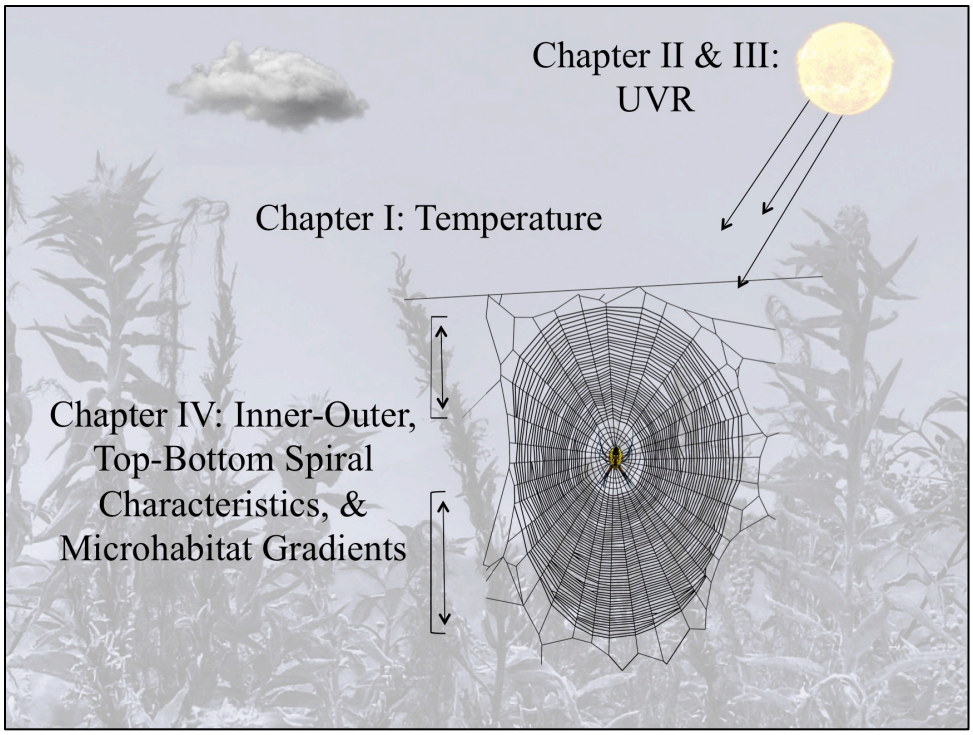

Figure 1. Integrated components of dissertation research questions.

REFERENCES

Blackledge, T. A., Kuntner, M. and Agnarsson, I. (2011). The Form and Function of Spider Orb Webs: Evolution from Silk to Ecosystems. In *Advances in Insect Physiology*, vol. Volume 41 (ed. C. Jérôme), pp. 175-262: Academic Press.

Chacón, P. and Eberhard, W. G. (1980). Factors affecting numbers and kinds of prey caught in artificial spider webs with considerations of how orb-webs trap prey. *Bulletin of the British Arachnological Society* **5**, 29-38.

Sahni, V., Blackledge, T. A. and Dhinojwala, A. (2011). A Review on Spider Silk Adhesion. *Journal of Adhesion* **87**, 595-614.

Sensenig, A. T., Lorentz, K. A., Kelly, S. P. and Blackledge, T. A. (2012). Spider orb webs rely on radial threads to absorb prey kinetic energy. *Journal of The Royal Society Interface*.

Slotta, U., Mougin, N., Römer, L. and Leimer, A. H. (2012). Synthetic Spider Silk Proteins and Threads. *Chemical Engineering Progress* **108**, 43-49,35.